UNIVERSITAT DE BARCELONA

Implications of astrocytic RTP801 in neuroinflammation and neurodegeneration in Alzheimer's disease

Almudena Chicote González

IMPLICATIONS OF ASTROCYTIC RTP801 IN NEUROINFLAMMATION AND NEURODEGENERATION IN ALZHEIMER'S DISEASE

Dissertation submitted by

Almudena Chicote González

This work was performed at the Department of Biomedical Sciences of the Faculty of Medicine and Health Sciences of the University of Barcelona, under the supervision of Dr. Cristina Malagelada Grau.

Dr. Cristina Malagelada Grau Almudena Chicote González

Doctoral program in Biomedicine

A mi familia.

“It’s not how much you do, but how much love you put in the doing”

-Mother Teresa

ACKNOWLEDGEMENTS

“Mamá, ya sé lo que quiero ser de mayor, ¡quiero ser científica!“. Y así empezaba esta historia, sin saber muy bien por qué. La tesis te hace transitar por todas las emociones que existen: ilusión, ansiedad, frustración, felicidad, tristeza, ira, miedo… En un camino que parece ser solitario, yo he estado rodeada de gente increíble que, sin duda, es lo mejor que me llevo de esta experiencia única.

Un 1 de octubre, hace tres años, llegaba a Barcelona con muchas ganas y mucha ilusión. Detrás de una puerta blanca muy difícil de encontrar, estaba la Unidad de Bioquímica, y no sabía que sería mi casa esos tres años. Y es que la sensación que tengo cada vez que llego es esa: la de estar en casa. Esta sensación es gracias a cada una de las personitas que trabajan conmigo cada día. Allí encontré mi refugio, y en los momentos más duros, esta gente me salvó la vida. Así que con ellos empiezo.

Primero me gustaría agradecerle a **Cris** que me diera la oportunidad de empezar mi tesis en el Malagelada’s lab. Cris, he aprendido mucho de ti, tanto de ciencia como de la vida. Ojalá todo el mundo tuviese las mismas ganas de vivir y disfrutar que tú. Gracias por ser siempre tan cercana, por todas nuestras charlas y salseos en el despacho. Gracias por todos los consejos y por darme consuelo cuando lo necesitaba, por estar tan pendiente de mí. Agradecerte también que nos abrieras las puertas de tu casa y por sacarnos de cerves y karaoke de vez en cuando. Gracias por transmitirme tú pasión por la ciencia, pero, a la vez, enseñarme que, al final, hay otras cosas también muy importantes en la vida. Sin duda, no te recordaré solo como directora de mi tesis, sino más bien como una amiga que estuvo presente en una de las etapas de más crecimiento de mi vida y que espero que siga estando.

Ahora les toca a mis senseis, los que me han enseñado todo lo que sé del lab. **Júlia** gracias por ser siempre tan buena conmigo, desde el primer día

tan preocupada de que me fuera bien. Júlia es esta persona estupenda de la cual todo el mundo quiere estar cerca; desprende buena energía por todos sus poros. Gracias por tratarme siempre con tanto cariño y por todos los momentos vividos dentro y fuera de la unidad. Siempre me acordaré de nuestra primera etapa en Mundet con una sonrisa, porque nos pasó absolutamente de todo, pero, gracias a ti, fue a la vez muy divertido. Aquella etapa nos unió mucho. Eres una de las personas más trabajadora que conozco, y sé que te irá genial y qué conseguirás todo lo que quieras en la vida, y aquí estaré yo para verlo.

A **Genís**, mi otro gran maestro. Genís es una de las personas más graciosas y divertidas que conozco; tiene una extraña afición que a todos nos acaba enganchando: hacer memes. Gracias, Genís, por hacerme siempre reír, por preguntarme cómo estaba. Gracias, por siempre echarme una mano, por tus trucos con el cálculo mental y por estar ahí cada vez que te he llamado para preguntarte por algún protocolo. Estar contigo en el lab cualquier tarde, con nuestra radio puesta, cantando mientras cada uno hace su experimento destinado al fracaso, ha sido todo un regalo. Ahora, fuera de bromas, no sé qué habría sido de mi sin ti. Gracias, por tanto.

A **Pol**, el pin de mi pon. Contigo me van a faltar palabras. Podemos decir que Pol y yo llegamos al lab casi a la vez, y quien nos conoce sabe que vamos siempre juntos a todo. Por dónde empezar… Gracias, Pol, por sacarme del lab a hacer el "café del drama" cada vez que lo necesitaba, gracias por abrirte tanto conmigo…Si la campana de disección o el lab de Mundet hablase... Pol es la persona más sabía que conozco, y es que sabe de todo, incluso de eso que pensarías que nadie sabe. Él lo sabe. Agradecida de poder siempre comentar contigo la ciencia, de tener ideas y llevar a cabo experimentos locos. Contigo aprendo cada día. Gracias por todo lo que has hecho en el proyecto del Parkinson y por estar conmigo en todas las reuniones. Cada día que me pasa algo, voy al lab corriendo a

contárselo a Pol, y él siempre tiene un abrazo guardado para mí. Gracias por tanto amor y tanta confianza, amigo, porque sin ti esta experiencia no habría sido ni la mitad de buena.

Gracias por estar presentes en el día de mi vida que más apoyo necesitaba. Os quiero.

Encontrar un grupo como el Malagelada's lab sería imposible, porque formamos el mejor equipo del mundo. Pero dentro de casa hay más grupos que son casi tan guays como el nuestro, y con ellos sigo.

Gracias **Mireia** por ser mi compañera del desahogo, por estar siempre ahí. Cuando yo llegué, Mireia llevaba en la unidad solo dos semanas, y ya parecía que fuera de toda la vida. Es una persona con un brillo especial, con mucho carácter, pero cuando necesitas cualquier cosa es la primera en ofrecerse. Gracias por todos los ratitos juntas, por escucharme, entenderme y aconsejarme. Gracias por nuestras tonterías y por los abrazos. Quiero que sepas que has sido un apoyo fundamental para mí; sin ti, casa no habría sido tan "casa". Ten por seguro que tú tesis va a ser increíble. Por último, quiero recordarte que tengo que ser dama de honor en tu boda.

A **Alazne,** eres sin duda la persona más empática y familiar que conozco. Alazne es esa persona que por fuera se come el mundo, pero por dentro lleva un oso de peluche. Gracias por tu sensibilidad y porque, junto con Mireia, hacéis una dupla muy especial para mí. Gracias por escuchar mis dramas y por apoyarme en todas mis ideas locas. Gracias por apuntarte a todos los planes y por ser tan natural, en definitiva, por darme tu mejor versión en cada momento. Trabajar bajo el mismo techo que tú ha sido un regalo que guardaré para siempre conmigo. Ojalá haberte conocido antes.

A **Esther,** si por alguien tenemos un grupo tan sano y unido es por ti. Esther es esa persona que intenta que todo el mundo sienta que forma parte de algo. Tú te encargabas de acoger a cada una de las personas que llegaban nuevas al lab. Me acuerdo cuando me hiciste el cuestionario el primer día. Tú no lo sabes, pero ayudaste mucho a que me sintiera más cómoda e integrada. No pudimos tener mejor presidenta de la comisión de fiestas. Mi fiel compañera de sitio, te eché mucho de menos cuando te fuiste de la unidad, y sinceramente creo que casa no es lo mismo sin ti. Esther, gracias por echarme un mano cuando lo necesitaba y por hacerme reír. Eres una persona maravillosa, y la vida te traerá seguro, infinitas cosas buenas.

A **Marina**, gracias por todos estos años de compartir historias. Marina es una persona súper sociable, de esas que tienen cientos de amigos, y es que no podría ser de otra manera. Gracias por todos los viajes juntas, por las risas cuando te miro el móvil y te pregunto: ¿con quién hablas? como compi tóxica, por todas tus super fiestas de cumpleaños y por compartir todas nuestras historias como leyendas solteras de la unidad. Sé que vas a triunfar allá donde vayas.

A **Ana,** aunque sea postdoc, ella pertenece 100% al grupo predocs. Gracias, Ana, por toda tu paz y nuestras conversaciones. Ana es esa persona que transmite serenidad allá donde va. Gracias por tener siempre buenos consejos y por ser tan cariñosa.

A **Laura,** desde que llegaste has sido una más. Gracias por abrirte tanto con nosotros y por ser siempre tan alegre. Laura, siempre que llega trae una sonrisa en la cara, y es inevitable que se te acabe pegando. Gracias, Laura, por transmitirme tu amor por la ciencia y tú alegría.

A **Laia,** durante estos años te he cogido un montón de cariño. Laia es un ser de luz, siempre dispuesta ayudar. Gracias Laia, por unirte a los planes

y por transmitirme tanta confianza. Gracias por abrirte tanto conmigo y por ser un lugar seguro donde poder hablar de todo. Eres una persona estupenda.

A **Alba,** recuerdo con mucho cariño los días que pasamos juntas en París cuando fuimos a la FENS. A Alba le cuesta abrirse, pero cuando lo hace, lo hace de corazón. Gracias por todas nuestras confesiones y ratitos por el lab, por esos días en que fuimos juntas a hacer las prácticas de experimentación animal y por hacer lo que yo no quería. Tú tesis irá genial, no lo dudes.

A **Blanca,** gracias por estar siempre tan pendiente de mí. Blanca siempre cuida a los demás. Gracias, Banca, por alimentarme y por intentar controlar mi afición al azúcar. Pero, sobre todo, gracias por estar siempre al tanto de todo, por escucharme y entenderme. Me llevo en el alma grandes recuerdos contigo. Los que te tenemos de amiga tenemos mucha suerte.

A **Lihong**, thanks for all the talks and laughs. Lihong is a very strong woman that has traveled very far to achieve her dreams. Thank you, Lihong for being there for me when I needed it and for the recommendations when I travelled to China. I hope you enjoy your time here.

A **María**, la artista de la unidad, gracias por invitarnos y dejarnos formar parte de ese mundo tan creativo tuyo.

También quiero agradecer a las nuevas incorporaciones: **Gisela**, siempre dispuesta a unirse a cualquier celebración o evento. Te has integrado genial y espero que disfrutes mucho de la unidad. Exprime cada momento. **Josep**, me habría gustado conocerte un poco más, porque creo que eres una persona encantadora. Disfruta mucho de esta etapa. **Andrés,** mi

nuevo compi de mesa, espero que seas muy feliz estos años que te quedan de tesis, y que Barcelona te trate igual de bien que me ha tratado a mí. **Jorge**, solo te conocemos de unos meses, pero ¡vaya fichaje para esta casa!, Tus ganas de vivir son difíciles de superar. Seguro que harás de tu vida algo maravilloso. **Núria**, eres una persona muy especial y súper trabajadora, me habría encantado coincidir contigo más tiempo. Quiero que te quedes con esta frase: al final todo sale bien, solo tienes que creer en ello.

Tengo la suerte de poder decir que durante 3 años he trabajado mano a mano con mis AMIGOS. Sois, sin duda, lo mejor que me llevo de esta experiencia. Os quiero mucho.

La unidad también me ha dado la oportunidad de coincidir con otros IPs. Gracias, **Manolo**, por ser siempre tan cercano con nosotros, por tu sabiduría y por contarnos las mejores historias de dinosaurio de la UB. Ha sido todo un placer compartir estos años. Gracias, **Eulàlia,** por transmitir siempre esa ilusión por la ciencia y por ser una gran jefa de unidad. Gracias, **Pedro, Hugo y Marga**, por pasaros por nuestro lado y darnos conversación, por vuestra simpatía y por vuestra participación en todos los eventos del lab.

No puedo olvidarme de los técnicos de la unidad, especialmente de **Carmen**, ¡Carmencita! Muchas gracias por todo lo que me has ayudado estos años, por todos los cortes de cerebro, por los pedidos, las conversas. Gracias por todo, porque eres la pieza fundamental de la unidad y gracias a ti todo funciona. Y gracias, **Mario,** por estar para arreglar las cosas cuando algo falla.

En el Institut de Neruociències también hay gente estupenda a la que me gustaría agradecer. A nuestros colaboradores, gracias, **Jordi** por ser siempre el que nos rescata cuando la economía no acompaña. Gracias,

Esther, por tu ayuda y generosidad. Gracias, **Lupe**, porque he aprendido mucho contigo de resonancias y por tu buena energía. **Albert**, gracias por enseñarme lo que sé de comportamiento y por tus buenos consejos científicos. A **Mercè** i a **Mar,** gracias por vuestro cariño cada vez que presentaba una comisión.

En la montaña rusa de la tesis, es muy importante tener cerca a gente que te acompañe y te apoye fuera del lab, así que ahora quiero agradecerles a ellos todo lo que me han aportado.

A mi **Familia sagrada: Mica, Coni, Miren, Leyre, Mariatu, Bea, María, Fer, Iñaki y Silvia.** Mica y Coni, gracias por ser mi hogar durante los dos primeros años en esta ciudad. Las tres empezábamos de cero, y habéis sido de mis pilares principales en esta aventura. A los demás, gracias por hacer de mi estancia en Barcelona algo tan especial: por todas nuestras comidas que se alargan hasta la noche, fiestas en el mojito o en cualquier discoteca random de Barcelona, días enteros de playa, días de maratones de pelis en casa, Biergartens, casas rurales… En definitiva, por compartir estos años conmigo. Habéis sido como mi familia aquí, y os estaré eternamente agradecida por la relación tan increíble que tenemos.

A mis chicas **Fritangas de Batukada: Bea, Babeth, Maria Carolina, María, Rosa, Tayrine y Olga** gracias por hacer de cada viernes un ritual, y por pasar noches enteras entre risas e historias en nuestro bar después de batukada. Sois gente estupenda.

I will thank to **Nadja, Sissi and Eleni**, the friends I made during my master in Stockholm, your videocalls have always been a way to disconnect and to remember the good days in Sweden. I miss you so much.

A mis amigas de Tresjuncos, mis **Pinchunches: Miriam, Lydia, Nat y Aroa**, cada vez que voy al pueblo no puedo ser más feliz con vosotras. Gracias por estar siempre disponibles para mí.

A mis dos inseparables de la uni, **Paula y Laura**, por cada almuerzo en la playa poniéndonos al día. Por contarnos todo lo que nos va pasando por el grupo, por hablar casi todas las semanas. Sois magia.

Gracias **a mis tios** y a mi prima **Paula** por vuestro apoyo continuo, vuestro amor infinito y por estar en todos los momentos importantes de mi vida.

Debo dar gracias infinitas a las de siempre, a mi núcleo duro de Valencia, las de toda la vida. **Laura**, ya sabes que eres el mayor apoyo que tengo en la vida, eres la primera persona a la que acudo siempre. Gracias por estar a mi lado en cada paso que doy y por hablarnos todos los días. La nuestra es una relación de 23 años, que sé que durará para siempre. **Mar**, gracias por ser también uno de mis pilares más fuerte, por acudir al momento siempre que te he necesitado, porque te puedo contar cualquier cosa sin sentirme juzgada. Gracias **Cami**, por ser tan divertida y por aguantarme todos estos años, por estar presente en todos los momentos decisivos de mi vida y por contarnos todo. Gracias **Bea** por ayudarme siempre, por los buenos momentos y por venir a verme. Me siento muy orgullosa de ti y sé que vas a conseguir todo lo que te propongas. Gracias, **Isa,** por estar siempre preguntándome como estoy, y por ser la persona que más calma transmite al grupo de locas que somos. Aun estando lejos, os siento cerca. Tengo una suerte enorme de teneros en mi vida. Sois familia.

A **Alex**, una de las últimas incorporaciones a mi vida y la más importante. Gracias, amor, por cuidarme tanto estos meses, por quererme como lo haces. Gracias por hacer que vuelva a creer en el amor, por apoyarme y animarme. Gracias por todos los viajes que haces a Barcelona, por alimentarme y gestionar tú solo todas las tareas, porque yo estaba

escribiendo la tesis. Eres la persona más valiente y alegre que conozco, siempre sacándole el lado positivo a todo. En el mundo hace falta muchísima gente como tú. Espero estar a tu lado toda mi vida.

Y por último los agradecimientos más importantes: allá voy.

A mi **madre**, la más guerrera y luchadora. Solo tú y yo sabemos lo duro que puede golpear la vida. Gracias por apoyarme durante toda mi vida, por dármelo todo y por encargarte, como dices tú, de "enderezar el árbol desde pequeña". Hoy soy la persona que soy gracias a ti y a papá. Sobre todo, y lo más importante gracias por darme todo el amor del mundo. Tengo la suerte de poder decir que me han criado mi madre y mi padre, y me han hecho muy feliz. Gracias, mamá, por no tirar la toalla y sacar una sonrisa siempre para mí. Gracias por tu confianza y por creer en mí.

Gracias, **papá**. Aún no me creo que no estes aquí para vivir este momento, porque sé que a ti en particular sería al que más ilusión le haría vivirlo. Él siempre decía con orgullo "mi hija es científica y está en el Clínic de Barcelona". Espero que ese orgullo perdure para siempre. Gracias, papá, por dármelo todo junto a mamá, por ser tan cariñoso, por quitarme el miedo a abrazar y a decir "te quiero", por ser el que siempre traía el sentido del humor a las situaciones. Espero que, donde estés, seas feliz. Yo te prometo seguir disfrutando de la vida y luchando por lo que quiero y por los que quiero. A ti te dedico esta tesis. Te echo infinitamente de menos.

Gracias Almu, porque como dice la canción: *"no puedes rendirte, hay que alzar el vuelo. Y si te tropiezas, dale un guiño al suelo, porque tú, tú, tú, solo tú sabes bien que puedes llegar a hacerlo".* Gracias por atreverte, aunque te dé miedo.

Gracias a todos. Esta tesis no habría sido posible sin cada uno de vosotros. Y gracias, ciencia, por haberme dado a gente tan maravillosa.

ABSTRACT

The central nervous system (CNS), consisting of the brain and spinal cord, is supported by various cells including neurons, glial cells, and blood vessel cells. Neurons are responsible for transmitting signals, while astrocytes, once considered merely support cells, are now recognized as vital for CNS function. Astrocytes maintain CNS balance, assist in brain defense, and regulate several processes. Historically, astrocytes were first identified in the mid-1800s and develop from radial glia, dividing and transforming into mature astrocytes during brain development. They continue to proliferate in the adult brain but at a low rate.

Astrocytes are critical in maintaining CNS homeostasis, including regulating ions, water, and neurotransmitter levels. They also play a key role in energy supply to neurons by converting glucose into lactate. Moreover, astrocytes are essential for synaptic regulation, promoting synapse formation and stability, and maintaining the blood-brain barrier. Astrocytes also contribute to neurovascular coupling and waste clearance via the glymphatic system, and they are involved in regulating blood flow and oxygen levels. In neuroinflammatory and neurodegenerative diseases, astrocytes can become reactive, leading to dysfunction. In diseases like Alzheimer's and Parkinson's, astrocytes lose their ability to support neurons and remove toxic substances, contributing to disease progression. Astrocyte reactivity is influenced by various signaling pathways, but the mechanisms of their dysregulation remain unclear.

Alzheimer’s disease is the most common form of dementia worldwide, affecting millions of people. It is both sporadic (1%) and hereditary, with age being the higher risk factor. Inherited Alzheimer’s disease is caused by mutations in the APP, PSEN1 or PSEN 2 genes. Having the APOE ε4 gene is the primary genetic risk factor for late-onset Alzheimer’s disease. The disease is characterized by cortical atrophy and enlargement of the ventricles. A central feature of AD is the accumulation of amyloid-β (Aβ)

peptides, derived from amyloid precursor protein, prone to forming plaques. These plaques are linked to cognitive decline, particularly in their oligomeric form. Another hallmark of AD is the formation of neurofibrillary tangles, caused by hyperphosphorylation of tau proteins, which disrupt neuron function and lead to cell death. Neuroinflammation also plays a key role, with microglia and astrocytes contributing to both Aβ clearance and neurodegeneration through inflammatory pathways like the NLRP3 inflammasome, exacerbating synaptic loss and further progression of the disease. AD treatments are divided into symptomatic and disease-modifying categories, although no cure exists yet. Promising new diagnostic biomarkers and therapies focusing on prevention and early intervention represent the future direction of AD management.

RTP801, is a stress-induced protein involved in regulating various cellular processes like metabolism, oxidative stress, autophagy, and cell fate. It plays a role in inflammatory, metabolic, neurodegenerative diseases, and cancer. Its expression is upregulated by stressors like hypoxia, DNA damage, and metabolic imbalances. RTP801 is primarily located in the cytoplasm but also in mitochondria, cell membranes, and the nucleus. A key function of RTP801 is inhibiting the mTOR pathway, which regulates cellular growth and autophagy. Elevated levels of RTP801 are linked to neurodegenerative diseases like Alzheimer's, Parkinson's, and Huntington's, where it suppresses mTOR activity, leading to neuronal damage. Its inhibition in disease models has shown potential therapeutic benefits by preventing cognitive decline and reducing inflammation.

This thesis aims to explore astrocytic RTP801's contribution to neurodegeneration and neuroinflammation in AD using the 5xFAD mouse model and a novel triculture *in vitro* model. The goals include determining its effects on cognitive deficits, neuron morphology,

functional connectivity, neuroinflammatory pathways, and intercellular crosstalk, as well as assessing its role in Aβ clearance.

In the first aim we discovered increased astrocytic RTP801 levels in the hippocampus of 5xFAD mice, which were linked to heightened Aβ toxicity. Behavioral testing demonstrated that silencing astrocytic RTP801 significantly improved cognitive functions in 5xFAD mice while also restoring anxiety-like behavior. Even though Aβ plaque load remained unchanged. On the other hand, Morphological studies of dentate gyrus DGCs cells showed that silencing astrocytic RTP801 reverted DGCs to a healthier phenotype, possibly contributing to improved cognition. Neuroimaging techniques revealed disrupted functional connectivity within the default mode network in 5xFAD mice, which could be restored by astrocytic RTP801 silencing. Altered resting-state networks indicated that astrocytic RTP801 impacts connectivity, essential for cognitive processes in AD. Previous investigations demonstrated that 5xFAD mice exhibited changes in GABAergic signaling, with lower GABA levels correlating with cognitive decline. Here, silencing astrocytic RTP801 mildly restored GABA levels and normalized functional connectivity. A reduction in parvalbumin^{+} interneurons was observed in 5xFAD mice, while astrocytic RTP801 silencing increased their numbers. Increased expression of GAD65/67 in astrocytes suggests compensatory mechanisms for GABA loss due to interneuron degeneration.

Overall, the first aim indicates astrocytic RTP801 as a promising target for AD treatments, linking glial function to cognitive decline. The findings present a new perspective on the role of astrocytes in neurodegeneration, emphasizing the importance of astrocytic RTP801 in therapeutic strategies.

During the second aim we discovered that astrocytic RTP801 has significant implications for neuroinflammation in a context of Alzheimer's disease. In published studies using the 5xFAD mouse model, researchers observed heightened microglial densities in the hippocampus as early as four months of age, with increased astrocyte densities by eighteen months. Investigating astrocytic RTP801 role in neuroinflammation revealed that silencing this protein can alleviate the neuroinflammatory response in these models, reducing the astrogliosis and the microgliosis. Specifically, astrocytic RTP801 was found to increase levels of inflammasome proteins like NLRP3, NLRP1, pro-caspase-1, and ASC. *In vitro* experiments corroborated these findings, indicating that RTP801 tightly regulates NLRP1 levels. However, the correlation between inflammasome components and cytokine levels, assessed via Luminex array, remains unclear. Notably, higher concentrations of osteopontin and macrophage colony-stimulating factor were noted in the 5xFAD mice hippocampus. Nevertheless, silencing RTP801 appeared to partially normalize only CCL3 levels, which is known to impair cognitive functions, indicating the need for further studies to clarify astrocytic RTP801's role in cytokine production. Previous research indicates that RTP801 can activate the NF-κB pathway, suggesting that its silencing may reduce the expression of inflammasome components influenced by NF-κB.

Neuroinflammation might also disrupt the balance between excitatory and inhibitory synapses, exacerbating neuronal damage. The proposed model suggests that neuroinflammation releases cytokines and reactive oxygen species harmful to neurons, particularly sensitive parvalbumin neurons. The findings of hyperconnectivity, reduced GABA levels, and fewer parvalbumin+ neurons in the hippocampus of 5xFAD mice suggest that astrocytic RTP801 suppression might offer protective effects. This silencing could potentially correct neuroinflammatory processes,

contributing to notable memory preservation in the 5xFAD model. Further research is essential to uncover the mechanisms by which astrocytic RTP801 regulates neuroinflammation.

Finally, in the third aim of the thesis we assess the role of RTP801 in an *in vitro* model of Alzheimer's disease using a novel triculture system composed of neurons, astrocytes, and microglia derived from the same animal. Traditional organotypic cultures and animal models of AD often provide limited and inconsistent representations of human AD pathology, sometimes a more controlled *in vitro* environment is needed. The triculture model allows researchers to study intercellular interactions among brain cell types more accurately. Astrocytic RTP801 is linked to morphological changes in reactive astrocytes. The study found no significant changes in astrocyte markers like GFAP after Aβ treatment, but silencing RTP801 reversed the morphological ramifications of astrocytes, indicating astrocytic RTP801 influence on cytoskeletal dynamics. Disruption in astrocytic morphology can impair their neuroprotective functions and contribute to neurotoxicity associated with Aβ oligomers.

Our research demonstrates that knocking out astrocytic RTP801 effectively reduces Aβ oligomer levels, a critical factor in AD progression. Even though *in vivo* experiments showed no significant change in Aβ plaque levels after RTP801 silencing, the complete knock out *in vitro* significantly decreased Aβ oligomers. This suggests RTP801 plays a key role in Aβ clearance. The findings support the idea that targeting RTP801 could be a promising therapeutic approach for AD, opening avenues for further research into its interaction with Aβ clearance pathways. Understanding these pathways will be crucial for developing more effective treatments, especially given the complex nature of AD. Future research should focus on the molecular mechanisms involved and the

long-term effects of RTP801 modulation on cognitive function and disease progression.

TABLE OF CONTENTS

ABBREVIATIONS

5xFAD	5 Familial Alzheimer's Disease
AAIC	Alzheimer's Association International Conference
AAV	Adeno-Associated Virus
Aβ	Amyloid Beta
AD	Alzheimer's Disease
ADAM10	A Disintegrin and Metalloproteinase Domain-Containing Protein 10
AICD	Amyloid Intracellular C-Terminal Domain
Akt	Protein Kinase B
ALDH1	Aldehyde Dehydrogenase 1
ALDOC	Aldolase C
ALS	Amyotrophic Lateral Sclerosis
ANTS	Advanced Normalization Tools
APOE	Apolipoprotein E
APP	Amyloid Precursor Protein
AQ4	Aquaporin 4
ASC	Apoptosis-Associated Speck-Like Protein Containing a CARD
ATF4	Activating Transcription Factor 4
ATP	Adenosine Triphosphate
BACE-1	Beta-Site Amyloid Precursor Protein Cleaving Enzyme 1
BDNF	Brain-Derived Neurotrophic Factor
BSA	Bovine Serum Albumin
C3	Complement Component 3
CA1	Cornu Ammonis

Ca^{2+}	Calcium Ion
CA3	Cornu Ammonis 3
CaMKI	Calcium/Calmodulin-Dependent Protein Kinase I
CDK5	Cyclin-Dependent Kinase 5
CEBP	CCAAT/Enhancer-Binding Protein
CEN	Central Executive Network
CHRM1	Cholinergic Receptor Muscarinic 1
Cl^-	Chloride Ion
c-myc	Cellular Myelocytomatosis Viral Oncogene
CN	Cognitively normal
CNS	Central Nervous System
CTF-α	C-Terminal Fragment Alpha
CUL4A	Cullin 4A
dACC	Dorsal Anterior Cingulate Cortex
DAM	Disease-Associated Microglia
DBS	Dried Blood Spot
DDB1	Damaged DNA-binding Protein 1
DDIT4	DNA Damage-Inducible Transcript 4
DG	Dentate Gyrus
DGC	Dentate Gyrus Granule Cell
DIAD	Dominantly Inherited Alzheimer's Disease
DMN	Default Mode Network
DMSO	Dimethyl Sulfoxide
DSM-5	Diagnostic and Statistical Manual of Mental Disorders, 5th Edition

EAAT1	Excitatory Amino Acid Transporter 1
EAAT2	Excitatory Amino Acid Transporter 2
EC	Entorhinal Cortex
eGFP	Enhanced Green Fluorescent Protein
EIF2α	Eukaryotic Translation Initiation Factor 2 Alpha
ELK-1	ETS Like-1
EPI	Echo Planar Imaging
EV	Extracellular Vesicle
FIC	Functional Imaging Contrast
GABA	Gamma-Aminobutyric Acid
GAD65/67	Glutamate Decarboxylase 65/67
GAP	GTPase-Activating Protein
GFAP	Glial Fibrillary Acidic Protein
GSK3β	Glycogen Synthase Kinase 3 Beta
GYP4	Glycerol-3-Phosphate Dehydrogenase 4
GYP6	Glycerol-3-Phosphate Dehydrogenase 6
HD	Huntington's Disease
HEPES	4-(2-Hydroxyethyl)-1-Piperazineethanesulfonic Acid
HFIP	Hexafluoroisopropanol
HIF-1α	Hypoxia-Inducible Factor 1 Alpha
HLOQ	High Limit of Quantification
HRP	Horseradish Peroxidase
IBA1	Ionized Calcium-Binding Adapter Molecule 1
ICA	Independent Component Analysis

IFN- γ	Interferon Gamma
IL-1β	Interleukin 1 Beta
IL-4	Interleukin 4
IL-6	Interleukin 6
JAK-STAT	Janus Kinase-Signal Transducer and Activator of Transcription Pathway
K^+	Potassium Ion
KIR4.1	Inwardly Rectifying Potassium Channel 4.1
KPI	Kunitz Protease Inhibitor
LLOQ	Lower Limit of Quantification
LOAD	Late-Onset Alzheimer's Disease
LTP	Long-Term Potentiation
LPS	Lipopolysaccharide
LRP1	Low-Density Lipoprotein Receptor-Related Protein 1
MAP2	Microtubule-Associated Protein 2
MAPK	Mitogen-Activated Protein Kinase
MAPS	Multiple-Associative Processing System
MAPT	Microtubule-Associated Protein Tau
MARK	Microtubule Affinity-Regulating Kinase
MCP-1	Monocyte Chemoattractant Protein 1
MCSF	Macrophage Colony-Stimulating Factor
MEGF10	Multiple EGF-Like Domains 10
MERTK	MER Proto-Oncogene Tyrosine Kinase
MFI	Mean Fluorescence Intensity
MGnD	Microglia Neurodegenerative Phenotype

MHtt	Mutant Huntingtin
MIP-1α	Macrophage Inflammatory Protein 1 Alpha
miRNA	microRNA
MMPS	Matrix Metalloproteinase
MOI	Multiplicity of Infection
MOPS	3-(N-Morpholino) Propanesulfonic Acid
mPFC	Medial Prefrontal Cortex
MRI	Magnetic Resonance Imaging
MRS	Magnetic Resonance Spectroscopy
mTORC1	Mechanistic Target of Rapamycin Complex 1
mTORC2	Mechanistic Target of Rapamycin Complex 2
MWM	Morris Water Maze
NAA	N-Acetylaspartate
nAChRs	Nicotinic Acetylcholine Receptor
NaCl	Sodium Chloride
NCD	Neurocognitive Disorder
NEDD4	Neural Precursor Cell Expressed Developmentally Downregulated Protein 4
NF-κB	Nuclear Factor Kappa B
NfL	Neurofilament Light Chain
NFT	Neurofibrillary Tangle
NG2	Neural/Glial Antigen 2
NGS	Next-Generation Sequencing
NH_4Cl	Ammonium Chloride
NKA	Na^+/K^+-ATPase

NLRP1 NOD-, LRR- and Pyrin Domain-Containing Protein 1

NLRP3 NOD-, LRR- and Pyrin Domain-Containing Protein 3

NMDA N-Methyl-D-Aspartate

O/N Overnight

OPN Osteopontin

PAM Proliferative-region-associated microglia

PAPS Perisynaptic astrocyte processes

PBS Phosphate-Buffered Saline

PD Parkinson's Disease

PEG Polyethylene Glycol

PEI Polyethylenimine

PERK PKR-Like Endoplasmic Reticulum Kinase

PET Positron Emission Tomography

PFA Paraformaldehyde

PKA Protein Kinase A

PNN Perineuronal Net

PP2A Protein Phosphatase 2A

PSD95 Postsynaptic Density Protein 95

PSEN1 Presenilin-1

PSEN2 Presenilin-2

PV Parvalbumin

RAGE Receptor for Advanced Glycation End Products

REDD1 Regulated in Development and DNA Damage Responses 1

ROC1 Regulator of Cullins 1

ROS	Reactive Oxygen Species
Rs-fMRI	Resting-State Functional Magnetic Resonance Imaging
RSN	Resting-State Network
RTP801	Regulated in Development and DNA Damage Responses 1
S100β	S100 Calcium-Binding Protein B
SCN	Suprachiasmatic Nucleus
SDS	Sodium Dodecyl Sulfate
SEM	Standard Error of the Mean
SH	Short-hairpin
SN	Substantia Nigra
SNARE	Soluble NSF Attachment Protein Receptor
SPARC	Secreted Protein Acidic and Rich in Cystein
SPARCL1	SPARC-Like Protein 1
STAT3	Signal Transducer and Activator of Transcription 3
SVZ	Subventricular Zone
Thios	Thiosulfates
TLRS	Toll-Like Receptors
TMD	Transmembrane Domain
TNF-α	Tumor Necrosis Factor Alpha
TRCP	Beta-Transducin Repeat-Containing Protein Complex
TKB	Tropomyosin-related kinase B
TSC1	Tuberous Sclerosis Complex 1
TSC2	Tuberous Sclerosis Complex 2
TSP1	Thrombospondin 1

TSP2 Thrombospondin 2

UPS Ubiquitin-Proteasome System

VGLUT Vesicular Glutamate Transporter

WFA Wisteria Floribunda Agglutinin

INTRODUCTION

1. Astrocytes

1.1. Definition and history

The central, peripheral, and autonomic nervous systems are the three components that make up the nervous system. Each of these contains neurons. The autonomic, peripheral, and central nervous systems all have different supporting cells. The brain and spinal cord make up the central nervous system (CNS), which is made up of several cell types that undergo a broad range of changes during pathologic processes. These cells include Neural cells, glial cells (glia, oligodendrocytes, ependymal cells, and microglia), and blood vessel and covering cells (leptomeninges and dura mater). Neurons have long been the most studied cells of the CNS, given their critical role in transmitting signals and processing information. However, astrocytes, once considered just support cells, have gained increasing recognition for their essential functions[1].

Astroglia or astrocytes are brain cells of ectodermal, neuroepithelial origin. They support homeostasis and offer defense for the CNS. With their remarkably adaptable plasticity and very varied structure and function, astrocytes determine the functional maintenance of the central nervous system during development and aging. Moreover, astrocytes are a part of neuronal networks and function in the CNS. They regulate the central nervous system's balance at every level of organization, from the molecular to the organ level[2].

The earliest description of a brain cell that was later identified as a glia was made by Heinrich Müller. He first described the Müller cell, a radial-like glial cell of the retina, in 1851[3] . Some years later, Max Schulze characterized these cells down to the smallest detail[4]. Since then, neuroscientists of the 19th century paid close attention to parenchymal glia, and a plethora of names were given to these cells, as

Bindesubstanzzlelle (binding substance cells) by Otto Deiters in 1865[5], *Leim erfüllten Interstitien* (glue-filled interstitium) in 1867 by Carl Frommann[6] or *Sternförmige Zellen* (star-form cells) by Albert von Kölliker in 1896[7]. However, Camillo Golgi in 1870, was the first to show that glia was a separate cellular population from nerve cells, and he started referring to them as neuroglia **(Figure 1)**. Golgi described glia as spherical cells with many tiny processes extending in all directions, many of which were oriented toward blood arteries. Golgi documented glial networks, detected glial end feet, and characterized a great diversity of glial cells in the brain using the silver-chromate staining technique[8].

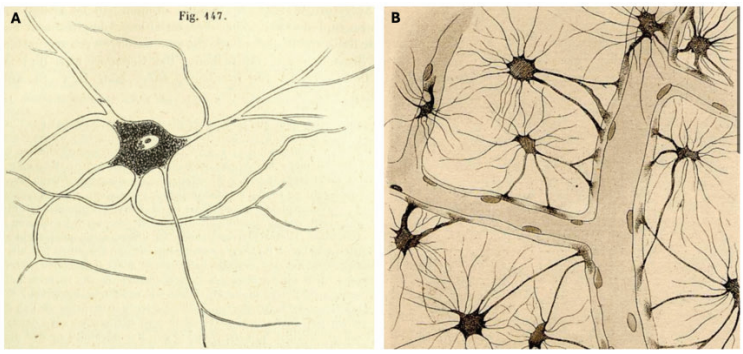

Figure 1. Historic glia drawings. A) Astrocyte drawing from Handbuch der Gewebelehre by Kölliker [7]**.** B) Drawing of astrocytes and blood vessels by Camillo Golgi[8].

Michael von Lenhossék coined the name "astrocyte" (αστρον κψτοσ; astron, star and kytos, a hollow vessel, later cell, i.e., starlike cell) in 1895[9]. Santiago Ramón y Cajal popularized the term "astrocytes" to refer to parenchymal neuroglia. In fact, Cajal created an astroglia-specific gold and mercury chloride-sublimate staining technique that labeled glial fibrillary acidic protein (GFAP). The GFAP staining allowed Cajal to verify that astrocytes originated from radial glia[10].

The first information on the dynamic interactions between neurons and glia emerged after the physiological examination of neuroglia in the late

1950s when these cells were probed using electrophysiological and radiotracer techniques applied to *in situ* and *in vivo* preparations from vertebrates and mammals[11,12]. Jean de Villis created pure neuroglial cell cultures in the late 1980s, enabling direct investigations of astrocyte physiology at the single-cell level[13].

1.2. Astrogliogenesis

Astrocytes are classical neural cells that develop from the neuroepithelium-derived radial glia, the universal neural progenitor[14]. In fact, astrocyte development is not the same as that of neurons because astrocytes not only can arise from glial intermediate progenitors, radial glia that have undergone metamorphosis, but also from differentiated astrocytes that have multiplied, and even Nerve/glial antigen 2 (NG2) glial cells, a kind of glial cells that express a chondroitin sulfate proteoglycan called NG2 **(Figure *2*)**[15].

In the brain development timeline, astrogliogenesis occurs after neurogenesis, since neurogenic factors like neurogenin 1, suppress astrogliogenesis simultaneously. In astrogliogenesis, radial glia divides asymmetrically in the subventricular zone (SVZ), generating intermediate glial progenitor cells that develop to immature proliferative astrocytes. These cells continue to proliferate while migrating across cortical layers[16]. Nevertheless, only a small portion of the astrocytes in the CNS are a result of embryonic astrogliogenesis; in rodents, the number of glial cells rises from approximately 4 million to over 140 million during the second and third postnatal weeks[17]. Indeed, half of the astrocytes present in the CNS are generated by symmetric division of differentiated astrocytes[18]. Furthermore, around 10-15% come from direct transformation of radial glia, which lose their apical processes at birth and reorganize into

protoplasmic astrocytes[19]. Finally, NG2 glial cells are another potential source of astroglia; these cells can produce protoplasmic astrocytes that remain exclusively in the ventral forebrain and do not move to other regions; also, this astrogenic route appears to be limited in time[20,21].

Numerous areas of the adult brain, such as the cerebral cortex, corpus callosum, striatum, hypothalamus, and septum, have been shown to exhibit astrocyte proliferation; nevertheless, the rate of division is extremely low, ranging from 0.05 to 0.45%[22].

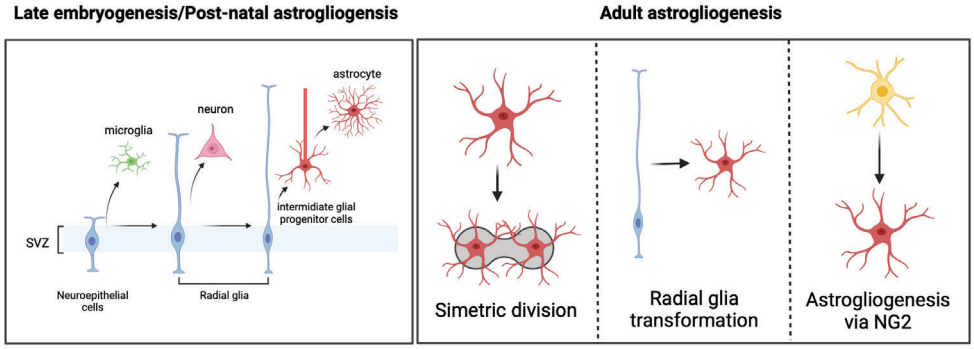

Figure 2. Astrogliogenesis processes in the embryonic and post-natal brain, and into the adulthood. Figure generated with Biorender software.

1.3. Astrocytic markers

It is far from simple to visualize and identify astrocytes, particularly in *in situ* preparations and in the *in vivo* brain. The notable morphological variation and lack of a universal marker, that can identify all cells in the astroglia lineage, provide challenges. Protein markers for astrocytes can be expressed as intracellular, membrane, or secreted components. These include energy metabolism markers, transcription factors, membrane channels and transporters, and structural proteins. They are not all restricted to astrocytes. Crucially, the amount and specific set of markers are highly dependent on the activation phenotype as well as its

physiological state. For the best interpretation of research findings, plural use of markers is highly recommended[23]. Principal astrocytic markers used are depicted in (**Table 1**).

Table 1. Principal astrocytic markers and function.

Marker	Full name	Protein type	Function
GFAP	Glial fibrillary acidic protein	Structural protein	BBB mechanical support
S100β	S100 calcium-binding protein β	Intracellular protein	Ca^{2+}-binding protein
AQ4	Aquaporin 4	Membrane protein	Water homeostasis
EAAT1 (GLAST)	Excitatory amino acid transporter 1	Membrane protein	Glutamate uptake
EAAT2 (GLT1)	Excitatory amino acid transporter 2	Membrane protein	Glutamate uptake
Ezrin	ezrin	Structural protein	Anchors membrane to cytoskeleton
ALDOC	Fructose-biphosphate aldolase C	Intracellular protein	Glycolytic enzyme
ALDH1	Folate enzyme aldehyde dehydrogenase 1 family member L1	Glucose related	Converts NADP to NADPH
C3	Complement component 3	Secreted protein	Upregulated in neuroinflammation
KIR4.1	Potassium inwardly-rectifying channels	Membrane protein	Uptake of K^+

1.4. Types

Since there are numerous cell subpopulations within the class Astroglia that have drastically different morphologies and functions, there has always been disagreement over how to classify and define astrocytic cells based on their shape and functions. However, there is a common classification for mammalian astrocytes which distinguish main different types including protoplasmic astrocytes, fibrous astrocytes, surface-

associated astrocytes, velate astrocytes, pituicytes, gomori astrocytes, perivascular and marginal astrocytes, ependymocytes, choroid plexus cells, and retinal pigment epithelial cells, radial astrocytes.

The major astroglia population in the grey matter are protoplasmic astrocytes, which consist of a round soma with 5-10 primary processes, high arborization and at least one process forms an end feet contact with a blood vessel[24]. On the other side, fibrous astrocytes typical of the white matter are characterized by longer processes and have less and less organized terminal processes than protoplasmic astrocytes[25]. The other types of astrocytes are minor, slightly different and specific of different brain regions; surface-associated astrocytes are in cortical surface with two processes projecting to layer I and surround pial vessels[26]. Velate astrocytes, pituicytes, gomori astrocytes, ependymocytes and retinal pigment epithelial cells belong to olfactory bulb, hypophysis, hypothalamus, ventricles and subretinal space, respectively[27–30]. Whereas perivascular and marginal astrocytes belong to the surrounding of pia mater, and they do not contact neurons[31]. Finally, radial astrocytes are only present in the developing brain.

In higher primates and specifically in human's other astrocyte types are present, including the interlaminar astrocytes present in the cortex and composed of several short processes with only one or two super long processes of around 1 mm long. On the other hand, the polarized astrocytes with one or two long processes are also described in the cortex. Varicose projection astrocytes only exist in human brains and are characterized by different long unbranched processes, which contain equally spaced varicosities[32].

1.5. Functions

In the CNS only neurons have the potential to produce electrical impulses. However, astrocytes have multiple functions which all contribute to CNS homeostasis[33,34]. This section will describe the different astrocytic functions **(Figure 3)**.

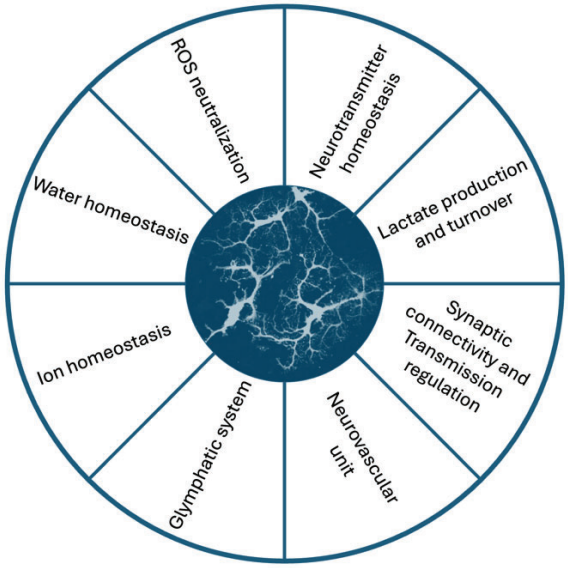

Figure 3. Principal astrocytes physiological functions in the CNS.

Astrocytes are the key for ion homeostasis in the CNS, which is fundamental for the proper functioning of the nervous system. Astrocytes regulate extracellular potassium (K^+) levels through several mechanisms, including energy-dependent pathways mediated by Na^+/K^+-ATPase (NKA), diffusion through K^+ channels, and transport by SLC transporters. These processes help buffer excess K^+ released during neuronal activity, ensuring stable neuronal function[35–37]. Astrocytes also contribute to chloride (Cl^-) homeostasis, particularly during intense GABAergic activity, by releasing Cl^- to sustain inhibitory neurotransmission[38]. Additionally, they help regulate extracellular calcium (Ca^{2+}) and pH levels, both of which are vital for proper synaptic transmission and overall brain

function[39,40]. In this way, astrocytes maintain the delicate ionic balance necessary for CNS stability.

Water homeostasis is also maintained by astrocytes, they regulate it through various pathways, most notably involving aquaporin 4 (AQP4) channels and membrane transporters. Astrocytes also influence extracellular volume, with AQP4 playing a key role. Deleting AQP4 increases extracellular volume and brain water content[41], dynamic changes in extracellular volume during neuronal activity are thought to be due to astroglia swelling from cotransport of water with K+, glutamate, and other molecules through transporters like EAAT1 and GAT-1[42].

Astrocytes are central to neutralize reactive oxygen species (ROS) generated by neuronal metabolism[43]. They are rich in glutathione, a key antioxidant that either directly scavenges ROS or acts as an electron donor for glutathione peroxidase[44]. Astrocytes supply neurons with cysteine and glutamylcysteine, essential for neuronal glutathione synthesis, as neurons have limited capacity to accumulate cystine[45]. Additionally, astrocytes store and regenerate ascorbic acid, releasing it in response to neuronal activity to protect neurons from oxidative damage[46,47]. This protective role is crucial, as it enables neurons to maintain high antioxidant levels, safeguarding them against ROS toxicity.

The brain's neurotransmitter turnover is largely dependent on astrocytes. Astrocytes eliminate and deactivate glutamate[48], Gamma-aminobutyric acid (GABA)[49], adenosine[50], and monoamines[51] via accumulation and metabolic conversion. Moreover, astrocytes generate glutamine, the necessary precursor for neuronal glutamate and GABA[52,53], which are essential for both excitatory and inhibitory neurotransmission.

Astrocytes are vital for brain energy supply by taking up glucose and converting it into lactate, which neurons use for adenosine triphosphate

(ATP) production, particularly during high activity[54,55]. While neurons primarily rely on oxidative metabolism, astrocytes use glycolysis, producing lactate as a byproduct. This supports the astrocyte-neuron lactate shuttle hypothesis, though some evidence suggests neurons also use glucose directly[56]. Additionally, astrocytes store glycogen, to efficiently store glucose, which helps sustain brain activity, especially during increased demand[57]. The precise balance and roles of glucose and lactate between neurons and astrocytes are still being studied.

Astrocytes cover around half of all synapses in the CNS with perisynaptic astroglial processes (PAPs). These processes are essential for synaptic function, expressing glutamate synthetase and transporters, but lacking GFAP and most organelles[58,59]. The extent of astrocyte coverage varies by brain region and synapse type, ranging from 29% to 90%, with more complex synapses generally having higher coverage[60]. The tripartite synapse model describes the close interaction between astrocytes and synaptic structures, recognizing astrocytes as integral components alongside pre- and postsynaptic neurons[61]. Additionally, astrocytes are essential for synapse formation, maturation, and elimination in the brain[62]. They release factors like cholesterol[63] and thrombospondins[64] that promote synaptogenesis and use proteins like hevin and secreted protein acidic and rich in cysteine (SPARC) to regulate it[65]. Astrocytes also stabilize synapses by dynamically covering them, influencing synaptic density and preventing unwanted synapse loss[66]. They play a role in synaptic pruning by tagging synapses for elimination[67] and can directly engulf synapses, especially in early development[68]. Additionally, astrocytes regulate neurotransmitter levels in the synaptic cleft, particularly glutamate and GABA, to maintain synaptic isolation and signaling specificity[69]. Their ability to morphologically adapt and change

synaptic coverage further modulates synaptic transmission and plasticity[70].

The involvement of astrocytes in neurovascular coupling supports the concept of a neurovascular unit, a network of neurons, astrocytes, pericytes and endothelial cells that work together to control cerebral blood flow. This unit ensures precise regulation of blood flow through coordinated signaling among its various components. Astrocytes play a crucial role in regulating local blood flow in the brain through a complex interplay of mechanisms. They release vasoactive agents, which can be converted to vasodilators (e.g., epoxyeicosatrienoic acids)[71] or vasoconstrictors (e.g., 20-hydroxyeicosatetraenoic acid)[72] depending on the context. Astrocytes also release ATP, which can either constrict[73] or dilate blood vessels, influencing vascular tone[74].

The lymphatic system is crucial for the elimination of extra fluid and metabolic waste from peripheral tissues[75]. In the brain, though, there is a well-organized arrangement for the brain's interstitial solute clearance that uses the perivascular space as a fast-moving fluid highway. Astrocytic end feet, which wrap approximately 99% of the vasculature, provide this distinct perivascular space[76]. Moreover, this system relies on astroglial AQP4 water channels and functions similarly to the peripheral lymphatic system. Therefore, this organization was named as the "glymphatic system"[77].

Astrocytes across various brain regions are equipped with oxygen sensors linked to Ca^{2+} signaling. When oxygen levels drop below ~17 mmHg, astrocytes experience increased intracellular Ca^{2+} levels, mediated by mitochondria and ROS. This hypoxia-induced Ca^{2+} signaling leads to the release of ATP from astrocytes, which in turn stimulates neuronal circuits involved in respiration[78].

The suprachiasmatic nuclei (SCN) in the anterior hypothalamus houses the circadian clock, driving rhythmical activity through transcription-translation feedback loops of core clock genes[79]. Astrocytes undergo molecular changes in SCN, with increased glial synaptic coverage at night[80]. Additionally, astrocytes may influence SCN neurons by releasing Tumor necrosis factor α (TNF-α)[81].

The hypothalamus's second most important glucose-sensing cellular population is represented by astrocytes called tanycytes[82]. Tanycyte processes create direct contact with the pituitary portal blood system's fenestrated capillaries, enabling them to examine the blood's molecular composition, which includes hormones and glucose[83].

In conclusion, the wide range of functions performed by astrocytes makes them essential for the proper functioning of the CNS.

1.6. Reactive astrocytes in neuroinflammation and neurodegeneration

Although the underlying processes of neurodegenerative disorders like amyotrophic lateral sclerosis (ALS), Parkinson's disease (PD), and Alzheimer's disease (AD) are still poorly understood, they are known to be drivers of neuroinflammation. Microglia, as well as infiltrating peripheral immune cells, such as T cells, play a major role in mediating the inflammatory response in the CNS. Nevertheless, astrocytes are also important downstream effectors[84].

Astrocytes lose key functions during acute inflammation and chronic neurodegenerative diseases **(Figure 4),** affecting their ability to support and regulate synapses. Typically, astrocytes secrete synaptogenic molecules like SPARC-like 1 (SPARCL1)[85], Thrombospondin 1 (TSP1),

Thrombospondin 2 (TSP2)[86], Glypican 4 (GYP4) and Glypican 6 (GYP6)[87], which are essential for synapse formation. However, these molecules are downregulated in neurotoxic reactive astrocytes, reducing their synaptogenic capacity[88]. The synapse pruning via MER Proto-Oncogene, Tyrosine Kinase (MERTK) and Multiple EGF Like Domains 10 (MEGF10) receptors, which are similarly downregulated in reactive astrocytes, impairs their phagocytic function[89]. This loss of function could lead to developmental issues and exacerbate neurodegenerative diseases by failing to clear debris or toxic proteins like amyloid β (Aβ)[90]. Additionally, astrocytes in a reactive state show impaired glutamate reuptake and recycling, potentially causing excitotoxicity, further contributing to synapse loss and neuronal death[91].

It has been demonstrated that an extensive range of extracellular stimuli, such as inflammation[92], illness[93], and ischaemia[94], can cause an increase or reduction in astrocyte calcium signaling. In a model of β-amyloidopathy, it has been demonstrated that normalization of these calcium transients rescues cognitive impairments[95]. One of the other potentially harmful impacts of astrocytic calcium dysregulation is the release of inflammatory cytokines[96]

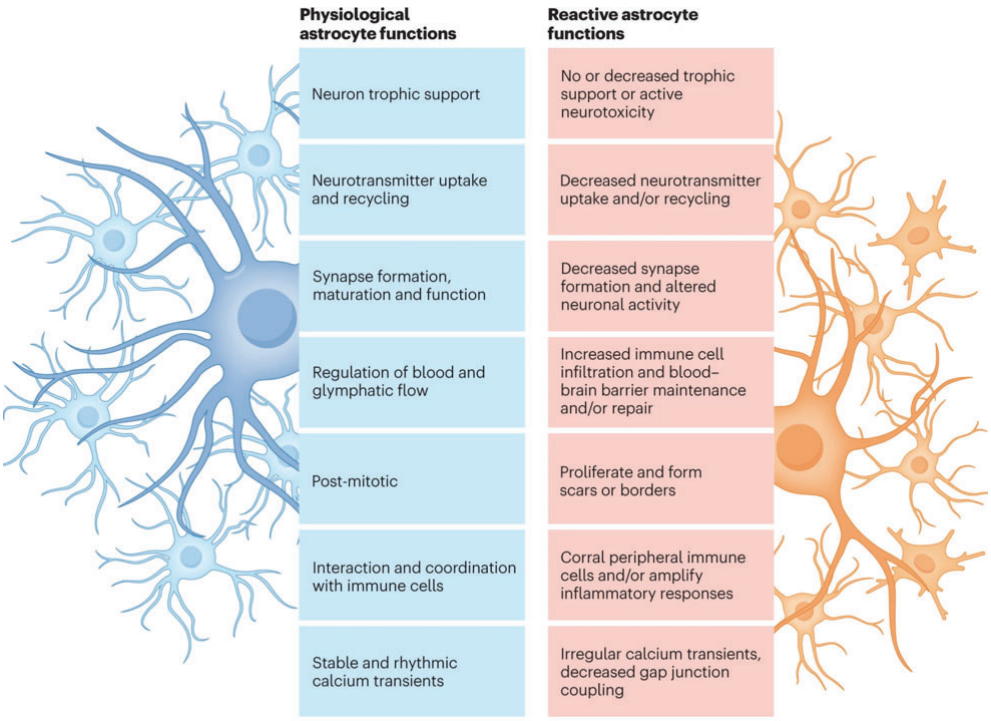

Figure 4. Physiological and reactive astrocyte functions. The right side (orange) displays functional alterations linked to various sub-states of reactive astrocytes, whereas the left (blue) displays the typical physiological functions of astrocytes. Models of inflammation and neurodegenerative disease were used to experimentally characterize the reactive astrocyte functions depicted in the picture. Extracted from Patani et al, 2023[97].

It is not clear if extrinsic signals from nearby cells trigger astrocyte reactivity or if disease-causing or disease-associated mutations drive astrocyte responses. However, in astrocyte models of AD, Huntington disease (HD), and PD, the Janus kinase/signal transducers and activators of transcription (JAK–STAT) pathway is activated downstream of cytokine or growth factor exposure[98]. This pathway is thought to be a key mediator of the production of astrocytic phenotypes, since downstream effects of Signal transducer and activator of transcription 3 (STAT3) activation include upregulation of morphology, migration, and proliferation, as well

as stimulation of GFAP expression and secretion of inflammatory cytokines[99].

Hence, the mechanisms by which astrocytic functions are dysregulated in a pathological scenario are not yet fully elucidated.

2. Alzheimer's disease

2.1. Epidemiology: Incidence and Prevalence

Alzheimer disease is the most common cause of dementia affecting millions of people worldwide[100]. AD is a sporadic and hereditary neurodegenerative disease. An amnestic cognitive impairment characterizes AD's prototypical appearance[101]. The epidemiology of AD and dementia (due to different causes) are linked, even though dementia can also be brought on by other neurodegenerative or cerebrovascular disorders, especially in elderly patients[102,103].

The Alzheimer's disease continuum describes how the disease progresses, from brain changes that are invisible to the affected person to brain changes that result in memory issues and eventually physical incapacity[104]. Individuals spend varying amounts of time in each area of the continuum. Age, genetics, biological sex, and other factors all have an impact on the duration of each segment of the continuum[105]. With age, the proportion of those who have Alzheimer's dementia substantially rises. Alzheimer's disease affects 5% of those in the 65–74 age group, 13.1% of those in the 75–84 age group, and 33.3% of those in the 85–plus age group[106]. People with Dominantly Inherited Alzheimer's (DIAD) are the estimated 1% or fewer of Alzheimer's patients who are affected by mutations in one of three particular genes, the amyloid precursor protein (APP), presenilin 1 (PSEN1) and presenilin 2 (PSEN2) genes **(Table 2)**. Before the age of 65, and perhaps as early as 30, symptoms often start to appear[107]. We see a genetically complex pattern of inheritance for Late onset Alzheimer's disease (LOAD), where lifetime risk for AD is determined by a combination of genetic risk factors, environmental factors, and life exposure events[108]. As a result, identifying novel LOAD loci with reliability is substantially more challenging. So far, the ε4 allele of the

apolipoprotein E gene (APOE) is the sole gene variant that is recognized as a LOAD risk factor[109].

Table 2. Genetic risk factors for early onset Alzheimer disease.

Gene	Protein	Reported mutations	Phenotype
APP	Amyloid β protein precursor	24	Increased $A\beta_{42}/A\beta_{40}$ ratio, Aβ production and aggregation
PSEN1	Presenilin 1	185	Increased $A\beta_{42}/A\beta_{40}$ ratio
PSEN2	Presenilin 2	14	Increased $A\beta_{42}/A\beta_{40}$ ratio

On the other hand, women make up over two thirds of Americans with Alzheimer's disease. 4.1 million of the 6.7 million Americans aged 65 and older who have Alzheimer's disease are female, whereas 2.6 million are male[110]. However, on average, women live longer than males, and the biggest risk factor for Alzheimer's is aging[111].

Eight modifiable risk factors were shown to be linked to roughly 37% of cases of Alzheimer's and other dementias in the United States in 2022, with midlife obesity ranking first among them, followed by physical inactivity and poor educational attainment[112].

Numerous research suggests that in the past 25 years, Alzheimer's and other dementias may have become less common in the United States and other high-income countries[112,113]. However, the total number of people

with dementia is anticipated to rise dramatically because of the rise in the population at the oldest ages, even though these findings suggest that a person's risk of dementia at any given age may be slightly decreasing[114].

The associated changes to dementia incidence and prevalence, both at the population level and within racial/ethnic, socioeconomic, and sex/gender categories, are unknown given the diverse life experiences of prospective older adult populations. Understanding risk factors and resilience in the coming decades will depend more and more on a birth cohort perspective, which considers how a particular group of people has progressed through various life stages[115].

2.2. Diagnosis and Progression

The degree of cognitive impairment can be categorized using a variety of terminologies, ranging from cognitively normal (CN) through dementia. The labels Mild Neurocognitive Disorder (NCD) and Major NCD are used in the Diagnostic and Statistical Manual of Mental Disorders (DSM-5) to define symptomatic conditions[116].

Memory, language, visuospatial function, and executive function are the key cognitive domains that are compromised in AD, and one or more cognitive domains may be impacted at any grade of cognitive impairment. The existence of non-AD illnesses further alters the clinical manifestations of people with AD pathology[117].

The prevalence of amnestic presentations increases with age of onset (>70 years), but non-amnestic presentations are more prevalent in younger people[118]. When cognitive deficits and neuropsychiatric symptoms co-occur, despair, anxiety, and social withdrawal may be the most noticeable symptoms in early dementia, whereas delusions,

hallucinations, emotional dysregulation, or physically aggressive behaviors may be seen in more severe stages[119].

Determining the presence and degree of cognitive impairment is the first step in the diagnostic process, plus a patient's cognitive evaluation by an experienced physician are the pillars of diagnosis. The use of biomarkers can then confirm this provisional diagnosis. At the end, the ability of the clinician to combine data from the informant, the mental status assessment, the neurological examination, and the technology is what makes a diagnosis[120]. There have been significant improvements in imaging and fluid-based diagnostic techniques that provide proof of the pathophysiology underpinning AD[121].

An important factor in delaying the onset of dementia is the timely and early detection of pathophysiological processes linked with AD, such as amyloid and tau pathology and neurodegeneration. It can be recognized utilizing various biomarker modalities [122].

The implementation of a blood test to detect AD patients is necessary. These blood tests will be used as a component of a diagnostic workup alongside other exams; they cannot be used as a stand-alone test to diagnose AD or any other dementia yet. Blood tests are based in the detection of AD biomarkers[123]. Exosomes from nerve cells and glial cells can be secreted into the peripheral blood, mediating intercellular communication and better reflecting the pathological changes in neurological diseases[124]. Some key pathological biomarkers found in AD patients' blood represent amyloid deposition and neurofibrillary tangles (NFTs) (Aβ1-42, P-T181-tau, P-S396-tau, and T-tau)[125]. At the Alzheimer's Association International Conference (AAIC) 2023, a new finger-prick blood test, which can be done at home was presented. Hanna Huber and associates investigated whether it was possible to measure the

biomarkers in dried blood spot (DBS) samples from a finger prick. The biomarkers measured were GFAP, Neurofilament light polypeptide (NfL) and P-T217-tau. The levels of these biomarkers coincided with its levels in plasma samples from the same patients[126].

We are shifting from a patient path that was primarily concerned with diagnosis and post-dementia care to one in which diagnostic biomarkers are increasingly employed for prediction, monitoring, and (preventive) treatment. Information sharing is essential throughout the patient journey and should, whenever possible, be supported by e-tools[121]. The rate of cognitive progression in AD patients is highly variable, according to both ordinary clinical practice and clinical trial experience[127]. Those with less severe cognitive impairment typically undergo a more gradual decline than those with more severe impairment[128].

Note that numerous comorbidities may not be clinically diagnosed in people with cognitive impairment caused by AD, which might increase cognitive dysfunction and performance in everyday tasks. These include pain, hearing loss, vision loss, depression, anxiety, and sleep difficulties[129].

2.3. Pathophysiology and molecular mechanisms

2.3.1. Macroscopic Brain changes

The multimodal association cortices and limbic lobe components exhibit the most pronounced cortical atrophy in the AD brain, which is frequently at least moderate. Primary motor and somatosensory cortices typically appear undamaged, in contrast to the frontal and temporal cortices, which frequently show increased sulcal gaps and atrophy of the gyri[130]. Precuneus and posterior cingulate gyrus atrophy are the most conspicuous examples of atrophy in the posterior cortical areas in AD.

Most affected people have lower brain weight as a result of this atrophy, which also frequently causes the frontal and temporal horns of the lateral ventricles to grow. However, none of the macroscopic characteristics are unique to AD, and clinically healthy individuals without the disease may exhibit significant cortical atrophy[131] **(Figure 5)**.

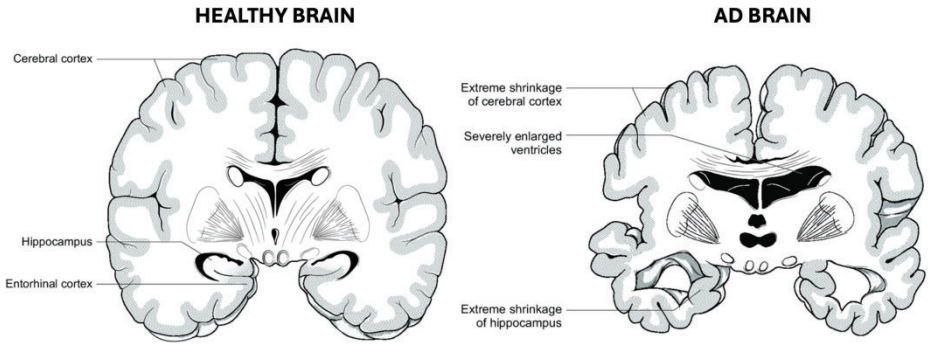

Figure 5. Macroscopic brain changes in AD patients' brains

Even though AD is regarded as a primary gray matter illness, AD patients also exhibit significant secondary alterations in their white matter[132].

2.3.2. Aβ

One of the major hallmarks of AD is the accumulation of Aβ aggregated peptides derived from APP. APP is a single-pass transmembrane protein, composed of a large extracellular domain, a transmembrane domain (TMD) and a small intracellular domain. The extracellular domain is composed of E1 and E2 subdomains with an acidic domain between them. The intracellular domain (AICD) mediates the interaction with several intracellular proteins[133].

The structure and function of APP can be influenced by post-translational modifications like N-glycosylation or O-glycosylation. APP is encoded by a

single gene and the three major isoforms are APP695, APP751 and APP770[134]. However the most expressed isoform in neurons is APP695, it is also the shortest one, because it does not contain the Kunitz protease inhibitor (KPI) and the OX-2 antigen domains.[34]

The APP molecule has several physiological functions and can act as a synaptic adhesion molecule *in vivo* forming dimers. This transmembrane protein can also act as a receptor-like molecule and induce intracellular signaling, as well as induce signaling in other cells by binding to receptors like Death receptor 6 (DR6). Furthermore, APP can also interact with synaptic proteins like soluble NSF-attachment protein receptor (SNARE) and has a role in synaptic plasticity and neuronal differentiation. Moreover, fragments of APP produced by the activity of secretases have also different functions[135].

APP can be processed by different enzymes, along canonical and non-canonical pathways. The canonical pathway can be subdivided into amyloidogenic processing and non-amyloidogenic processing. During the amyloidogenic pathway β-secretase (mainly β-secretase 1 (BACE1)) cleaves the N-terminal of APP generating the APPsβ fragment and CTFβ, the latter is then cleaved by the γ-secretases complex to produce AICD, and Aβ that will form plaques in AD[135]. In the non-amyloidogenic processing, α-secretase (normally ADAM metallopeptidase domain 10 (ADAM10)) cleaves APP in the extracellular domain, in the region that links E2 with the TMD, forming the APPsα and the C-terminal fragments of APP reflecting alpha-secretase processing (CTFα). CTFα, is then cleaved by the γ-secretases complex to form p3 and AICD. However, as α-secretase cleaves in the middle of the sequences of Aβ, no Aβ will be formed from this pathway. However, the p3 fragment is also an amyloid peptide and it also accumulates in the neuritic plaques. Moreover, the role of p3 is still not well characterized[136]. Another difference is that APPsβ (formed in

amyloidogenic pathway) is 16 amino acids sorter than APPsα, eliminating its neuroprotective and neurotrophic effects in comparison to APPsα. Some *in vivo* studies demonstrate that while APPsα improves synaptic activity, facilitating long-term potentiation (LTP), APPsβ do not show any such effect[137] **(Figure 6)**

In both amyloidogenic and non-amyloidogenic pathways, γ-secretase cleavage of the respective CTF can generate AICD, which translocate to the nucleus and regulates gene expression. However, AICD coming from non-amyloidogenic pathway does not contribute to gene expression regulation as it has been suggested that it is rapidly degraded[138]. Some genes directly or indirectly regulated by AICD are cellular myelocytomatosis oncogene (c-myc), p53 andcyclin D1[139].

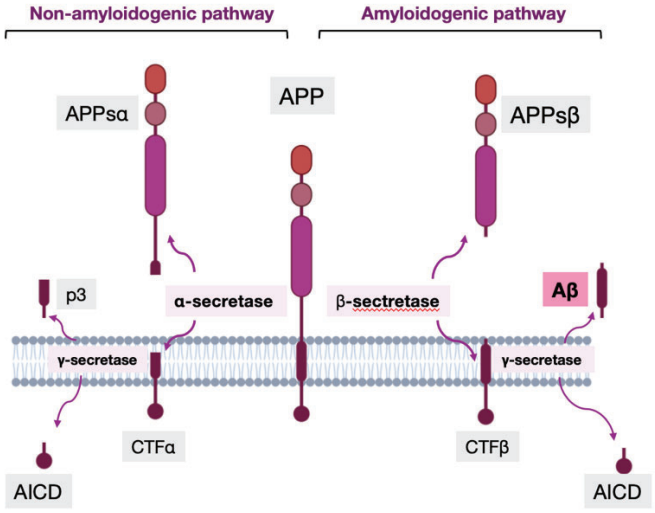

Figure 6. Canonical pathway of APP processing, non-amyloidogenic processing by α-secretase and amyloidogenic processing by β-secretase.

Senile plaques are microscopic abnormalities in the brain's parenchyma that are characterized by an aberrant buildup of protein. They frequently include reactive glial cells and dystrophic neuronal processes. The isoform of Aβ that is most frequently produced by neurons is $Aβ_{40}$; however, $Aβ_{42}$

has two hydrophobic residues at the C-terminus that increase its propensity to self-assemble into plaques. Therefore, compared to $A\beta_{40}$, more plaques exhibit immunoreactivity for $A\beta_{42}$[140]. Moreover, Aβ multimerizes into a variety of oligomeric species that can interact with cells and affect brain function, in addition to plaques. It seems that oligomers are a crucial intermediary step in the assembly of all forms of polymeric amyloid[141]. In fact, the quantity of oligomeric Aβ is more closely correlated with cognitive loss than is the total number of plaques[142].

The prevailing molecular explanation for the abnormal self-assembly and spread of misfolded proteins in the brain is now the prion paradigm. According to the prion paradigm, misfolded proteins rich in β-sheets conformation into oligomeric/polymeric assemblies that can cause other protein molecules of the same kind to take on a similar shape at the molecular level. The proteins in this disease tend to clump together, and the assemblies frequently form amyloid deposits[143].

The progression of amyloid plaques has been divided in 5 phases, called the Thal phases for amyloid deposition, determined by immunostaining of Aβ in brains of post-mortem patients. In the first phase Aβ is found in isocortical regions; after, in phase two, Aβ appears in the limbic regions; during the third phase, plaques occur in basal ganglia; at the fourth phase, amyloid aggregates appear in the forebrain and midbrain; and finally in the fifth phase, medulla oblongata and cerebellum are affected[144].

2.3.3. Neurofibrillary tangles (NFT)

The second major hallmark of AD is the presence of neurofibrillary tangles. Hyperphosphorylated tau proteins aggregate and separate from microtubules to produce NFT, which are twisted threads. The NFT

conform a dynamic neuronal lesion that progresses through three distinct stages in AD: pretangle, mature tangles and ghost tangles[145] **(Figure 7)**

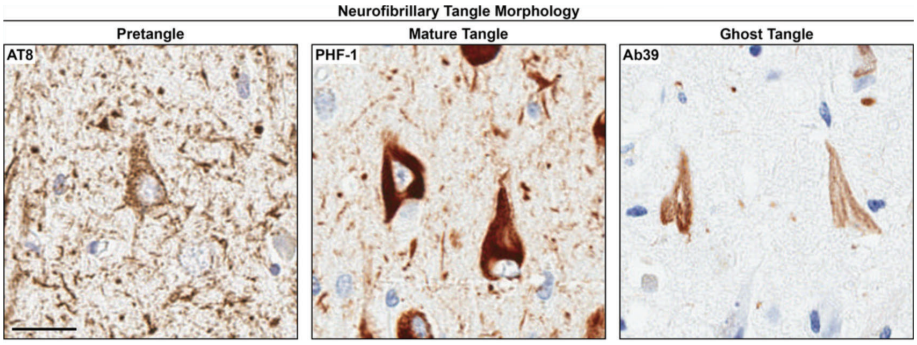

Figure 7. Different stages of the NFT. Pretangles, mature tangles and ghost tangles are shown To distinguish the different stages AT8 marked the pretangles, PHF-1 marked neuritic plaques and Ab39 ghost tangles. Figure modified from Moloney *et al.,* 2021[146].

Tau, a member of the family of microtubule associated proteins (MAPs), is largely found on the axonal tracts of neurons and, to a lesser extent, in glia, which can be either oligodendrocytes or astrocytes[147]. Six distinct Tau protein isoforms result from alternative splicing of the microtubule associated protein Tau (MAPT) gene. A balance between assembly and disassembly is maintained in healthy neurons by Tau function. Recent data suggests that tau has additional roles. For instance, by maintaining β-catenin, tau phosphorylation allows neurons to avoid an abrupt apoptotic death. Additionally, by regulating the anterograde transport by kinesin and the retrograde transport driven by dynein, tau plays a crucial part in maintaining the equilibrium of microtubule-dependent axonal transport of organelles and biomolecules[148].

The proper functioning of Tau is dependent on phosphorylation, which lowers Tau affinity in the microtubules. Hyperphosphorylation, however, may take place in neurodegenerative disorders, resulting in a loss of neurons. Two to three tau residues are phosphorylated in the healthy

brain. However, tau is substantially more phosphorylated in AD and other tauopathies, with about nine phosphates per molecule[149]. Notably, alterations in tau kinase and tau phosphatase expression and/or activation have been well-documented in AD and associated diseases[150]. Glycogen synthase kinase 3β (GSK 3β), cyclin-dependent protein kinase 5 (CDK 5), cAMP-dependent protein kinase (PKA), mitogen-activated protein kinases (MAPK), calcium-calmodulin-dependent kinase II (CaMK II), and microtubule affinity-regulating kinase (MARK) are the key tau kinases[151]. The protein phosphatase 2 (PP2A) enzyme has been linked to the dephosphorylation of aberrant tau more than any other phosphatase[152].

In 1991 Braak and Braak developed the Braak stages of AD that classifies the NFT progression in the brain. It is composed of 6 stages, divided in the Transentorhinal (stages I-II), limbic (stages III-IV) and neocortical stage (stages V-VI)[153].

2.3.4. Neuroinflammation in AD

The healthy brain is an immunologically active organ that is protected by resident immune cells as well as peripheral immune cells that infiltrate[154]. It is now obvious that the adaptive immune system exists under homeostatic settings. Despite their low levels, adaptive immune cells, such as T cells and B cells, which can penetrate the brain meninges and occupy the dura via skull channels. They play critical roles in brain maintenance such as neuronal function, brain development, and spatial learning[155]. Changes in brain-resident (microglia and astrocytes) and peripheral immune cells (neutrophils, monocytes, T cells, and B cells), as well as interaction between innate and adaptive immune cells, have been linked to the development of AD neuropathology[156].

Microglial cells have several roles in the etiology of AD. Microglia has been classified as M1 (pro-inflammatory) or M2 (neuroprotective)[157]. However, single-cell transcriptome and comprehensive proteomic studies have revealed multiple functionally different microglial cell types covering a range of activities in the healthy brain and during AD. This includes disease-associated microglial cells (DAM)[158], microglia neurodegenerative phenotype (MGnD)[159], morphologically activated microglia (PAM), and a slew of unidentified subgroups[160]. The uptake and removal of debris by microglia is crucial for maintaining tissue homeostasis. In fact, microglia phagocytose a range of substrates, including Aβ[161]. Moreover, microglia mediate synapse loss via complement in AD[162], it also worsens tau pathology through the same mechanism[163] . As disease-associated molecular patterns, β-Amyloid plaques and oligomers can activate Toll-like receptors (TLRs) and the NOD-like receptor protein 3 (NRLP3) inflammasome, which causes microglia to produce Tumor necrosis factor α (TNFα), interleukin-1β (IL-1β), and other inflammatory cytokines[164]. The hypothesis that "classical" inflammation exacerbates AD pathogenesis is supported by the findings that genetic deletion of NLRP3, caspase-1, and TLRs ameliorates Aβ accumulation and cognitive deficits in amyloidosis mice models[165–167].

Astrocytes can also exacerbate neurodegeneration by acquiring the reactive phenotype. A1 reactive astrocytes (pro-inflammatory), with high expression of glial fibrillary acidic protein (GFAP), complement C3 (C3), and S100 calcium-binding protein β (S100β) have been identified in AD patients' brains[168]. A1 reactive astrocytes exhibited elevated expression of genes involved in the classical complement cascade, which are linked to synaptic loss[169]. Furthermore, in mice models of AD, A1 reactive astrocytes released proinflammatory cytokines such TNF-α, IL-6, IL-1β, and IL-1α[170].

Matrix metalloproteinases (MMPs) secreted by astrocytes help remodel the extracellular environment and degrade Aβ[171]. Transport proteins like Low density lipoprotein receptor-related protein 1 (LRP1) and Receptor for Advanced Glycation Endproducts (RAGE) play crucial roles in Aβ clearance, but dysregulation can lead to increased Aβ levels and toxicity[172]. Furthermore, astrocytes can transfer tau to nearby neurons through mechanisms like exocytosis and exosome release, further spreading tau pathology[173]. Hyperphosphorylation of tau is partly mediated by astrocytes, with ApoE4 influencing this process via the astrocyte-secreted protein glypican-4[174].

Astrocytic dysfunction may have a substantial impact on glutamate homeostasis. Dysregulation or dysfunction of the excitatory amino acid transporters (EAATs), particularly EAAT2, which is mostly expressed in astrocytes, can result in excitotoxicity, neuronal death, and cognitive impairment[175].

Finally, Astrocytes play a crucial role in cholinergic dysfunction by supporting neurogenesis in the hippocampus through cholinergic receptors like Cholinergic Receptor Muscarinic 1 (CHRM1), mediated by Brain-derived neurotrophic factor (BDNF) signaling[176,177]. In AD, astrocytes' α7 nicotinic acetylcholine receptors (nAChRs) are linked to the regulation of Aβ accumulation. Overexpression of α7 nAChRs in regions like the prefrontal cortex and hippocampus correlates with the formation of Aβ plaques[178]. Dysfunctional astrocytic α7 nAChRs may contribute to Aβ buildup, exacerbating AD progression and cognitive decline[179].

2.4. Treatments

Even though no definitive cure has been found yet, a variety of drugs are available for the treatment of AD decline. These drugs are categorized into two main groups: symptomatic treatments and disease-modifying treatments. Symptomatic treatments are designed to alleviate cognitive symptoms such as memory loss and confusion[180]. Among these, cholinesterase inhibitors, like Donepezil (Aricept), Rivastigmine (Exelon), and Galantamine (Razadyne), work by increasing the levels of acetylcholine, a neurotransmitter critical for memory and judgment. Donepezil is approved for all stages of AD[181], while Rivastigmine[182] and Galantamine[183] are used in mild to moderate stages of the disease. Another class of symptomatic treatments includes NMDA receptor antagonists, such as Memantine (Namenda), which help regulate glutamate, a neurotransmitter that can be excitotoxic in excess[184]. Memantine is approved for moderate to severe AD and is sometimes combined with Donepezil in a combination therapy known as Namzaric, also approved for moderate to severe cases[185].

In addition to these symptomatic treatments, there are disease-modifying therapies that aim to slow the progression of AD by targeting its underlying causes. One of the key focuses of these therapies is on reducing Aβ plaques, a hallmark of AD pathology. Aducanumab (Aduhelm) was the first of these anti-amyloid therapies, controversially approved in 2021 for early-stage AD[186], followed by Lecanemab (Leqembi) in 2023, which also targets Aβ plaques in the early stages of the disease[187]. Donanemab, another anti-amyloid therapy, was also approved in 2023 and specifically targets a modified form of beta-amyloid[188]. While these therapies represent significant advancements, research into anti-tau therapies is ongoing, though no drugs have yet been approved in this category.

Beyond these approved treatments, various experimental and off-label therapies are being explored. Drugs like Bapineuzumab and Solanezumab, continue to be studied in clinical trials. Researchers are also investigating the potential of gene therapies and stem cell treatments, though these remain experimental and are not yet available for general use[189,190].

The medications, often used alongside lifestyle interventions and supportive therapies, form part of a comprehensive approach to managing AD, aiming not only to alleviate symptoms but also to slow the disease's progression[191].

3. RTP801

3.1. Structure and expression regulation

The stress-induced protein known as Regulated in Development and DNA Damage-Response 1 (REDD1), also known as RTP801 or Dig2, regulates several cellular processes, including metabolism, oxidative stress, autophagy, and cell fate. RTP801 also plays a role in the etiology of inflammatory and metabolic diseases, neurodegeneration, and cancer[192].

Low amounts of RTP801 expression are seen ubiquitously[193]. As a protein, RTP801 is an acidic, serine-rich protein with 232 amino acids and a projected molecular weight of 25 kDa[194]. In 2010, a section of human RTP801 was crystallized by Vega-Rubin-de-Celis *et al.*, and the crystal structure included two α-helices and four β-sheets[195] **(Figure 8)**. However, no RTP801/REDD1 enzymatic activity has been reported yet. Although it is predominantly located in the cytoplasm, RTP801 is also present in the mitochondria, the cellular membranes, and the nucleus[196,197]. RTP801 has a variety of biological roles; nevertheless, amino acid sequence analysis has not been able to definitively identify its functional motifs or domains.

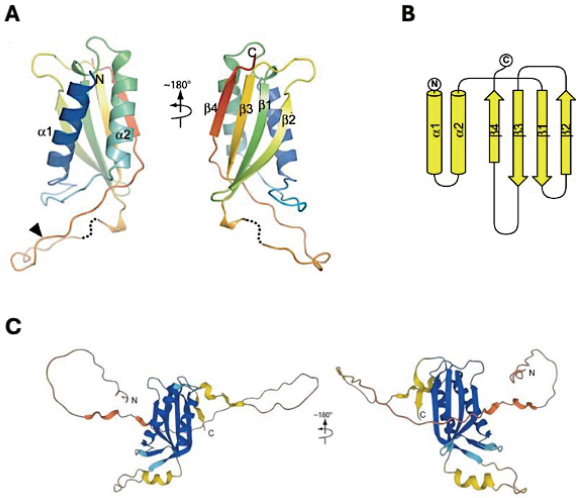

Figure 8. RTP801 protein structure. A) RTP801 crystalized structure from residues 89 to 226. B) Topology diagram. Figure obtained from Vega-Rubin-de-Celis *et al.*, 2019[195], C) RTP801 predicted structure by AlphaFold software.

RTP801 is encoded by the gene called *DNA damage-inducible transcript 4* (*DDIT4*) on chromosome 10[193]. *DDIT4* gene expression is upregulated, not only by cellular stressors such as hypoxia[198], ischemia[199], DNA damage[194] and ROS[197], but also by metabolic imbalances brought on by an excess or shortage of nutrients (e.g., high glucose levels[200] ,amino acid depletion[201] or high free fatty acid levels[202], fasting or starvation[203]. The previous mentioned stressors and metabolic imbalances activate different transcription factors with binding sites at the RTP801 promoter, including p53[194], E-26-like protein 1 (Elk-1), CCAAT enhancer-binding protein (CEBP), hepatic nuclear factor-4, Hypoxia-inducible factor 1-alpha (HIF-1α) and nuclear factor kappa B (NF-κB)[204]. Different expression mechanisms have been described for RTP801, for instance during ER stress or amino acid shortage conditions the double stranded RNA-activated protein kinase-like ER kinase-eukaryotic initiation factor-2α (PERK–eIF-2α) axis activates the stress-induced transcription factor Activating transcription factor 4 (ATF4), which in turn causes RTP801 expression[205]. Furthermore, through their unique nuclear receptors, other hormones like vitamin D and estrogen also promote the expression of RTP801[206]. Inflammatory factors as lipopolysaccharides (LPS) can also upregulate RTP801 expression[207].

Many cell types express low levels of RTP801 protein due to its brief half-life of 5–10 minutes[208]. It is known that the stability of the RTP801 protein is controlled by proteasomal breakdown[209]. A further investigation revealed that glycogen synthase kinase 3 beta (GSK3β) phosphorylates RTP801 at Ser19, Thr23, and Thr25. Subsequently, RTP801 is swiftly degraded by the ubiquitin-mediated degradation pathway, which is facilitated by the Cullin 4A-damage specific DNA binding protein 1- RING-box protein 1- β - Transducin repeat-Containing Protein (CUL4A–DDB1–ROC1–β–TRCP) E3 ligase complex[210]. Indeed, RTP801 is ubiquitinated to

target it for the ubiquitin-proteosome system (UPS) and the endolysosomal system by Parkin[211] and neuronal precursor cell-expressed, developmentally down-regulated gene 4 (NEDD4)[212].

3.2. Function

One of the most popular functions of RTP801 is the inhibition of the mammalian target of rapamycin (mTOR), which is a serine/threonine protein kinase and a major signaling hub that unifies networks involved in cellular metabolism, energy management, and cell development[213]. The mTOR kinase is found in two different complexes, mTORC1 and mTORC2. In addition to promoting the manufacture of lipids, proteins, and nucleotides needed for cell growth and proliferation, mTORC1 suppresses autophagy and lysosome biogenesis to prevent catabolism, which breaks down intracellular bulk proteins and damaged organelles[213]. The mTORC1 has two upstream negative regulators, RTP801 and a complex consisting of Tuberous sclerosis (TSC1) and Tuberous sclerosis (TSC2). RTP801 keeps TSC1/2 active, which suppresses mTORC1 activities. Mostly found in endomembranes, TSC1 forms a complex with TSC2 to stabilize it[214]. On the other hand, TSC2 acts as a GTPase-activating protein (GAP) towards the small GTPase Rheb[215]. RTP801 binds to 14-3-3 proteins and dissociates the inactive TSC2/14-3-3 complex, this preserves GAP activity and inhibits mTORC1 activation. In the endomembrane system, RTP801 colocalizes with TSC2, grows in local concentration in relation to 14-3-3 proteins, and improves its capacity to sequester 14-3-3 proteins, hence blocking the connection between TSC2/14-3-3[198]. Another mechanism for mTOR inhibition via RTP801 is by affecting mTORC2 activity over Protein kinase B (Akt), an upstream regulator of TSC2, through the action of protein phosphatase 2A (PP2A)[216] **(Figure 9)**.

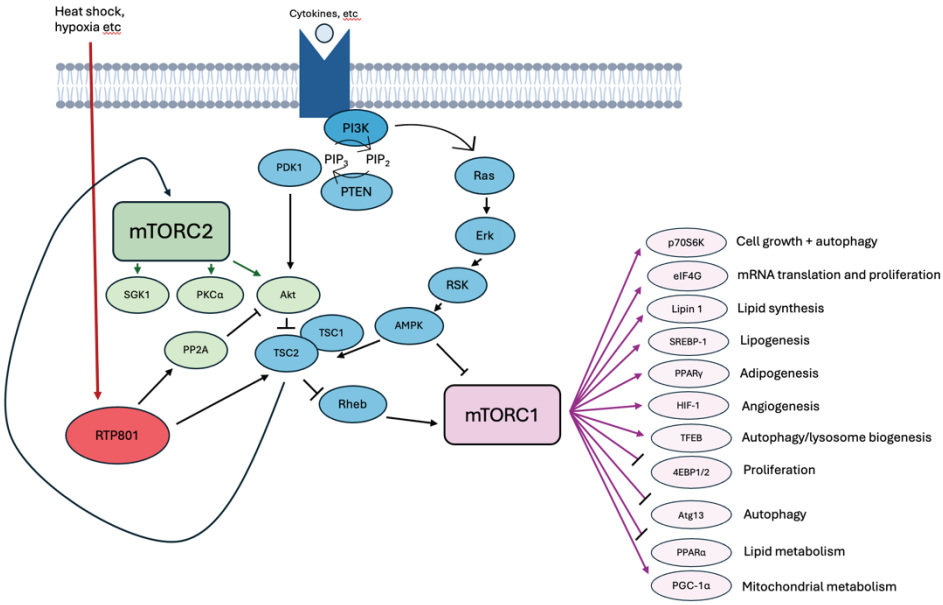

Figure 9. Simplified mTOR pathway and RTP801 function.

RTP801 has a role in developmental neurogenesis and neuron migration, noting its dynamic expression in neuroprogenitors and subsequent decline as neurons mature in the cerebral cortex. *In vitro* studies also reveal an RTP801 upregulation in response to differentiation signals, suggesting a role in neuroprogenitor differentiation. On the other hand, by in-utero electroporation, knocking down RTP801 in the ventricular zone neuroprogenitors forced their cell cycle exit and promoted early neuron migration and differentiation in the developing cortex. On the other hand, RTP801 over expression hinders neuronal differentiation, emphasizing its role as a temporal brake [217].

RTP801 is likely an important risk factor for the development of various diseases, including cancer, muscle atrophy, obesity, osteoarthritis and neurodegenerative diseases, such as Alzheimer's or Parkinson's[192].

In metabolic diseases like obesity, RTP801 stimulates adipogenic differentiation and adipogenesis. RTP801 is enough to cause weight gain

and eventually obesity through aberrant NF-κB activation[218]. In other diseases as skeletal muscle atrophy, glucocorticoids promote protein breakdown and disrupt protein synthesis, which results in muscular atrophy. Skeletal muscle atrophy is associated with RTP801, which in turn promotes anabolic and inhibits catabolic pathways by phosphorylating target substrates[219].

In cultured neurons, RTP801 was either overexpressed or silenced, and the extracellular vesicles (EVs) were characterized. By administering RTP801-EVs to healthy cultured neurons and measuring apoptotic cell death and branching, the toxicity of these EVs was evaluated. RTP801 produced a unique proteomic signature of EVs, with a greater number of pro-apoptotic markers. Via EVs, RTP801-induced toxicity was transmitted to neurons, where it triggered apoptosis and reduced the complexity of neuronal morphology. On the other hand, recipient neurons showed increased arborization in response to shRTP801-EVs. All these findings point to the possibility that RTP801-induced toxicity is spread by EVs and may thus accelerate the development of neurodegenerative disorders[220] **(Figure 10)**.

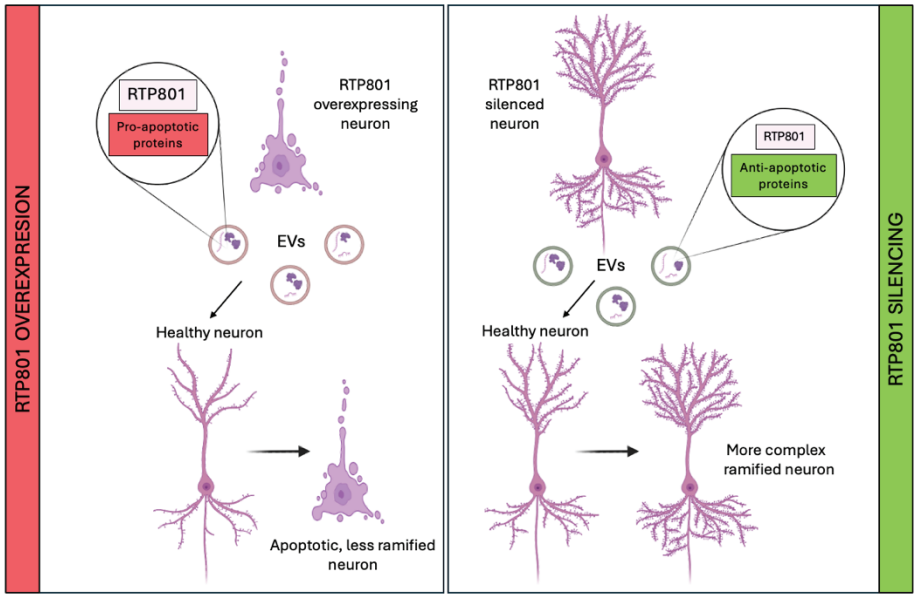

Figure 10. Extracellular vesicles contain RTP801. When neurons overexpress RTP801, the EVs protein cargo is proapoptotic and toxic (left panel) while when RTP801 is silenced in neurons, EVs contain anti-apoptotic proteins and have a trophic function (right panel).

3.3. RTP801 in neurodegenerative diseases

In neurodegenerative diseases RTP801 has been shown to play an important role. In the hippocampal regions of gerbils [221] and in the post-mortem brain tissues of individuals suffering from neurodegenerative diseases such as AD [222] and Parkinson's disease (PD), RTP801 is elevated and suppresses mTOR signaling[223]. RTP801 overexpression in the central nervous system in neuropsychiatric and neurodegenerative diseases may have a deleterious effect on neuronal activity and function. For instance, chronic unpredictable stress exposure increased the expression of RTP801 in the rat prefrontal cortex, as was also seen in patients with major depressive disorder. This, in turn, resulted in a decrease in mTORC1 activation and protein synthesis-dependent synaptogenesis, which in turn

caused synaptic loss, neuronal atrophy, and behaviors resembling those of depression and anxiety[224].

In PD, the specific molecules causing neuron loss are not well understood. One study identified RTP801 as a gene highly induced in PD cellular models and animal models. RTP801 protein levels were elevated in postmortem brains of PD patients, particularly in substantia nigra neurons. Overexpressing RTP801 led to neuron death, and its induction was found to be necessary for cell death in PD models. The mechanism involves the repression of the mTOR and Akt kinase activities[225]. According to this work, a plausible explanation for the early stages of many neurodegenerative diseases could be that cellular stressors that induce RTP801 lead to mTOR depression to maintain neuron viability and function. However, as suggested by the PD research, at more advanced stages, persistent RTP801 overexpression can finally lead to neurodegeneration and neuronal death through mTOR and pro-survival enzyme Akt inactivation[223].

In Huntington Disease (HD), RTP801 mediates mutant huntingtin toxicity and is elevated in human samples. RTP801 was increased in the synapses of cultured neurons by ectopic mutant Huntingtin (mhtt). In both animal models and striatal synapses from HD patients, RTP801 was also upregulated. Impairment to motor learning was avoided in the R6/1 mouse striatum by knocking down RTP801. These findings suggest a potential role for mhtt-induced RTP801 in mediating motor impairment[226]. In another study, gliosis markers and elevated RTP801 levels in the hippocampal regions of HD patients are correlated. Although the expression of RTP801 remains unaltered in the R6/1 mouse model, RTP801 silencing in the hippocampal region ameliorates cognitive deficits, restores synaptic markers, and lowers inflammation, indicating

RTP801 as a possible marker and therapeutic target for hippocampal neuroinflammation associated with HD[227].

RTP801 is elevated in the hippocampus of both human AD patients and murine models of AD, such as 5xFAD and tauopathy. RTP801 levels in postmortem human hippocampal samples correlate with disease progression stages and astrogliosis markers. Inhibition of RTP801 in the 5xFAD mouse hippocampus prevents cognitive decline associated with Aβ deposition and exhibits an anti-inflammatory effect, reducing astrogliosis, microgliosis, and inflammasome sensor proteins. RTP801 elevation is observed in compromised structures of the 5xFAD and tauopathy mouse models, with dysregulation specifically noted in the synaptosomal compartment. Moreover, behavioral testing confirms the rescue of cognitive skills in 5xFAD mice by silencing RTP801 in neurons, suggesting RTP801's role in mediating associative and declarative memory loss. RTP801 is also involved in inflammatory pathways, demonstrating its silencing effect on Tropomyosin-related kinase B (TrkB.T1) and implicating astroglia response in RTP801-dependent cognitive alterations. Genetic RTP801 inhibition in hippocampal neurons shows a general anti-inflammatory response, potentially mediated by downregulating inflammasome receptors and their effector. The study suggests that targeting RTP801 levels, commonly upregulated in neurodegenerative conditions, could be more effective than mTOR modulation, positioning RTP801 as a promising biomarker and pharmacological target for AD[222].

HYPOTHESIS AND AIMS

RTP801, also known as REDD1, is a stress responsive protein that is expressed ubiquitously and presents a wide variety of biological functions. Nevertheless, the full structure and the functional motifs are not yet identified. Indeed, RTP801 does not present any known canonical enzyme activity either. Among the RTP801 physiological functions the most studied one is the negative regulation of mTOR/Akt axis, followed by the NF-κB activation.

RTP801 has been widely studied in different diseases as cancer and muscle atrophy. Nevertheless, RTP801 have also an important role in neurodegenerative diseases including Huntington's, Parkinson's and Alzheimer's where its RNA and protein levels are upregulated. The participation of RTP801 in different diseases is proven, nonetheless the exact underlying mechanisms are still unknown.

AD is a devastating neurodegenerative disease characterized by the presence of Aβ plaques and neurofibrillary tangles which in turn causes neuroinflammation and neuronal death. For more than 100 years of AD research, no cure has been found yet. Investigating the role of RTP801 in AD is crucial to understand its pathophysiology and it approaches us a bit more to an effective treatment.

Although RTP801 is expressed in neurons and astrocytes, all the prior investigations focus on neuronal RTP801, whereas the potential contribution of astrocytic RTP801 to hippocampal pathology and cognitive dysfunction of neurodegenerative diseases such as AD has never been investigated.

We hypothesized that astrocytic RTP801 is contributing to the severity of Alzheimer's disease, exacerbating the cognitive symptoms and neuroinflammation.

Overall, the general objective of this thesis is to **investigate the putative role of astrocytic RTP801 in neurodegeneration and neuroinflammation in Alzheimer's disease.**

AIM I. To investigate the putative role of astrocytic RTP801 in cognitive impairment and neurodegeneration in AD using the 5xFAD mouse model.

1. To evaluate whether RTP801 increases in astrocytes in the AD mice model 5xFAD and whether its genetic normalization in hippocampus prevents cognitive deficits.
2. To study whether astrocytic RTP801 affects hippocampal neurons morphology.
3. To determine whether astrocytic RTP801 changes the functional connectivity, metabolism and neighboring neurons' integrity in the 5xFAD mice model.

AIM II. To investigate the contribution of astrocytic RTP801 in neuroinflammation in the context of AD using the 5xFAD mouse model.

1. To elucidate astrocytic RTP801 influence on astrogliosis and microgliosis.
2. To explore the signaling pathways by which RTP801 mediates neuroinflammation.

AIM III. To identify the neuroinflammatory intercellular crosstalk induced by astrocytic RTP801 using a novel *in vitro* AD model based on primary tricultures of neurons, microglia, and astrocytes.

1. To establish and characterize a new *in vitro* AD model.
2. To determine whether astrocytic RTP801 can influence the neuroinflammatory crosstalk between neurons, microglia and astrocytes.

3. To study the effect of astrocytic RTP801 in the Aβ oligomers clearance.

METHODOLOGY

4. Animals

4.1. *DDIT4*$^{flx/flx}$ mice

For the mice primary tricultures, the hippocampi were obtained from *DDIT4*$^{flx/flx}$ mice (generated by Notini et al.,(2012) and provided by our close collaborator Dr. Florian Britto (Cochin Institute, Paris, France). Briefly, Ozgene Pty Ltd (Canning Vale, W.A., Australia) used the Cre/loxP technique to produce RTP801-deficient mice.

In the DDIT4$^{flx/flx}$ mice , the gene coding for RTP801 is flanked by specific DNA sequences called *loxP* sites. The enzyme Cre recombinase recognizes the *loxP* sites and delete the gene between them.

To knock out the expression of *DDIT4*, the overexpression of Cre recombinase is needed. For our experiments we transduce the primary cultures prepared from the DDIT4$^{flx/flx}$ mice with adenoassociated viral particles (AAV) containing the Cre recombinase gene construct under a GFAP promoter. The Cre recombinase recognizes the *LoxP* sequences, cleave them and then the *DDIT4* gene fragment is eliminated. As a result, a knockout for RTP801 is generated in a cell specific manner.

4.2. 5xFAD mice model of AD

The transgenic mouse line 5xFAD (MMRRC catalog #034840-JAX, RRID:MMRRC_034840-JAX) was utilized in this study as an AD mouse model. The 695-amino acid isoform of the human amyloid precursor protein (APP695), which carries the Swedish, London, and Florida mutations and is overexpressed in 5xFAD mice, is controlled by the murine Thy-1 promoter. Additionally, human presenilin-1 (PSEN-1)

carrying the M146L/ L286V mutation is also overexpressed in these mice. The animals were all six months old and male. The animals were housed at 19-22º and 40-60% humidity, with food and water in a colony room. Animals were under a 12:12 h light/dark cycle. The ethical guidelines (Declaration of Helsinki and NIH Publication no. 85-23, revised 1985, European Community Guidelines, and Spanish guidelines (RD53/2013) for handling animals and approved by the local ethical committee (University of Barcelona, 225/17 and Generalitat de Catalunya, 404/18) were followed.

The 5xFAD model of AD shows Aβ plaques at 2 months old[228] and hyperphosphorylation of Tau protein[229]. At 2-4 months the gliosis associated to the amyloid pathology can be detected[230]. The model also presents a decline in the neurogenesis[231]. This model also presents significant early caspase-3 activation and at 9 months old shows neuronal loss[232]. Lower levels of synaptic markers have also been detected as well as alterations in synaptic transmission[233] . Importantly 5xFAD mice model show cognitive impairment at 6-month-old[234,235] (**Figure 11).**

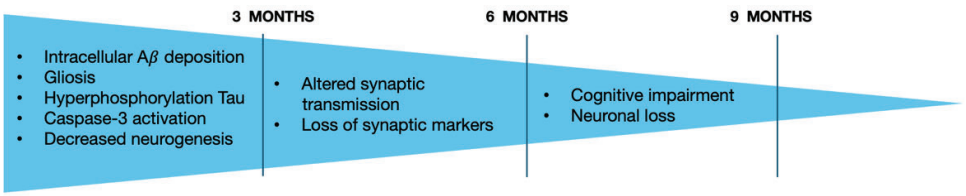

Figure 11. Alterations found in the 5xFAD mouse model of AD. The alterations start as soon as 1 month old with early intracellular Aβ deposition, micro and astrogliosis, hyperphosphorylation of Tau protein, caspase-3 activation and decreased neurogenesis. After 3 months mice shown altered synaptic transmission and loss of synaptic markers. Later at 6 months old the cognitive impairment starts and the neuronal loss.

5. Cell cultures

5.1. Rat primary hippocampal cultures

Rat primary hippocampal cultures from embryonic day 18 (E18) Sprague-Dawley rats (Envigo) were prepared by dissecting out the hippocampi, as previously described[236]. The hippocampi were digested for 15 minutes with 0,05 % trypsin (Thermo Fisher Scientific). Following the digestion, the tissue was mechanically dissociated with rounded-end glass pipettes. Previously to the cell culture 12 mm coverslips were coated with 0.25 mg/ml poly-L-lysine (Sigma). Following mechanically dissociation of the embryonic hippocampus cells were count and 300 cells/mm2 were seeded.

During the first hour cells were cultured with MEM medium supplemented with 10% Horse serum. Afterwards, cultures were maintained in Neurobasal medium supplemented with B27 (1:50), 2mM GlutaMAX and penicillin/streptomycin (all the media and supplements from Thermo Fisher Scientific).

Every 7 days one third of the medium was replaced by new media. Rat primary hippocampal cultures were maintained in a 5% CO_2 atmosphere at 37ºC. The neurons were used for experiments at DIV14.

5.2. Mice primary hippocampal triculture

One day before starting the triculture protocol all the media and plate coating was prepared. For the coverslip coating poly-L-lysine was diluted in a prepared B buffer containing boric acid 3,1 g/L and Borax 4,75 g/L. Final concentration of Poly-L-lysine of 0,5 mg/mL. The plates were

washed four times with Mili-Q water prior cell plating, after the last wash Mili-Q water was replaced with 500 µL of plating media, containing Neurobasal A, 0,1% Horse serum, 0,02% of B27, 0,02% of 1M HEPES pH =7,5 and 0,01% of GlutaMAX

The hippocampi of postnatal day 1 or 2 (P1-P2) were dissected and digested equally to previously described in the rat primary hippocampal culture. After the enzymatic digestion with the 0,05% trypsin the tissue was washed twice with plating media following a mechanical dissociation with the rounded-end glass pipettes. Cells were counted and seeded in a p24 at a density of 421 cells/mm^2 or 263 cells/mm^2.

After four hours growing the plating media was changed by the growth media, containing Neurobasal A with 0,02% B27, 0,01% GlutaMAX, 0,001% IL-34, 0,0005% TGF- β and 0,001% cholesterol (all the media and supplements were from Thermo Fisher Scientific). After 3 days, 500µL of new triculture growth media was added at DIV7, 500µL of the medium were replaced with new 500µL of new growth media. Half of the media was changed every 4 days. Cultures were maintained in a 5% CO_2 atmosphere at 37ºC. The tricultures were used for experiments at DIV 13-14.

6. Cell Culture treatments

6.1. Aβ oligomer preparation and culture treatment

The lyophilized $A\beta_{1-42}$ (Abcam) was re-suspended under the fume hood in ice cold 100% 1,1,1,3,3,3-Hexafluoro-2-propanol (HFIP) until obtaining a 1mM solution with a GasTight Hamilton syringe (Teknorama). Following

the resuspension the solution was aliquoted and concentrated under a SpeedVac centrifuge (800 g, maximum 25ºC). The aliquots were stored at -80ºC until 48 hours before treatment. $A\beta_{1-42}$ film as resuspended by adding DMSO up to 5mM $A\beta_{1-42}$. the mixture was sonicated in the water bath at room temperature for 10 minutes to ensure complete resuspension. Afterwards, the oligomers were prepared by diluting them in PBS with 2%SDS at a concentration of 400µM and then incubated for 24 hours at 37ºC. The following day the oligomers were diluted again only in PBS to a final concentration of 100µM and incubated for 18 hours at 37ºC. At treatment day the oligomers were added to the media until reach a concentration of 0,5 µM for the triculture or 1 µm to the glial culture for 24 hours **(Figure 12)**.

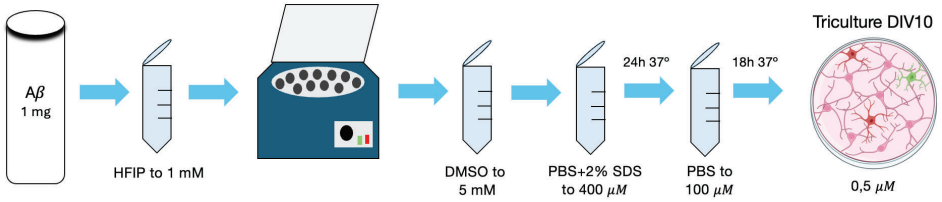

Figure 12. Protocol for $A\beta_{1-42}$ oligomerization for cell culture treatment. Astrocytes were treated at day 7 with 1µM of $A\beta_{1-42}$ oligomers and tricultures were treated with 0,5 µM of $A\beta_{1-42}$ oligomers.

6.2. Plasmid description

The plasmid constructs used in this thesis and their specifications are listed below **(Table 3)**. The plasmid sequences used for over expressing or knocking down RTP801 were previously validated in Malagelada *et al.* (2006). For the lentiviral production the plasmids used were pCMV-VSV-G (envelope vector) and pCMV-dR8.2 dvpr (packaging vector) (Addgene).

For the *in vitro* astrocytic infection of primary tricultures and glial cultures AAVs with serotype 5 (rAVV5) were used. This serotype is preferred to infect astrocytes. For the *in vivo* experiments the plasmids packed in AAV with serotype 2 and 5 (rAVV2/5) were used for the same reasons. Furthermore, for the *in vivo* experiments the construct were packed into a miRNA instead of a shRNA because of the GFAP promoter plus the sequence to target DDIT4 transcript was to big.

Table 3. List of plasmids used. CMV = Cytomegalovirus; sh = short hairpin; HIV1 = Human immunodeficiency virus 1; UBC=Ubiquitin-C.

Empty vector	Promoter	Resistance	Reporter	Construct	Source
pLL3.7	U6	Ampicillin	CMV-eGFP	pLL3.7-shCT	Addgene
				pLL3.7-shRTP801	
FUGwm	CMV-HIV1	Ampicillin	UBC-eGFP	FUGWm-eGFP	Provided by Dr. Clarissa Waites
				FUGWm-eGFP-RTP801	
rAAV2/5	GFAP	Ampicillin	eGFP	rAAV2/5-GFAP-miCT	Viral vector production Unit
				rAAV2/5-GFAP-miRTP801	
rAAV5	GFAP	Ampicillin	eGFP	rAAV5-GFAP-eGFP	University of North Carolina-Vector Core
				rAAV5-GFAP-GFP-Cre	

6.3. Bacterial transformation and DNA plasmid amplification

Escherichia coli DH5α competent cells were used to amplify DNA plasmids for posterior cell culture lentiviral infection. The DNA vector and E.coli were mixed and exposed to 40ºC for 30 seconds. The mix was then

placed at 4ºC for 5 minutes. Next the mixture was diluted in S.O.C media (thermos Fisher Scientific) and kept at 37ºC for 1 hour. Afterwards the transformed bacteria were seeded on lysogeny broth agar (LB agar Sigma) plates containing 100μg/ml ampicillin (Thermo Fisher Scientific) and incubated overnight (O/N) at 37ºC.

A single colony containing the plasmids of interest was grown in Terrific Broth medium supplemented with 100 μg/ml ampicillin (Thermo Fisher Scientific) at 200 rpm until reaching saturation. The plasmid was isolated using the commercial kit HiPure Plasmid Filter Midiprep Kit (Thermo Fisher Scientific). Finally, the DNA concentration was measured with NanoDrop™ One Microvolume UV-VIS Spectrophotometer (Thermo Fisher Scientific).

6.4. Lentiviral preparation

Lentiviral particles were prepared using HEK293T cells at a confluency of 80% in P100 plates. The cell line cultures were transfected with polyethyleneimine (PEI) (Cliniscience). PEI in 1xPBS was mix with the following DNA vectors, previously prepared (ratio 1:4): pCMV-VSV-G, pCMV-dR8.2 dvpr, and the target vector (PLL 3.7 – shCT, pLL3.7-shRTP801, pCMS-eGFP or pCMS-eGFP-RTP801). The mix was incubated at room temperature for 20 minutes. After the mentioned time HEK293T were transfected with the mix. Three days later, lentiviruses were purified from the cell medium by the polyethylene glycol (PEG) precipitation. The media was collected and centrifuged for 5 minutes at 5000 x g to remove cell debris. The supernatant was then incubated 90 minutes at 4ºC with a mix of 8,5% PEG 6000 and 0.5 M NaCl, it was mixed every 20 minutes. The

mix was centrifuged at 7.500 x g for 15 minutes in a SS-34 fixed angle rotor in a Sorvall R5-5C Superspeed Centrifuge. Finally, the pellet was resuspended with PBS-Ca^{2+}/Mg^{2+} and stored at -80ºC. Transduction of several viral dilutions was used to assess viral titer.

7. Protein expression in cell cultures

7.1. Lentiviral transduction: RTP801 knock down

Rat primary hippocampal neurons and astrocytes were transduced at DIV 7 with lentiviral particles containing the shRNA vector against RTP801(pLL3.7-shRTP801) or the scrambled control sequence (pLL3.7-shCt) or at DIV 12 with the lentiviral particles containing the eGFP or eGFP-RTP801 constructs. Using a MOI of 100.000 and for 4 days.

7.2. Adenoviral transduction: RTP801 knock out

Mice tricultures of neurons, astrocytes and microglia and glial cultures were transduced at DIV10 or DIV 7 respectively with the Adeno-associated viral particles containing the constructs (rAAV5-GFAP-eGFP or rAAV5-GFAP-GFP-Cre). The cultures were infected at a MOI of 100.000 viral units /cell. Cre recombinase was expressed for 5 days.

8. Immunocytochemistry staining

Primary cultures were fixed with 4% paraformaldehyde (PFA) (Santa Cruz) followed by a permeabilization step using 0,25% Triton X-100 (Sigma-Aldrich) for 5 minutes. The blocking was carried out with Superblock™ PBS Blocking Buffer (Thermo Fisher Scientific) for 20 minutes. Primary antibodies diluted in Superblock-PBS were incubated

shaking and at 4°C O/N. Primary antibodies information is listed in the table below **(Table 4)**.

Following the primary antibodies incubation, cells were washed three times with 1xPBS and incubated with the secondary antibodies **(Table 4)** and Hoechst 33342, to visualize the nuclei, diluted in SuperBlock-PBS for 2 hours at RT. Coverslips were mounted with ProLong® Gold Antifade Mountant (Thermo Fisher Scientific).

Table 4. Primary and secondary antibodies used for immunofluorescence of cultured cells.

Antibody	Host Specie	Dilution	Source
GFP	Chicken pAb	1:1000	Synaptic systems (#132006)
GFP	Rabbit mAb (D5.1)	1:500	CST (#2956)
GFAP	Mouse mAb (G-A-5)	1:500	Sigma (#G3893)
GFAP	Rabbit pAb	1:500	Proteintech (#16825-1-AP)
RTP801	Chicken mAb	1:200	Davids Biotechnologie, GE. (specially customized for us)
NLRP1	Rabbit pAb	1:500	Proteintech (#2981)
MAP2	Mouse mAb [AP-2]	1:500	Abcam (#ab11268)
Iba1	Goat pAb	1:500	Abcam (#ab5076)
Aβ	Mouse mAb (NT78)	1:500	Synaptic system (#218 111)
S100β	Rabbit pAb	1:500	Proteintech (#15146-1-AP)
Parvalbumin	Rabbit	1:500	Proteintech
PSD95	Mouse mAb(6C6-1C9)	1:500	Thermo Fisher (#MA1-045)
VGLUT	Rabbit pAb	1:500	Synaptic system (#135303)
AlexaFluor488 anti chicken IgG	Donkey polyclonal	1:500	Jackson Immunoresearch (#703-545-155)

AlexaFluor 555 anti rabbit IgG	Donkey polyclonal	1:500	Thermo Fisher Scientific (#A31572)
AlexaFluor 647 Anti rabbit IgG	Donkey polyclonal	1:500	Thermo Fisher Scientific
AlexaFluor 647 anti mouse IgG	Donkey polyclonal	1:500	Thermo Fisher Scientific (#A31571)
AlexaFluor 488 Anti goat IgG	Donkey polyclonal	1:500	Thermo Fisher Scientific (#A11055)
AlexaFluor 488 anti rabbit IgG	Goat polyclonal	1:500	Thermo Fisher Scientific (#A11070)
AlexaFluor 647 anti mouse IgG	Goat polyclonal	1:500	Thermo Fisher Scientific (#A21237)
AlexaFluor 488 Anti mouse IgG	Goat polyclonal	1:500	Thermo Fisher Scientific (#A11017)
AlexaFluor 555 anti chicken IgG	Goat polyclonal	1:500	Thermo Fisher Scientific (#A32932)
AlexaFluor 488 anti chicken IgY	Goat polyclonal	1:500	Thermo Fisher Scientific (#A11039)

9. Hippocampal injection of adeno-associated viral particles in 5xFAD mice

6-month 5xFAD animals were anesthetized with a mixture of 2% oxygen and isoflurane (2% induction, 1’5% maintenance), after that, we performed bilateral hippocampal injections of rAAV2/5-GFAP-miRNA-CONTROL-GFP and rAAV2/5-GFAP-miRNA-RTP801-GFP sequences under the GFAP promoter, expressing GFP and packed in AAV serotypes 2/5. To achieve widespread hippocampal AAV transduction, stereotaxic surgery was performed using the following coordinates (millimeters) from

Bregma (anteroposterior and lateral) and from the skull (dorsoventral); anteroposterior: −2.0; Lateral +/−1.5, and dorsoventral: −1.3 (CA1) and −2.1 (DG) **(Figure 13)**. We delivered 1ul of 1:1 Virus in each depth for 4 minutes, followed by 2 minutes to complete virus diffusion. Mice had 2 hours of carefully monitoring after surgery and were returned to their home cage. Total recovery took place in 1 month before starting the behavioral tests.

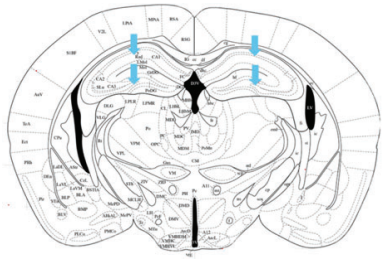

Figure 13. Specific brain coordinates for hippocampal injection of adeno-associated viral particles. rAVV2/5 were bilaterally injected to knock down RTP801 or control in CA1 and DG.

10. Behavioral assessment

10.1. Plus maze

To evaluate the anxiety level of the animal, mice were placed at the Plus maze for 5 minutes. The maze is composed of two opposing 30 x 8 cm open arms, and two opposing 30 x 8 cm arms enclosed by 15 cm-high walls. The apparatus was placed 50 cm above the floor and dimly lit (60 lx).

10.2. Morris water maze

To evaluate the spatial memory, mice were placed at the Morris water maze (MWM). The water maze test was performed in a circular pool of

100 diameter and 40 cm high, with a water depth of 25 cm. the first day to discard visual or physical deficiencies each animals underwent four trials without any distal cue and with a visible platform. The following phase (learning/acquisition phase) last 6 more days, including a four trials per day. The pool had four positions north (N), south (S), east (E) and west (W), where the visual cues were adapted (round, star, square and triangle). The platform was then submerged 1 cm below the water and placed in a midpoint between two coordinates. Time and distance to arrive to the platform in each trial was measured.

11. MRS and resting-state fMRI acquisition

Mice were scanned, on a 7.0T BioSpec 70/30 horizontal animal scanner (Bruker BioSpin, Ettlingen, Germany) with an actively shielded gradient system (400 mT/m, 12 cm inner diameter). Each animal underwent magnetic resonance spectrometry acquisition (MRS) to determine the concentration of metabolites. Afterwards, functional magnetic resonance imaging (rs-fMRI) was used to assess functional brain connectivity. Thus, mice were fastened using tooth and ear bars, adhesive tape, in prone position in a Plexiglas holder. A combination of medetomidine (bolus of 0.3 mg/kg, 0.6 mg/kg/h infusion) and influsiorane (0.5%) was used to sedate the animals using a nose cone in the holder.

The head was precisely positioned at the magnet's isocenter using 3D-localizer images. Reference T2-weighted images were acquired in axial, coronal and sagittal orientations to accurately position the MRS voxel in the hippocampus (voxel size 5.4 uL). MRS was acquired with PRESS localization (TE = 12 ms, TR = 5000 ms) using local 1st and 2nd order

shimming (MapShim) performed in the voxel, followed by a reference water spectrum acquired with 8 repetitions, to ensure a peak full width at half-maximum ≤ 12 Hz; then, MRS was acquired with 256 repetitions and VAPOR water suppression, adjusted to keep the water peak amplitude 30–50% higher than the upfield metabolite peaks.

Rs-fMRI acquisition was performed using an Echo Planar Imaging (EPI) sequence with TR = 2 s, TE = 19.4, voxel size 0.21 0.21 mm2, and slice thickness 0.5 mm. 420 volumes were acquired, and the total scan time was 14min.

12. Rs-fMRI processing and analysis

The resting-state fMRI acquisition was processed to extract functional brain networks by independent component analysis (ICA) and evaluate differences between experimental groups as described previously[237]. Each fMRI acquisition was pre-processed including slice timing, motion correction, pass-band frequency filtering, spatial normalization to a mice brain atlas template and smoothing (ANTs and Python 3). All the pre-processed images were considered to extract the group ICA using FSL MELODIC. The resulting ICs were compared with the functional networks described in Grandjean et al 2020[238] .to identify the components corresponding to functional networks of interest. Afterwards, dual regression was performed to identify voxel-wise differences by using fsl-randomize, that performs non-parametric permutation test including family-wise error correction on neuroimaging data[239].

13. Histology staining techniques

13.1. Fluorescence immunohistochemistry

After the behavioral and MRI assessment, animals were euthanized by cervical dislocation. Left hemispheres where isolated and fixed for 1 day in 4% paraformaldehyde in PBS. Free-floating coronal brain sections of 40 µm were obtained using a cryostat (Leica CM1950).

For the immunofluorescence experiments, brain sections were washed twice in PBS-T (1xPBS 0.3% Triton X-100) and incubated in 50 mM NH_4Cl for 30 minutes. For the blocking and permeabilization PBS-T with 3% NGS and 0.2 % BSA was used for 1 hour. For amyloid plaque staining a 4-hour blocking was performed, the blocking buffer in this case was PBS 0.25% Triton X-100 with 10% donkey serum. Primary antibodies were diluted in blocking solution. Slices with primary antibodies were incubated at 4ºC in agitation overnight. Brain sections were washed with PBST-T and incubated with secondary antibodies diluted in blocking solution for 2 hours at room temperature. Finally, Hoechst33342 (Thermo Fisher Scientific, #H3570) 1:5000 in PBS was added to stain the nuclei, for 15 minutes. Sections were washed with PBS-T and mounted with ProLong Gold Antifade Mountant. The antibodies used are listed below **(Table 5)**.

Table 5. Primary and secondary antibodies used for fluorescence immunohistochemistry.

Antibody	Host species	Dilution	Source
GFP	Rabbit mAb (D5.1)	1:1000	CST (#2956)
GFAP	Mouse mAb (G-A-5)	1:1000	Sigma(#G3893)
GFAP	Rabbit pAb	1:500	Proteintech (#16825-1-AP)
RTP801	Chicken mAb	1:200	Davids Biotechnologie, GE. (specially customized for us)
Iba1	Goat polyclonal	1:500	Abcam (#ab5076)
NeuN		1:500	Abcam (#ab104224)
Parvalbumin	Mouse	1:500	Sigma
Parvalbumin	Rabbit	1:500	Proteintech
AQ4	Rabbit pAb	1:200	Proteintech (#16473-1-AP)
S100β	Rabbit pAb	1:500	Proteintech (#15146-1-AP)
ASC	Rabbit mAb (D2W8U)	1:500	CST (#67824S)
APP	Rabbit mAb (6E10)	1:1000	Novus Biologicals (#NBP2-62566)
AlexaFluor 488 anti chicken IgY	Goat polyclonal	1:500	Thermo Fisher Scientific (#A11039)
AlexaFluor 647 anti mouse IgG	Goat polyclonal	1:500	Thermo Fisher Scientific (#A21237)
AlexaFluor 555 anti rabbit IgG	Goat polyclonal	1:500	Thermo Fisher (#A21429)
AlexaFluor 555 anti rabbit IgG	Donkey polyclonal	1:500	Thermo Fisher Scientific (#A31572)
AlexaFluor555 anti goat IgG	Donkey polyclonal	1:500	Thermo fisher Scientific(#A21432)

For the Aβ plaques visualization, we immunostained brain sections for ThioS/APP. Briefly, slices were blocked for 4 hours with blocking buffer composed of 10% normal donkey serum in PBS 1x 0.25% Triton X-100. Thioflavin S (ThioS, Sigma #T1892) staining was performed as described in [240] and APP antibody (#NBP2-62566) was also added. Free-floating slices were washed for 1 minute sequentially in 70% and 80% ethanol after the secondary antibody, next they were incubated with 1% ThioS in 80% ethanol for 15 minutes. Before mounting with ProLong Gold Antifade Mountant slices were washed twice first with 80% ethanol followed by 70% ethanol (1 minute each).

13.1.1. Perineuronal networks staining in brain sections

To visualize the perineuronal networks that surrounds hippocampal parvalbumin-positive interneurons, we used biotinylated Wisteria Floribunda lectin (WFA) (1:250, VectorLabs #B-1355-2), reagent that binds to the carbohydrate structures terminating in N-acetylgalactosamine. Alexafluor555-Streptavidin (Thermo Fisher Scientific) was used to detect the biotinylated conjugates, along with the other secondary antibodies used in each occasion.

Images were obtained with confocal microscopy (Zeiss LSM 880 and ZEN Software) at the Microscopy Service (Campus Clínic) with a ×10, ×25, or ×40 magnification and standard (1 airy disc) pinhole (1 AU). Two sections from the dorsal hippocampus were analyzed per animal.

13.2. Golgi staining and neuron morphology analysis

After cervical dislocation, mouse hemispheres were collected in fresh for Golgi-Cox staining. The FD Rapid GolgiStain™ (FD Neurotechnologies) kit was used following manufacturer's protocol.

Superfrost slides were prepared with a gelatin solution (5 g/L) and 0,5 g/L of chromium potassium sulfate dodecahydrate and air dried prior to use. Brains were sliced (100μm each slice) using a Leica Vibratome and mounted on the abovementioned slides before final staining steps. Finally, slices were dehydrated with 50%, 75%, 95% ethanol and a final incubation with 100% ethanol and xylene, twice for 5 minutes each. Finally, samples were mounted with DPX mountant medium (Sigma). Neurons were analyzed with Image J.

14. Western Blotting

For western blot analyses hippocampi were dissected out and stored at -80ºC. Samples (15–20 μg) were resolved with NuPAGE polyacrylamide gels (12% and 4–12%) using MOPS SDS running buffer. Proteins were transferred to nitrocellulose membranes with the iBlot2 system. All reagents and machinery were obtained from Thermo Fisher Scientific. Membranes were blocked with 5% non-fat dry milk (BioRad) diluted in TBS-T (Tris-buffered saline containing 0.1% Tween-20). Primary antibodies were diluted in TBS-T with 5% BSA (Sigma) and incubated overnight at 4 °C by shaking. The primary antibodies are listed below **(Table 6)**. Mouse anti-actin primary antibody was already conjugated to horseradish peroxidase, so it was incubated for 30 min before chemiluminescent protein detection. Anti-mouse and anti-rabbit

secondary antibodies produced in goat and conjugated to HRP (Thermo Fisher Scientific, #31460 and #31430) were diluted 1:10.000 in blocking solution for 1 h at room temperature. Proteins were detected with SuperSignalTM West Pico Plus chemiluminescent substrate (Thermo Fisher Scientific). Images were acquired with ChemiDocTM (Bio-Rad) and quantified by densitometric analysis with ImageJ software (NIH).

Table 6. Primary and secondary antibodies used in western blot.

Antibody	Host species	Dilution	Source
GFP	Rabbit	1:1000	CST (#4858)
NLRP1	Mouse	1:1000	Santa Cruz Biotechnology (#sc-166368)
NLRP3	Rabbit mAb (D4D8T)	1:1000	CST (#15101)
Caspase 1	Rabbit mAb (E2Z1C)	1:1000	CST (#24232T)
ASC-TM1	Rabbit mAb (D2W8U)	1:1000	CST (#67824S)
IKBα	Rabbit	1:500	Proteintech (#
β-actin	Mouse mAb (Ac-15)	1:10000	Merck (#A3854)
HRP Anti-mouse IgG	Goat polyclonal	1:10000	Thermo Fisher Scientific (#31430)
HRP Anti-rabbit IgG	Goat polyclonal	1:10000	Thermo Fisher Scientific (#31460)

15. Cytokine Luminex

A customized panel for Luminex detection of cytokines and chemokines was used (R&D Systems). The panel included the following analytes: interleukin-4 (IL-4), IL-6, IL-10, IL-1α/IL-1F1, IL-1β/IL-1F2, IL-17A, interferon gamma (IFN-γ), macrophage colony-stimulating factor (M-CSF), osteopontin (OPN), tumor necrosis factor alpha (TNF-α), monocyte chemoattractant protein-1 (MCP-1/CCL2), macrophage inflammatory protein-1α (MIP-1α/CCL3). Briefly, 50 µL of all samples were tested in single replicates following manufacturer's instructions. The assay plate included 11 2-fold serial dilutions in single replicates of a standard sample provided by the vendor with known concentration of each analyte. Two blank controls were included in the plate for quality control purposes. Samples were acquired on a Luminex 100/200 instrument and analyzed in xPONENT software 3.1. The standard curve was fitted based on five-parameter log-logistic model. To account for background noise, median fluorescent intensity (MFI) of blank controls was subtracted to MFI of samples. The higher limit of quantification (HLOQ) was based on the higher dilution of the standard curve; and the lower limit of quantification (LLOQ) was calculated as the mean of blanks plus 2SD. Results were reported as pg/ml.

16. Experimental design and statistical analysis

The power analysis approach was used to calculate sample sizes: 0.05 alpha value, 1 estimated sigma value, and 75% of power detection. Data is expressed as mean ± SEM. With the d'Agostino and Pearson omnibus normality tests, the normal distribution was examined. If the test was

passed, a parametric statistical analysis was used to do the statistical analysis. We used the F test to examine variances prior to pairwise comparisons. In trials with a normal distribution, statistical analyses were carried out using t-test, one-way ANOVA or two-way ANOVA with Bonferroni's or Tukey's post hoc tests as stated in the figure legends, as well as the unpaired, two-sided Student's t test (95% confidence interval). The T test with Welch's correction is used when the variances were not equal. The significant outlier values were identified using the Grubbs and ROUT tests. Blocks of animals were used to blind and randomize each experiment in this investigation. All the mice were divided randomly into experimental groups. Data were randomly gathered, prepared, and examined and data was analyzed blindly. Statistics were judged significant at P equal to 0.05 or lower.

RESULTS

17. Role of astrocytic RTP801 in neurodegeneration

In neurodegenerative diseases overexpression of neuronal RTP801 is detrimental to neuronal activity and function. The hypothesis is that at early stages of a neurodegenerative disease mTOR is hyper activated, inducing an upregulation of RTP801 expression. Then, progressively, RTP801 starts to inactivate mTOR as a regulatory loop. However, at more advanced stages of these diseases, chronic overexpression of RTP801 can over-inactivate mTOR activities, inhibiting protein synthesis and the pro-survival kinase Akt, among others [241].

Building on the previous point, postmortem brains of PD patients showed increased amounts of RTP801 protein, specifically in the neuromelanin positive substantia nigra neurons. Besides, RTP801 overexpression resulted in the death of neurons, and in PD models, its induction was sufficient and necessary for cell death[242]. Interestingly, in HD, higher levels of RTP801 were found in the striatum of both animal models and in human postmortem samples[243,244].

Not surprisingly, in AD postmortem hippocampal samples RTP801 was also elevated and the levels correlated with the Braak and Thal stages of the disease. Indeed, RTP801 levels were upregulated in the 5xFAD mouse model of AD and silencing its neuronal expression prevented cognitive impairment and exhibited anti-inflammatory effects. Interestingly, silencing neuronal RTP801 in hippocampal neurons in the 5xFAD mouse model, led to an indirect reduction of RTP801 in astrocytes, suggesting that astrocytic RTP801 could contribute to the AD phenotype in these mice. Moreover, this suggested that RTP801 could be mediating a crosstalk between neurons and astrocytes worthy to investigate[222].

Hence, to investigate the contribution to cognitive impairment and neuroinflammation of astrocytic RTP801, we knocked down RTP801,

specifically in astrocytes in the 5xFAD mice model of AD and investigate the effect on neurodegeneration and brain homeostasis.

17.1. RTP801 levels are elevated in hippocampal astrocytes in the 5xFAD mice.

Six-month-old animals were anesthetized, and we bilaterally injected adeno-associated virus (AAV) vectors expressing either scrambled microRNA (rAAV2/5-GFAP-miCT) or microRNA targeting RTP801 (rAAV2/5-GFAP-miRTP801) under the GFAP promoter into the dorsal hippocampus of wild-type (WT) and 5xFAD mice model of AD. After one moth recovery when 5xFAD already presents cognitive symptomatology, we performed a behavioral characterization followed by MRI analyses. Then, we sacrificed the animals at 7 months and 3 weeks old and performed all the immunohistochemistry and biochemical characterization **(Figure 14A)**. This experimental design resulted in four groups of mice: WT miCT, WT miRTP801, 5xFAD miCT, and 5xFAD miRTP801. First, we confirmed that viral transduction after the injections in the DG and CA1 of the dorsal hippocampus was performed correctly **(Figure 14B).**

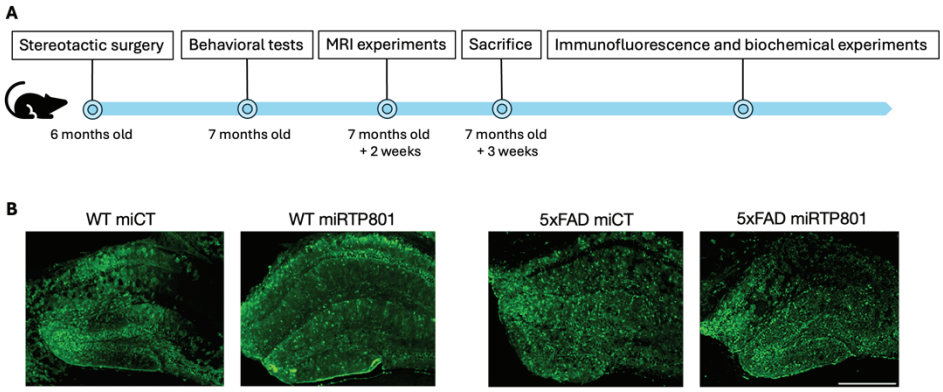

Figure 14. Experimental design and AAVs infection of the four groups. (A) Schematic representation of the experimental procedure. AAVs expressing GFAP-miCT or GFAP-miRTP801 were bilaterally injected in the dorsal hippocampus of 6-month-old WT males (WT miCT or WT miRTP801 groups) or 5xFAD males (5xFAD miCT or 5xFAD miRTP801 groups). Four weeks later, behavioral tests were performed, followed by MRI analyses and biochemical characterization. (B) Representative immunostaining of GFP fluorescence, showing the specific transduction with AAV2/5 in the CA1 and DG in the four groups. Scale bar = 500µm

Next, we confirmed that the AAV2/5 containing the GFAP promoter had specific tropism for astrocytes. Hence, by immunostaining we observed that indeed the transduced cells (eGFP$^+$ cells) were astrocytes (GFAP$^+$ cells), but not neurons (NeuN$^+$ cells) or microglia (Iba1$^+$ cells) **(Figure 15)**.

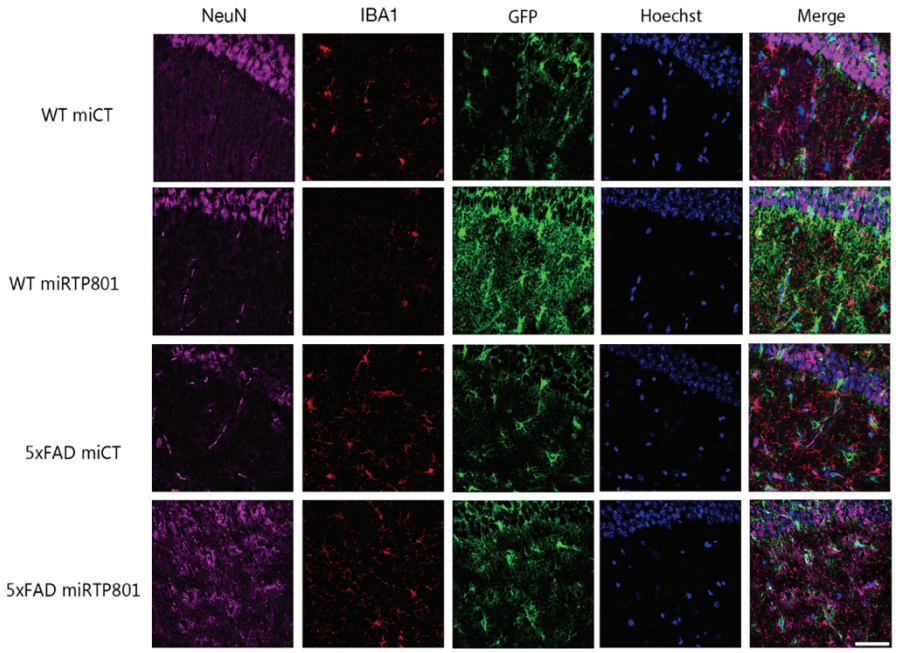

Figure 15. Specific transduction of astrocytes in the dorsal hippocampus of the rAAV2/5-GFAP-miCT and rAAV2/5-GFAP-miRTP801. (A) Representative NeuN, Iba1 and GFP staining immunofluorescence microscopy imaging.

As expected, the levels of RTP801 in the 5xFAD astrocytes were elevated in both CA1 and DG compared with the WT animals and the miRTP801 decreased the astrocytic RTP801 levels around a 30% at the CA1 **(Figure 16)** and the DG **(Figure 17)** as judged by immunofluorescence image analysis.

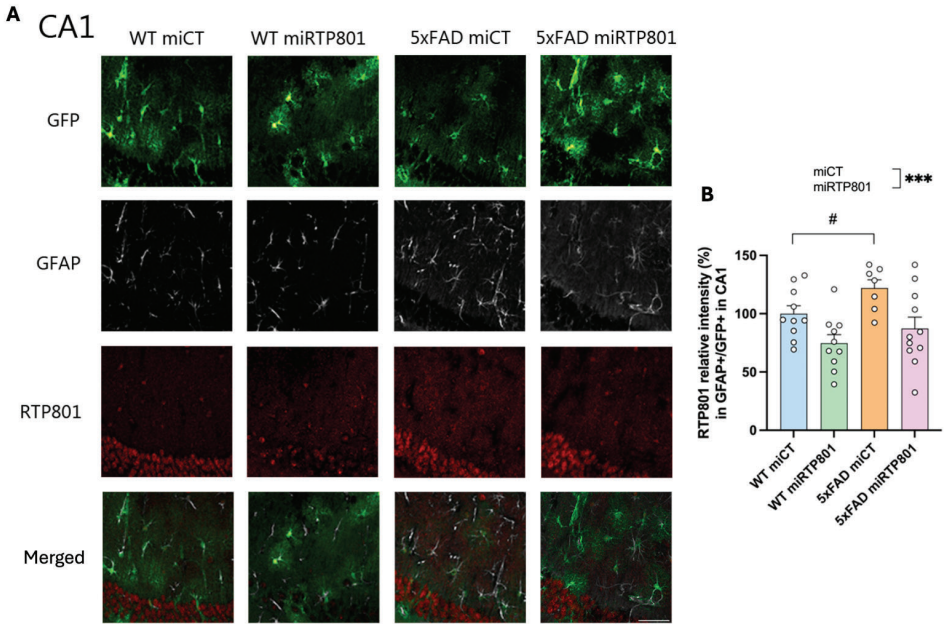

Figure 16. Hippocampal CA1 astrocytes show higher levels of RTP801 in the 5xFAD mouse model and the miRTP801 normalizes this upregulation. A) Representative CA1 images from dorsal hippocampus where transduced cells (GFP$^+$, astrocytes (GFAP$^+$, white), and RTP801 (red) are depicted. Scale bar = 50 μm. **B)** Immunofluorescence quantification of RTP801 protein levels in GFP$^+$ astrocytes of the CA1 in the four groups is shown (treatment effect: $F_{(1,\ 34)} = 12{,}99$, $P = 0.001$, genotype effect #P < 0,05).

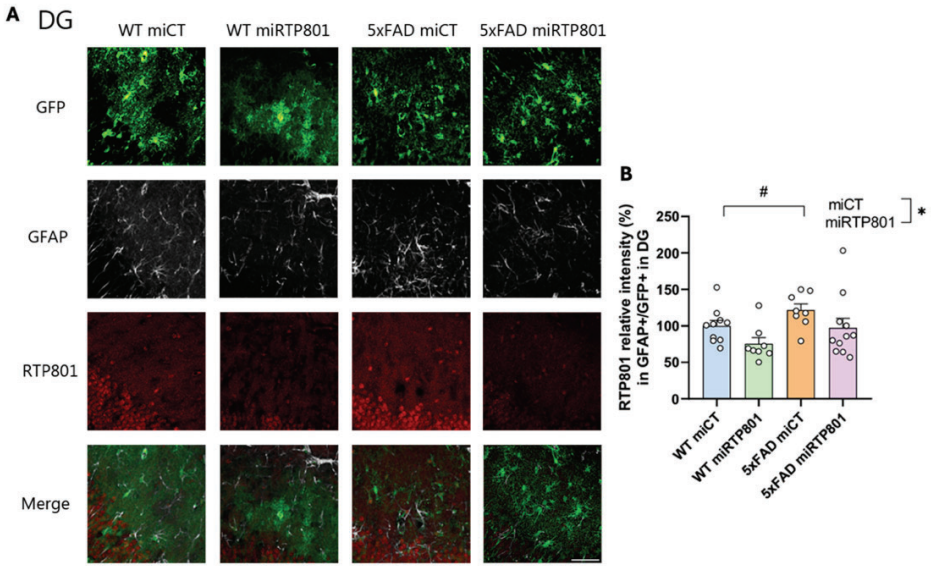

Figure 17. Hippocampal DG astrocytes show higher levels of RTP801 in the 5xFAD mouse model and the miRTP801 normalizes this upregulation. A) Representative DG images from dorsal hippocampus where transduced cells (GFP⁺, astrocytes (GFAP⁺, white), and RTP801 (red) are depicted. Scale bar = 50 μm. **B)** Immunofluorescence quantification of RTP801 levels in GFP⁺ astrocytes of the DG in the four groups is shown (treatment effect: $F_{(1, 34)} = 12{,}99$, $P = 0.05$, genotype effect #P < 0,05).

17.2. Astrocytic RTP801 silencing does not affect the number of Aβ plaques.

To investigate whether astrocytic RTP801 silencing affects the number of Aβ plaques, one of the major hallmarks of AD, we performed an immunohistochemistry combining Thioflavin S staining with an antibody that recognizes APP protein. Interestingly, RTP801 silencing (miRTP801) did not have any effect on APP or Aβ plaque load in the dorsal hippocampus in the 5xFAD mice in comparison to the 5xFAD injected with the miCT (**Figure 18)**.

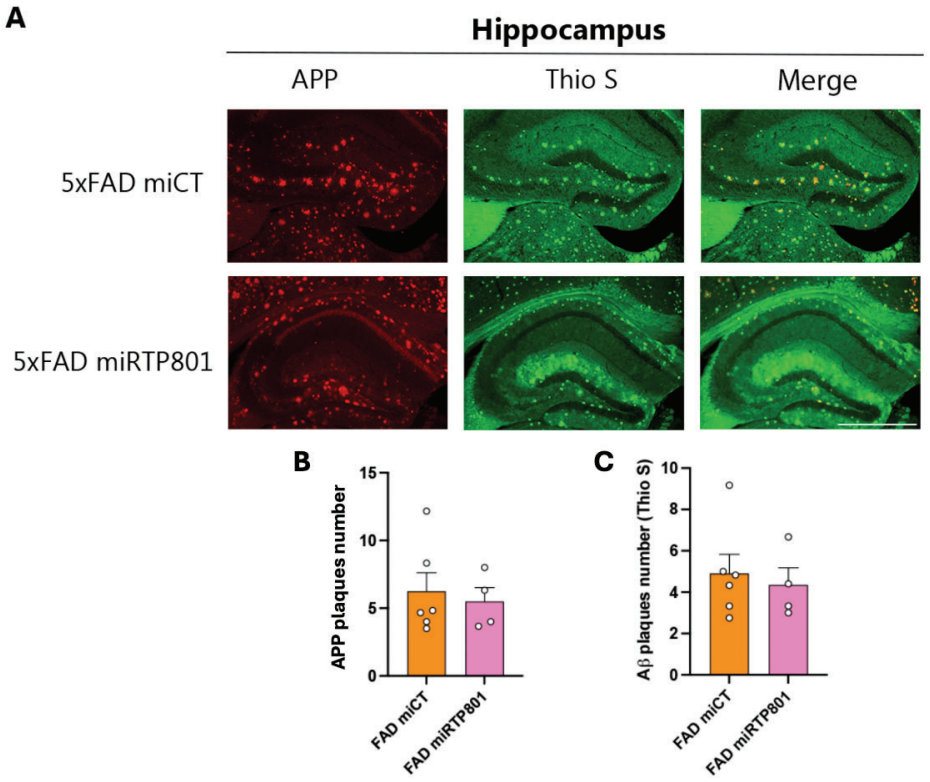

Figure 18. Amyloid plaques in 5xFAD miCT and 5xFAD miRTP801 mice's dorsal hippocampus. A) Representative dorsal hippocampi from 5xFAD miCT and 5xFAD miRTP801 immunofluorescence images 7'5 months after injection. Amyloid plaques were co-stained with Thioflavin S (ThioS, green) and for APP protein (red). Scale bar = 500 μm. B) Quantification of the APP+ plaques/field. C) Quantification of Aβ+ plaques/field in the hippocampus. Data are means ± SEM. T-test was performed.

Our findings collectively demonstrate that astrocytic RTP801 is elevated in the hippocampal region of 5xFAD mouse model, and it is sensitive to our GFAP-miRTP801 AAV particles. However, silencing astrocytic RTP801 does not change the Aβ plaque load.

17.3. Genetic normalization of astrocytic hippocampal RTP801 levels in 5xFAD mice prevents cognitive deficits and mildly restores anxiety.

To investigate whether astrocytic RTP801 silencing could contribute to prevent the appearance of cognitive impairment, one month after AAVs injection, we performed a battery of behavioral tests. We started with the plus-maze paradigm to test the levels of anxiety in the four experimental groups. We observed that 5xFAD mice, independently of the treatment, spent more time in the open arm, meaning that these animals were less anxious. However, when we silenced astrocytic RTP801 in the 5xFAD mice, we lost this trait in comparison to the WT miCT. Interestingly, the difference between the time they spend in the open and the closed arm is also lost **(Figure 19)**

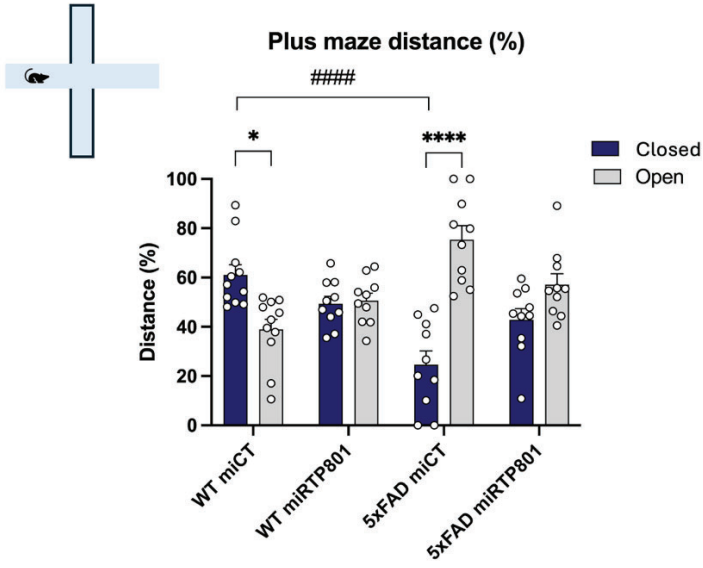

Figure 19. Astrocytic RTP801 regulates anxiety-like behavior. Animals were put in the elevated plus maze to measure their anxiety-like behavior. The time spent in the open arms was monitored for 5 min. Two-way ANOVA showed a significant general time effect. Bonferroni post hoc test was performed (open vs close *p< 0.05., **** p < 0.0001 and genotype effect WT vs 5xFAD ####p<0.0001).

Next, we investigated whether astrocytic RTP801 contributed, in the 5xFAD mouse model, to associative and spatial learning impairment by using the Morris water maze (MWM). First of all, the grid test revealed that all groups had normal muscular strength, indicating that any potential changes in the MWM are not the result of deficiencies in muscular strength. The grid test consists on testing the ability of the rodents to hang on the inverted mesh measured by seconds to fall (WT miCT 51.06 ± 4.393, 5xFAD miCT 49.71 ± 5.022, WT miRTP801 49.33 ± 4.882 and 5xFAD miRTP801 43.67 ±5.154 ; two-way ANOVA genotype effect P = 0.4786; two-way ANOVA miRNA effect: P = 0.4323). Second, although 5xFAD mice showed decreased body weight, as previously reported in [245], we did not find any differences in mice weight (g) associated with astrocytic RTP801 silencing (WT miCT 32.15 ± 0.592, 5xFAD miCT 28.61 ± 0.6715, WT miRTP801 32.15 ± 0.5435, and 5xFAD miRTP801 29.66 ± 0.5460; two-way ANOVA treatment effect: P = 0.3791; two-way ANOVA genotype effect P = <0.0001). Third, all the 5xFAD groups were tested in the visible platform task (four trials/mouse) to rule out poor vision, changed motivation, and/or sensorimotor disabilities. We compared escape latencies during training with the visible platform between WT miCT, WT miRTP801, 5xFAD miCT, and 5xFAD miRTP801 mice and found no differences between groups from trial 1 to trial 4, meaning that they could learn to identify the visible platform **(Figure 20A)**. Afterwards, all the animals went through the hidden version of the MWM to assess spatial learning. We observed that 5xFAD miCT mice did not significantly improve throughout training from day 1 to day 6, in comparison to WT miCT. However, in the 5xFAD miRTP801 mice, after silencing RTP801, this trait was prevented. **(Figure 20B)**.

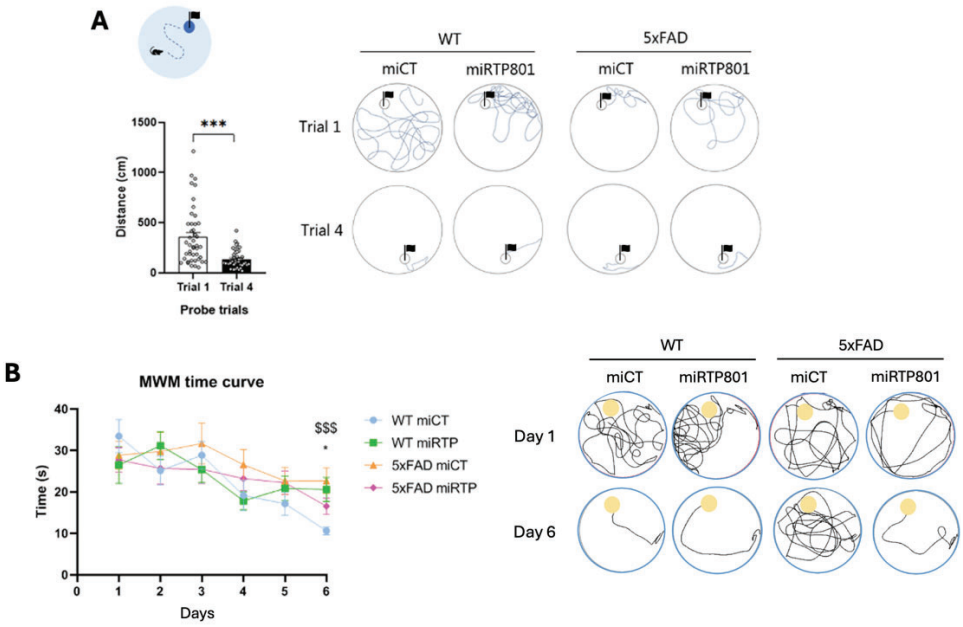

Figure 20. Astrocytic RTP801 affects spatial memory. A) The distance (in cm) to reach the visible platform was monitored in a 4-trials session to evaluate potential visual or physical impairments in 7-month-old mice. Paired t-test showed a significant general time effect in this procedural version of the MWM (***p < 0.0001) indicated that animals significantly improved their latencies in trial 4 compared to trial 1. C) Morris water maze time curve, Time (in s) to reach the hidden platform was monitored in a daily 4-trials session performed for 6 days to evaluate spatial learning. The distance (in cm) to reach the hidden platform was monitored in a daily 4-trials session performed for 6 days to evaluate spatial learning in 7-month-old mice. Two-way ANOVA showed a significant general time effect in this spatial version of the MWM (F(1,76) = 29.37, P<0.001) and post hoc (Tukey's test) multiple comparisons indicated that WT miCT groups and 5xFAD miRTP801 significantly improved their latencies to reach the hidden platform on the day of training 6 compared to the day of training 1, the 5xFAD shCt group who showed no significant differences comparing its latencies on day 6 with those on day 1 (see graph). The number of mice in F, G, WT shCt (n = 11), WT shRTP801 (n = 10), 5xFAD shCt (n = 10), and 5xFAD shRTP801 (n = 10). Two-way ANOVA showed a significant general time effect. Turkey's post hoc test was performed *p< 0.05, *** p < 0.001, $$$ < 0.001.

Overall, these data demonstrate that 7.5-month-old 5xFAD mice miCT show associative and spatial learning deficits that are prevented when astrocytic RTP801 levels are silenced in the hippocampus.

17.4. Astrocytic RTP801 shows a partial recovery of the apical dendrite neurons.

The literature reported that the dentate granule cells (DGCs) in AD patients have early morphological changes that worsen with the course of the illness. The initial morphological alteration seen in patients at Braak-Tau I/II stages is an abnormally elevated number of DGCs with multiple main apical dendrites. This change continues as AD progresses[246].

One of the primary cortical inputs that reach the DG is the perforant pathway, which is built with the axons of pyramidal neurons in the entorhinal cortex (EC). The dendrites of DGCs form the initial synaptic connection with the previously stated axons and its morphological maturity is essential for the establishment appropriate afferent connections from the perforant route. Hippocampal areas CA3 and CA2 are in touch with DGC axons, also known as Mossy fibers[247]. The dendrites of CA1 pyramidal neurons, which project back to the subiculum and the EC and the axons of CA3 pyramidal neurons. For learning and memory, the traditional hippocampus trisynaptic circuit (EC-DG-CA3-CA1) is essential[248].

Given that silencing astrocytic RTP801 prevented cognitive deficits in the 5xFAD mice, we investigated whether this involved a morphological change in the DGC apical dendrites.

By Golgi staining, we analyzed the total dendritic width, the total dendritic length, the number of ending tips and the % of neurons with only one apical dendrite. Our results reveal that there was no difference in total dendritic width or number of ending tips. However, 5xFAD mice presented neurons with shorter dendritic length in comparison to WTs. Interestingly, the DGCs in the 5xFAD mice showed more than one apical dendrite compared to the WT, and silencing astrocytic RTP801 mildly

prevented this trait, since this significant difference was lost in the 5xFAD miRTP801 group. **(Figure 21)**.

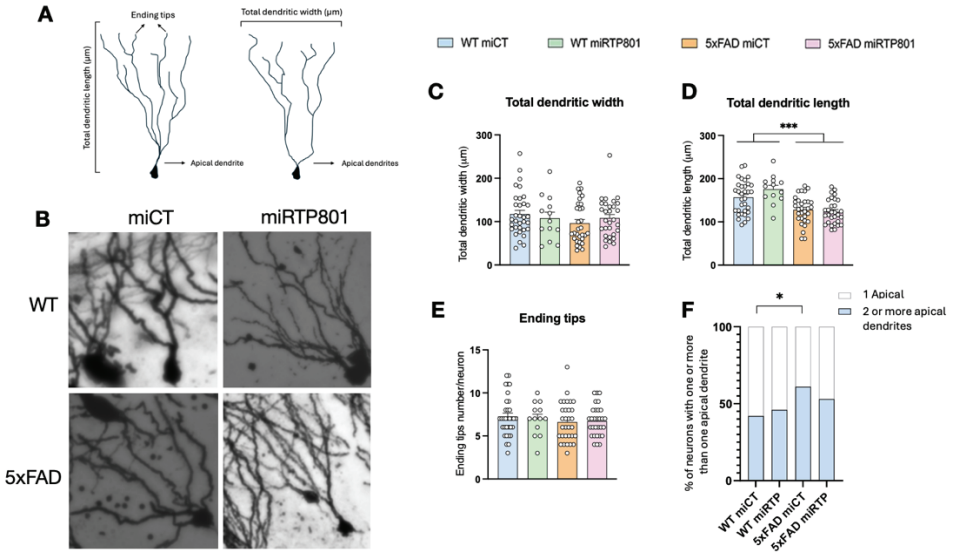

Figure 21. Astrocytic RTP801 mildly affects DGCs morphology. A) Schema of a neuron showing the primary apical dendrite, the ending tips, the dendritic length and the dendritic width. B) Representative images of Golgi staining. C) Quantification of total dendritic width (µm). D) Quantification of total dendritic length (µm). E) Quantification of number of ending tips in each neuron. F) Quantification of the % of neurons with more than one apical dendrite. Data are means ± SEM. In all panels Two-way ANOVA with Bonferroni's post hoc test was performed: *p < 0.05, ***p < 0.001.

17.5. Resting-state functional connectivity is restored by knocking down astrocytic RTP801 in 5xFAD mice

To investigate whether the brain connectivity was affected in the 5xFAD mice and whether astrocytic RTP801 could be involved, MRI analyses were conducted one week after the behavioral tests. We explored the functional brain connectivity in established resting-state networks (RSNs) obtained by independent component analysis (ICA). From ICA20, six components were identified representing these functional networks.

Based on their relevance to functional alterations related to aging and AD[249–251], the selected RSN were named by their main representative hubs, and were the following: 1) cingulate-cortex (as part of the default mode network), 2) amygdala – insular cortex (as part of the salience network), 3) hypothalamus – mammillary bodies (as part of the autonomic network), 4) ventral hippocampus-ventral striatum, 5) sensory cortices including piriform, auditory, somatosensory and visual (also known as lateral cortical network), and 6) pons - striatum. The anatomical structures comprised in these networks were selected by visual inspection of their spatial maps based on previous studies[252].

Significant perturbations in brain functional connectivity were evidenced by statistical maps showing significant differences (green voxels) in multiple networks in 5xFAD mice comparing with age-matched controls at 7.5 months of age (comparison 5xFAD miCT>WT miCT; $p < 0.01$) ($n = 7$). The significant voxels were used as a mask to plot the Z-score values of the 3 experimental groups. We observed that the functional connectivity was higher in the 5xFAD mice compared to that in WT mice, while the connectivity decreased when astrocytic RTP801 was silenced, likely to the WT animals. Focusing on the different networks, we found significant higher connectivity of the cingulate cortex in the 5xFAD mice that significantly deceased in 5xFAD miRTP801 mice. As previously mentioned, this region is considered a central region of the default mode network which has been widely studied in the AD field, both in humans[253] and animal models[254]. A similar effect was observed in the amygdala-insular cortex. These regions represent part of the salience network whose function is linked to the default mode network and has been also been shown to be altered in both normal aging and AD progression[255]On the other side, the autonomic network includes connectivity of hypothalamus and mammillary bodies. Again, a significant increase of

functional connectivity was observed in 5xFAD miCT compared to WT miCT. In this case a strong decrease was observed in 5xFAD miRTP801 mice when comparing to both WT miCT and 5xFAD miCT. Similar effects were observed for ventral hippocampus-ventral striatum and the association cortices. Dysregulation of the corticothalamic network may be a common denominator that contributes to the diverse cognitive and behavioral alterations in AD. The only network we saw a different pattern was the pons striatum where no significant differences were observed between WT miCT and 5xFAD miCT. Moreover, 5xFAD miRTP801 showed significant hyperconnectivity compared to both miCT groups).

Hence, data suggest that elevated levels of astrocytic RTP801 mostly produce a functional hyperconnectivity in different RSN of the 5xFAD mouse model, contributing to the typical cognitive impairment of AD. When astrocytes normalize their expression of RTP801 the resting state functional connectivity is decreased, except for pons-striatum connectivity **(Figure 22).**

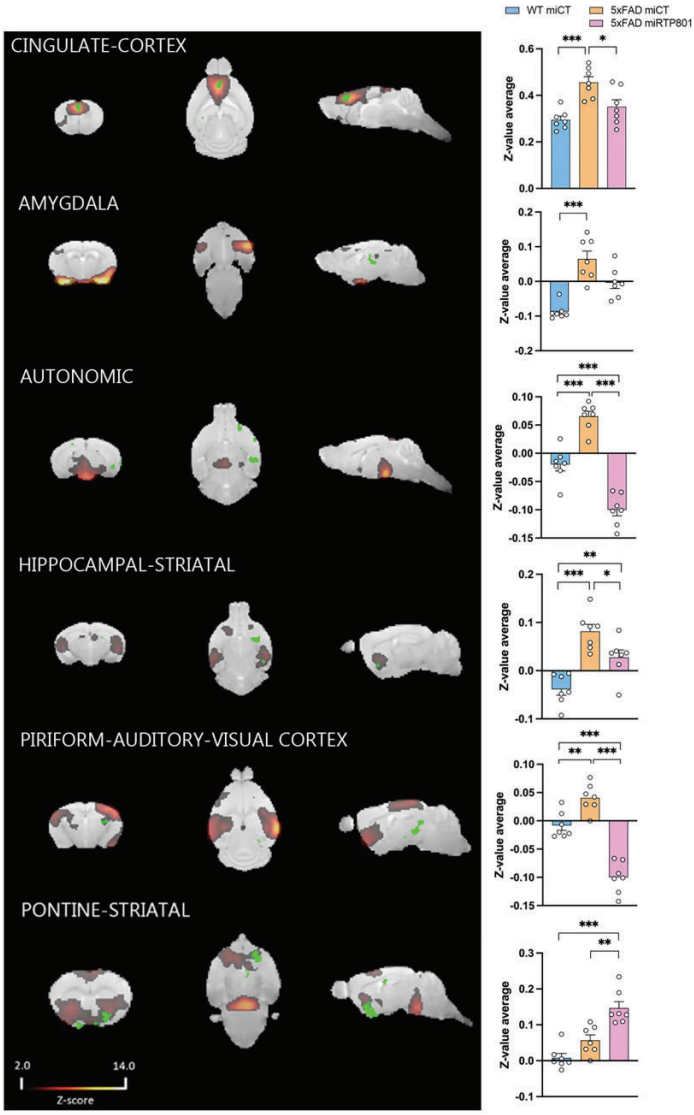

Figure 22. Silencing astrocytic RTP801 in 5xFAD mice changes functional connectivity. (A) Spatial maps of the independent components of the resting-state functional Magnetic Resonance. Imaging data, grouped into six resting state networks, namely. Statistical maps showing significant differences (green voxels) in the corresponding ICA connectivity in WT and FAD miCT animals (FAD miCT>WT; $p < 0.01$) (n = 7). (B) Cingulate-Cortex (C) Amygdala (D) autonomic network (E) Hippocampal-striatal (F) Piriform-auditory-visual cortex and (G) Pontine-striatal. Values of Z-score in these voxels were plotted for the 3 experimental groups. Data are means ± SEM. In all panels one-way ANOVA with Bonferroni's post hoc test was performed: *$p < 0.05$, **$p<0.01$,***$p < 0.001$

Hence, data suggest that elevated levels of astrocytic RTP801 mostly produces a functional hyperconnectivity in different RSN of the 5xFAD mouse model, contributing to the typical cognitive impairment of AD. When astrocytes normalize their expression of RTP801 the resting state functional connectivity is decreased, except for pons-striatum connectivity.

17.6. Astrocytic RTP801 mediates the loss of DG and CA1 Parvalbumin+ interneurons, negatively affecting the levels of GABA in the 5xFAD mouse model.

Silencing RTP801 in the 5xFAD mouse astrocytes led so far to prevent the loss of spatial memory and to prevent the percentage of DGCs with one apical dendrite. Moreover, it also contributed to conserve the resting state functional connectivity as in the WT. Hence, to investigate the mechanisms by which silencing astrocytic RTP801 was beneficial, we first assessed the metabolites in the dorsal hippocampi of WT miCT, 5xFAD miCT and 5xFAD miRTP801 mice by Magnetic resonance spectroscopy (MRS).

To normalize the metabolites' concentrations we used creatine, since it's the common value to normalize in MRI experiments because its concentration tends to remain stable under physiological and pathological conditions. Furthermore, it helps to reduce the variability cause for other experimentation factors as voxel size differences or magnetic field inhomogeneities[256]. **(Figure 23A)**. We observed no differences in the levels of aspartate, glutamine, glutamate, glycine or glutathione **(Figure 23B-F)**. However, we detected a decrease in an important precursor of the neuropeptide N-acetylaspartylglutamate (NAAG), the NAA (N-acetyl aspartate), in the 5xFAD mice injected with the miCT and the miRTP801 compared to the WT mice **(Figure 23G).** Glucose

was diminished in the 5xFAD miRTP801 compared to the WT miCT **(Figure 23H)**. We detected also lower levels of the neurotransmitter and neuroprotector taurine and in the 5xFAD mice **(Figure 23J).**

Interestingly, we observed a reduction of GABA levels in the 5xFAD miCT compared to WT miCT which was partially rescued after knocking down astrocytic RTP801 in the 5xFAD **(Figure 23I)**.

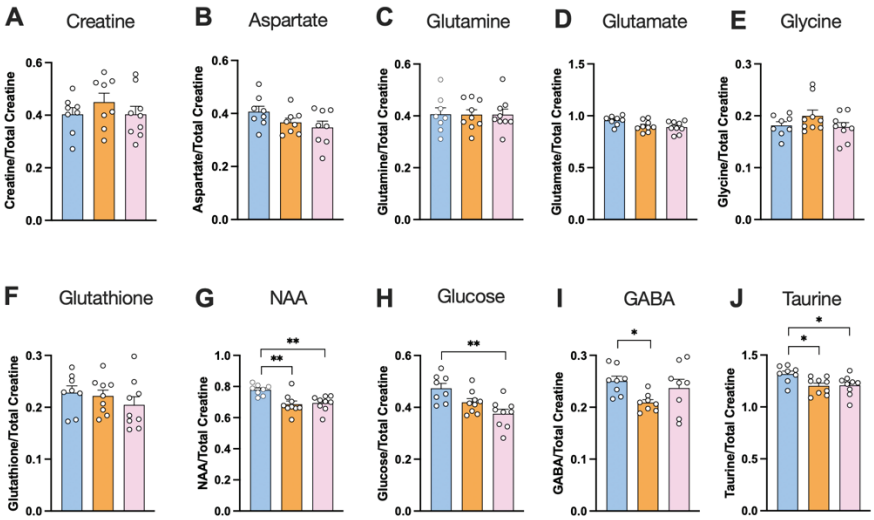

Figure 23. Changes in hippocampal metabolites in the 5xFAD mouse model. Metabolites concentration quantification (mmol/kg w.w) was measured using MRS (Magnetic resonance spectrometry). A) Creatine, B) Aspartate, C) Glutamine, D) Glutamate, E) Glycine, F) Glutathione, G) NAA, H) Glucose, I) GABA, J) Taurine. Each point represents data from an individual mouse. Data are means ± SEM. One-way ANOVA with Bonferroni's post hoc test was performed *p < 0.05, **p < 0.01. Abbreviations: GABA: Gamma-aminobutyric acid; NAA: N-Acetylaspartate.

Since the reduced GABA levels observed in 5xFAD miCT could explain their hyperconnectivity which seemed to be sensitive to the levels of RTP801 in astrocytes, we aimed to investigate the possible reasons for this GABA deficit. Hence, we first examined the number of GABAergic interneurons by quantifying the number of Parvalbumin^{+} (PV) cells in the CA1 and DG regions across the three experimental groups. We also measured their perimeter and their area. As expected, the number of PV+

neurons was lower in the 5xFAD miCT group, silencing astrocytic RTP801 preserved the amount of CA1 and DG PV⁺ interneurons in comparison to 5xFAD miCT mice. Moreover, these interneurons were bigger in the 5xFAD miRTP801 mice in the DG **(Figure 24)**.

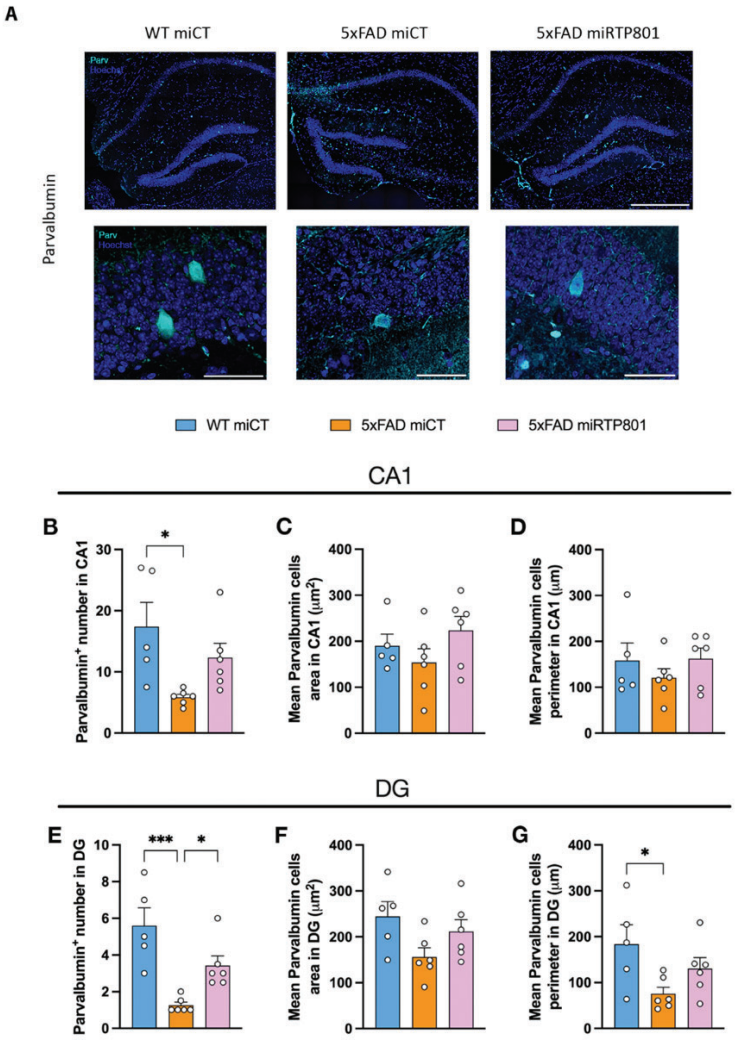

Figure 24. Astrocytic RTP801 protects Parvalbumin⁺ interneurons from neurodegeneration. A) Representative immunostaining of hippocampal PV⁺ interneurons in the different groups. Scale bar = 500 μm and 50 μm. B) Number of PV⁺ interneurons in the CA1. C) Area covered by PV⁺ interneurons in the CA1. D) Mean perimeter of PV⁺ interneurons in the CA1 E) Number of PV⁺ interneurons in the DG. F) Area covered by PV⁺ interneurons in the DG. Each point represents data from

an individual mouse. G) Mean perimeter of PV+ interneurons in the DG. Data are means ± SEM. One-way ANOVA with Bonferroni's post hoc test was performed *p < 0.05, ***p < 0.001.

Interestingly, differences in the levels of GABA-producing enzymes GAD65/67, which is expressed by GABAergic neurons[257] and astrocytes[258]. were observed between WT and 5xFAD mice but they were not prevented by silencing astrocytic RTP801 **(Figure 25).**

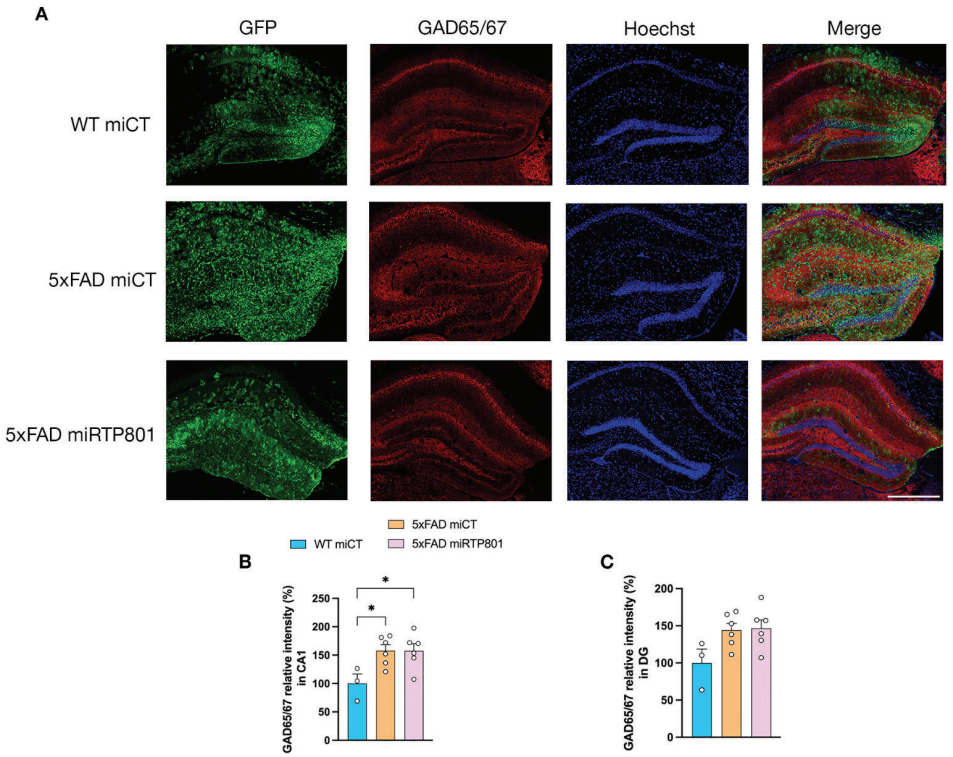

Figure 25. GAD65 and GAD67 in WT miCT, 5xFAD miCT and 5xFAD miRTP801 mice's dorsal hippocampus. (A) Representative GAD65/67 immunofluorescence microscopy imaging from the CA1 and DG. (B) Quantification of GAD65/67 intensity in CA1 and (C) DG. Data are means ± SEM. One-way ANOVA with Bonferroni's post hoc test was performed: *p < 0.05.

Hence, our results suggest that the hyperconnectivity seen in the 5xFAD brains could be explained in part, by the toxicity of astrocytic RTP801 over

hippocampal PV+ interneurons, one of the main sources of the GABA neurotransmitter.

17.7. Astrocytic RTP801 might be involved in the PNN degradation observed in the 5xFAD

Perineuronal nets (PNN) surrounds some neurons' soma and proximal dendrites as a part of the extracellular matrix. These PNNs are made up of link proteins, hyaluronan, tenascin, and highly charged chondroitin sulfate proteoglycans (such as aggrecan, neurocan, and brevican)[259]. PNNs surround different kinds of neurons within the regions where they are located, and their distribution is similar in different mammalian species[260]. Interestingly, most cells ensheathed by a PNN are GABAergic interneurons, particularly PV+ interneurons[261]. Due to their high metabolic requirement and increased mitochondrial density, and fast-spiking features make PV+ cells more susceptible to oxidative stress than other interneurons like calretinin and calbindin cells[262]. In this line, PNN seems to protect PV+ interneurons from oxidative stress[263,264].

Glia is an important source of PNNs components during development and adulthood[265]. Importantly, astrocytes release a wide range of matrix-remodeling proteases and their inhibitors to closely regulate PNN structural integrity[266,267].

Considering that in the 5xFAD mice model showed a decrease of PV+ interneurons and that silencing astrocytic RTP801 seems to prevent PV+ interneurons loss, we next assessed whether RTP801 contribute to PNN impairment in our animal model. To do so, we used lectin Wisteria floribunda agglutinin (WFA) to stain the PNNs. WFA, which has been frequently employed as a PNN marker in histology examinations, can be

bound by a wide variety of PNNs, but not all of them. Hence, it is noteworthy that WFA-negative PNNs exist, as well[268].

We stained the brain slices with WFA-biotin and Streptavidin-AlexaFluor555. In the CA1 we observed a reduction in the number of PNN in the 5xFAD mice, while in the 5xFAD miRTP801 there are more PV^+ surrounded by a PNN and more PNN structures in general.

On the other side, in the DG there are lower numbers of PNN in the 5xFAD with no differences after knocking down astrocytic RTP801, probably due to the low amount of PV^+ interneurons in this area. However, the proportion of PV^+ neurons wrapped with PNN was not different among groups **(Figure 26)**.

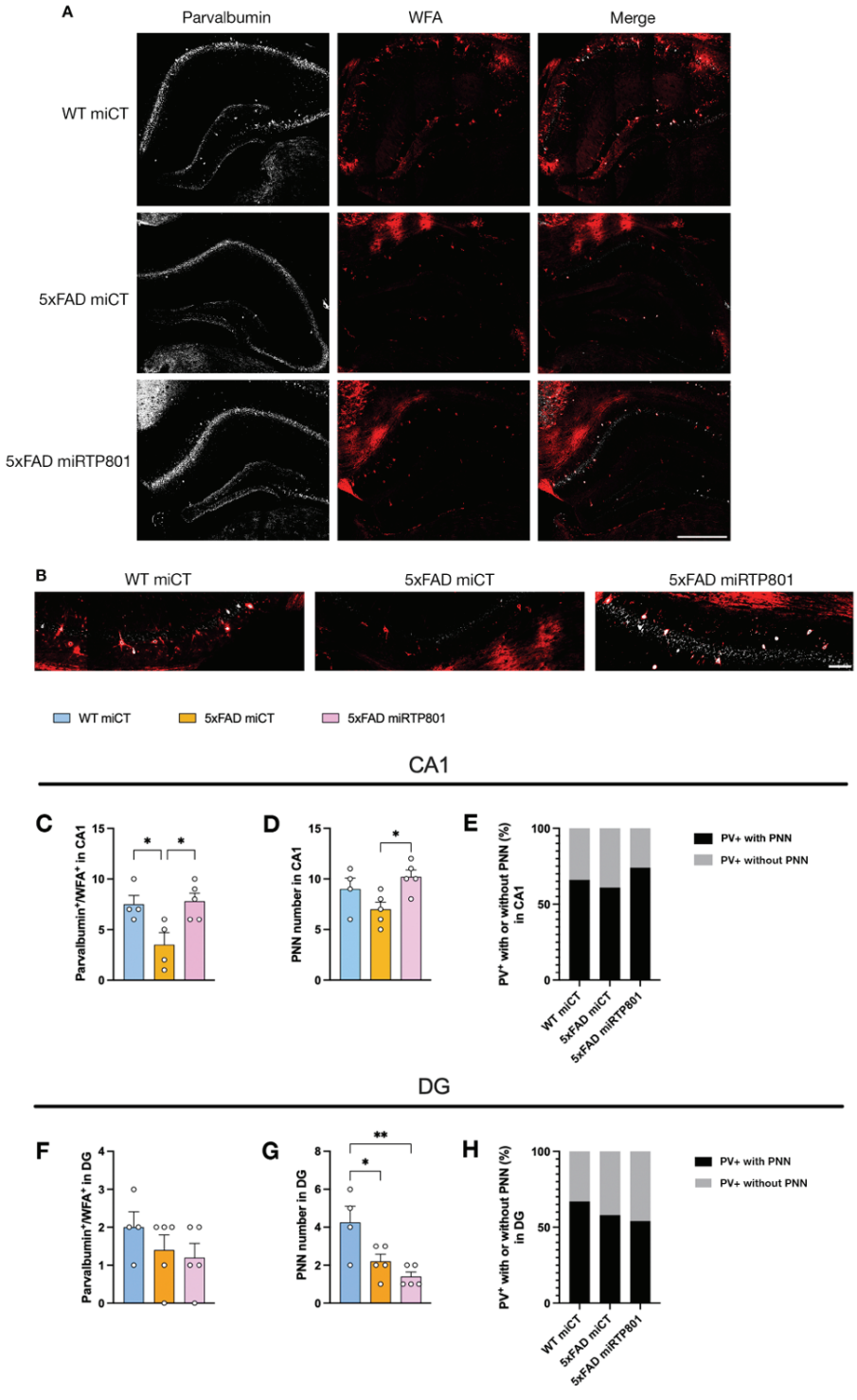
A
Parvalbumin
WFA
Merge
WT miCT
5xFAD miCT
5xFAD miRTP801
B
WT miCT
5xFAD miCT
5xFAD miRTP801
WT miCT
5xFAD miCT
5xFAD miRTP801
CA1
C
Parvalbumin+/WFA+ in CA1
D
PNN number in CA1
E
PV+ with or without PNN (%) in CA1
PV+ with PNN
PV+ without PNN
WT miCT
5xFAD miCT
5xFAD miRTP801
DG
F
Parvalbumin+/WFA+ in DG
G
PNN number in DG
H
PV+ with or without PNN (%) in DG
PV+ with PNN
PV+ without PNN
WT miCT
5xFAD miCT
5xFAD miRTP801

Figure 26. RTP801 negatively affects the PNN integrity at least in the CA1 of 5xFAD mice. A) Representative immunostaining of hippocampal Parvalbumin$^+$ interneurons (grey) and PNN (red). Scale bar = 500 μm B) Representative immunostaining of hippocampal Parvalbumin+ interneurons (grey) and PNN (red) in CA1. Scale bar = 50 μm . C) Number of Parvalbumin$^+$ interneurons with PNN in the CA1. D) PNN number in the CA1. E) Parvalbumin$^+$ interneurons with or without PNN (%) in the CA1 F) Number of Parvalbumin$^+$ interneurons with PNN in the DG. G) PNN number in the DG. H) Parvalbumin$^+$ interneurons with or without PNN (%) in the DG. Data are means ± SEM. One-way ANOVA with Bonferroni's post hoc test was performed *$p < 0.05$, **$p < 0.01$.

18. Role of astrocytic RTP801 in neuroinflammation

In AD, Aβ plaques accumulation causes neuroinflammation due to over-reacting microglia and astrocytes. Thus, this inflammation. When becomes chronic, leads to a sustained release of cytokines, chemokines, prostaglandins and ROS[269], which in turn causes synaptic dysfunction[270], neuronal death[271] and inhibition of neurogenesis[272]. Therefore, neuroinflammation is a major hallmark of AD.

Astrogliosis have been described as a process by which astrocytes undergo biochemical, morphological, metabolic, physiological, and transcriptionally regulated program modifications in response to pathology. These modifications ultimately lead to the acquisition of new functions or the loss or upregulation of homeostatic ones[273]. On the other hand, microgliosis is the term used to describe the morphological, molecular, and functional remodeling of microglia in response to brain stressors, such as the deposition of Aβ or α-synuclein[274] .

Inflammasomes are cytoplasmic multiprotein complexes formed by sensor and adaptor proteins along with inflammatory caspases. Briefly, activation of inflammasomes by endogenous and/or exogenous stimuli, leads to enzymatic activation of caspase 1, resulting in secretion of interleukins, and committing the cell to a consequent programmed cell death, such as apoptosis or pyroptosis[275]. Therefore, fine-tuned modulation of the inflammasome activity is imperative for cell survival.

In a previous work of our group, neuronal RTP801 upregulation in the 5xFAD contributed to astrogliosis, microgliosis and to the inflammasome activation, by upregulation caspase 1, NLR family pyrin domain containing 1 (NLRP1), NLR family pyrin domain containing 3 (NLRP3) and apoptosis associated speck-like protein containing a CARD (ASC)[222].

In the previous section of the thesis, we described the role of astrocytic RTP801 in cognitive impairment, metabolism, functional brain connectivity, DGCs morphology and interneuron numbers in the 5xFAD mice model of AD. To investigate whether astrocytic RTP801 also contributes to neuroinflammation and to explore in-depth its precise mechanisms, here we investigated astrogliosis, microgliosis, inflammasome and cytokines levels in the 5xFAD mouse model after silencing RTP801.

18.1. Astrocytic RTP801 contributes to astro- and microgliosis in the in 5xFAD mouse model.

In this aim we focused on neuroinflammation. To investigate the levels of astrogliosis we monitored the levels of glial proteins GFAP and S100β. The major constituent of astrocyte intermediate filaments is GFAP, and it has been the most widely used marker for astrogliosis[276]. Nevertheless, GFAP is not the only and absolute marker of reactivity, for this reason we used it in a combination with S100β. The Ca^{2+} -binding protein S100β is mainly found in reactive astrocytes[277].

By immunofluorescence, we observed that 5xFAD presents higher intensity and numbers of $GFAP^+$ astrocytes in the CA1 and the DG as well. Interestingly, silencing RTP801 in the 5xFAD mice mildly decreased the $GFAP^+$ intensity of in both regions **(Figure 27)**. On the other hand, the intensity and the number of $S100\beta^+$ cells diminished after knocking down astrocytic RTP801 only in the DG of both WT and 5xFAD **(Figure 28)**.

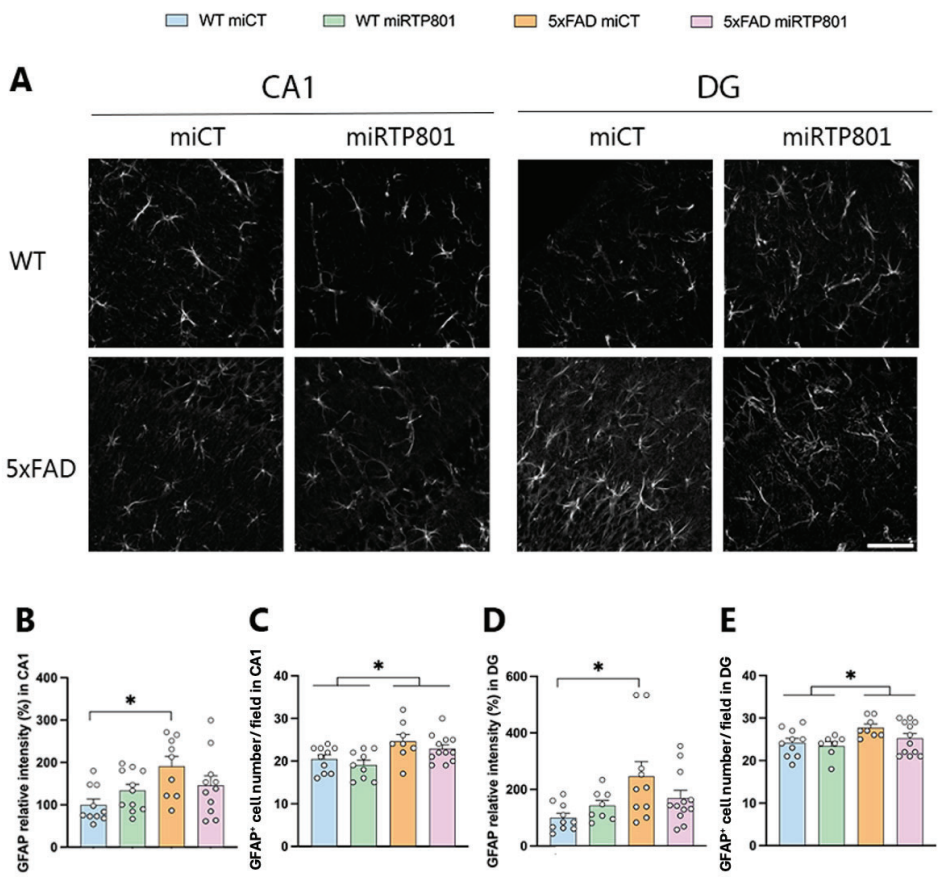

Figure 27. Silencing astrocytic RTP801 mildly recovers astrogliosis in the 5xFAD mice. A) Representative GFAP immunofluorescence microscopy imaging from the CA1 and DG. Scale bar = 50μm. B) Quantification of GFAP intensity in CA1. C) Quantification GFAP+ cells number /field CA1. D) Quantification of GFAP intensity in DG. E) Quantification GFAP+ cells number /field DG. Data are means ± SEM. Two-way ANOVA with Bonferroni's post hoc test was performed: *$p < 0.05$.

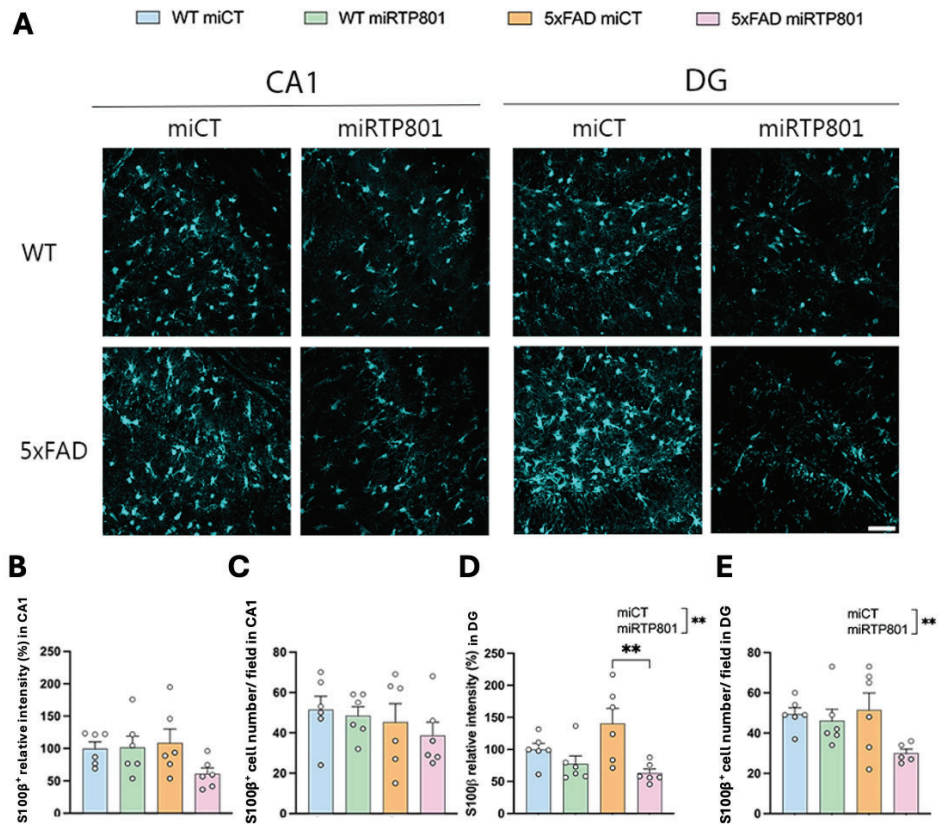

Figure 28. Silencing astrocytic RTP801 recovers astrogliosis in the 5XFAD mice
A) Representative S100β immunofluorescence microscopy imaging from the CA1 and DG. B) Quantification of S100β intensity in CA1. Scale bar = 50μm. C) Quantification S100β+ cells number /field CA1. D) Quantification of S100β intensity in DG. E) Quantification S100β+ cells number /field DG. Data are means ± SEM. Two-way ANOVA with Bonferroni's post hoc test was performed: **p< 0.01.

The removal of interstitial metabolic waste products is accomplished by the glymphatic system, the central nervous system version of the lymphatic system composed by the end-feet of the astrocytes surrounding the blood vessels. AQ4 is a water channel protein, that regulates the extracellular medium's composition and clearance. AQ4 can be found in the perivascular space, in the astrocytic end-feet close to this blood-brain barrier. Furthermore, AQ4 aids in the removal of tau protein and Aβ, which

are linked to AD[278]. Depolarization of AQ4 and a decrease in the clearance of AD-associated proteins are observed in AD pathogenesis[279]. For the abovementioned reason we decided to investigate whether astrocytic RTP801 could affect the levels of AQ4 in a pathological condition such as AD. We observed a significant decrease in AQ4 intensity in the CA1 between the WT and the 5xFAD mice but we did not observe changes after silencing RTP801 in any genotype **(Figure 29).**

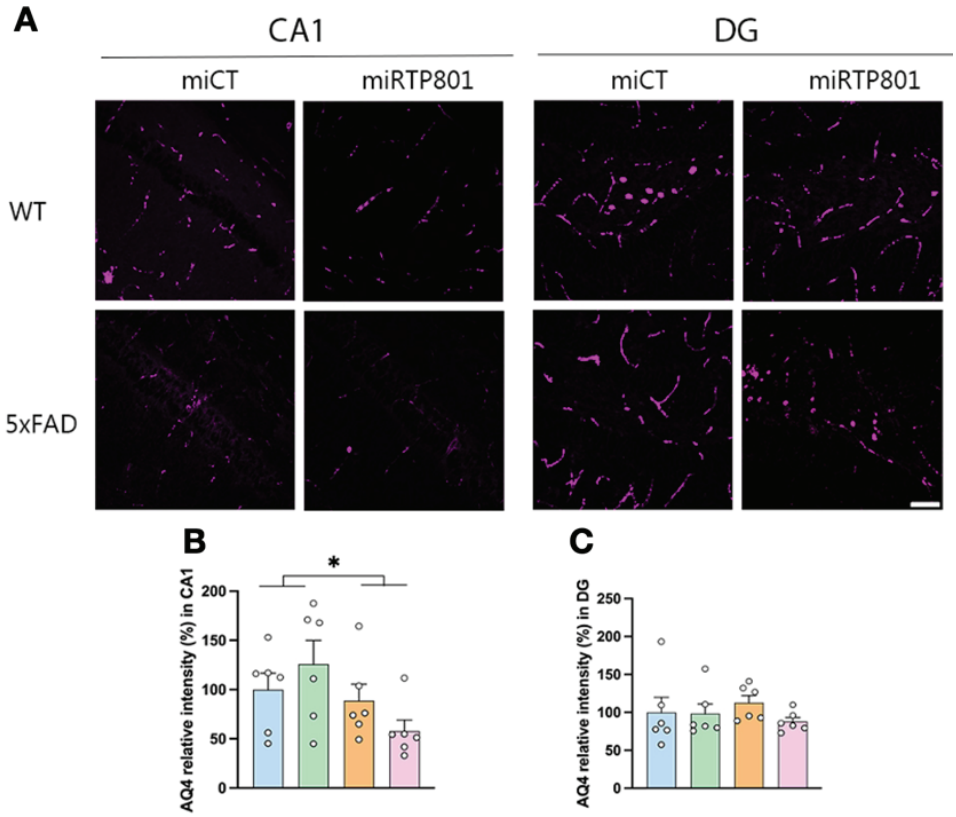

Figure 29. AQ4 protein levels are decreased in the 5xFAD mouse model and are insensitive to astrocytic RTP801 levels. A) Representative AQ4 immunofluorescence microscopy imaging from the CA1 and DG. Scale bar = 50μm. B) Quantification of AQ4 intensity in CA1. C) Quantification of AQ4 intensity in DG. Data are means ± SEM. Two-way ANOVA with Bonferroni's post hoc test was performed: *$p < 0.05$.

We next investigated whether astrocytic RTP801 can affect microgliosis, as we saw with neuronal RTP801 in the 5xFAD mouse model. Indeed, we observed the same effect seen in our previous work after silencing neuronal RTP801[222]. Not surprisingly, in the 5xFAD mice model there are more Iba1^{+} cells both in the CA1 and the DG compared to the WT mice. Interestingly, silencing astrocytic RTP801 mildly prevented this elevation in Iba1+ cells in the 5xFAD mice. This effect was more evident in the DG probably because there were more microglia cells in comparison to CA1. **(Figure 30A-C)**. Unfortunately, this mild effect was not translated to significant changes in microglia morphology in either CA1 or DG **(Figure 30D-G)**.

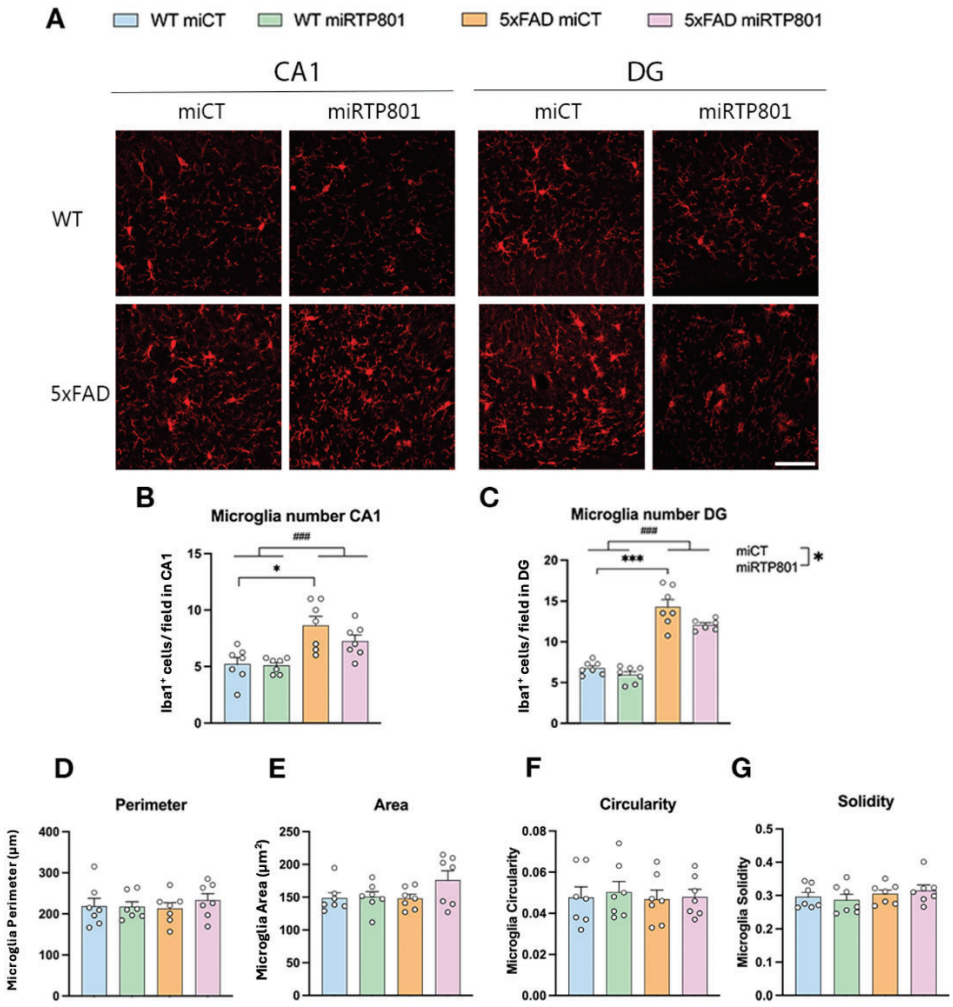

Figure 30. Silencing astrocytic RTP801 mildly prevents microgliosis in the 5xFAD mouse model of AD. A) Representative Iba1 immunofluorescence microscopy imaging from the CA1 and DG. Scale bar = 50µm. B) Quantification Iba1+ cells number/field CA1. C) Quantification Iba1+ cells number/field DG. D) Microglia mean perimeter (µm). E) Microglia mean area (µm^2). F) Microglia mean circularity. G) microglia mean solidity. (Data are means ± SEM. Two-way ANOVA with Bonferroni's post hoc test was performed: *p < 0.05, ***p<0.001, ###p<0.001.

Altogether, these results suggest that normalization of astrocytic RTP801 levels in the CA1 and DG ameliorates astrogliosis and microgliosis, suggesting an important role in neuroinflammation.

18.2. Silencing astrocytic RTP801 change the inflammasome protein levels but does not change the cytokine profile of the 5xFAD mice.

To further gain insight into the hippocampal neuroinflammatory processes mediated by astrocytic RTP801 in the 5xFAD mice, we then evaluated the level of inflammasome effectors and their constituent parts by WB, including NLRP1, NLRP3, ASC and pro-caspase 1. We confirmed that they are upregulated in the 5xFAD vs WT hippocampal lysates and then, we observed that silencing RTP801 in astrocytes reduced the inflammatory response by decreasing the levels of both NLRP1 and NLRP3 **(Figure 31A-B)** in the 5xFAD mouse model. Interestingly, we also observed the same effect over the adapter protein ASC **(Figure 31C)** and the effector pro-caspase 1 **(Figure 31D)**.

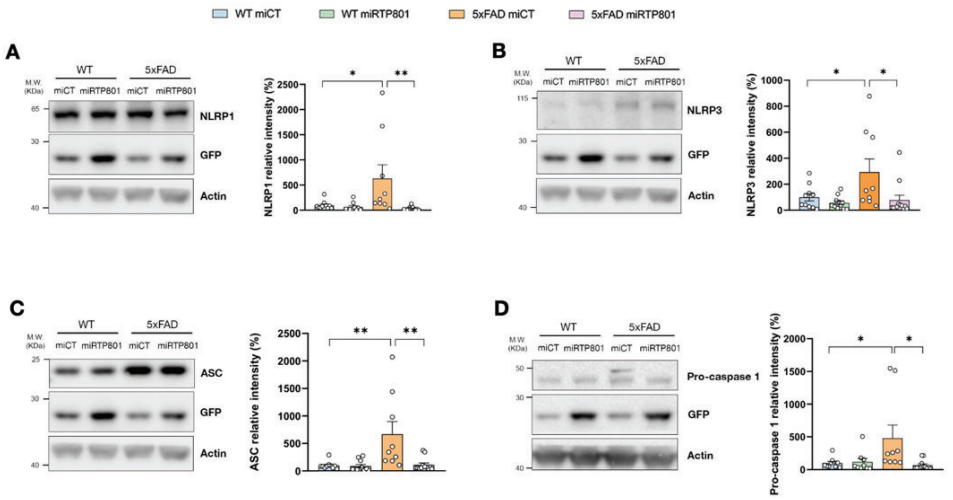

Figure 31. Astrocytic RTP801 contributes to inflammasome activation in a context of AD. Immunoblottings for A) cleaved-NLRP1, B) NLRP3 C) ASC and D) pro-caspase 1 and GFP as loading control for transduced astrocytes in the dorsal hippocampus of 7-month-old WT miCT, WT miRTP801, 5xFAD miCT, and 5xFAD miRTP801 groups of mice. Densitometric quantifications were normalized by GFP levels as readout of astrocytic infection. Data are means ± SEM. Two-way ANOVA with Bonferroni's post hoc test was performed: *p < 0.05, **p< 0.01.

Next, we investigated whether these significant changes in the inflammasome after silencing RTP801 could be translated in differences in the production of hippocampal cytokines and chemokines. We used a customized panel for Luminex detection of cytokines and chemokines in hippocampal lysates from the 4 experimental groups. Although we did not observe significant differences in the levels of IL-1β, IL-6 or IL-4 between any of the 4 experimental groups, we observed an up regulation of osteopontin (OPN), Macrophage colony-stimulating factor (MCSF) and C-C Motif Chemokine Ligand 3 (CCL3) between the WT and 5xFAD mice. However, only CCL3, was mildly affected by RTP801 silencing in the 5xFAD mice, since the statistical difference between WT miCT versus 5xFAD miRTP801 was lost. Overall, further studies with more sensitive techniques will be needed to investigate in depth the role of astrocytic RTP801 in cytokine production **(Figure 32)**.

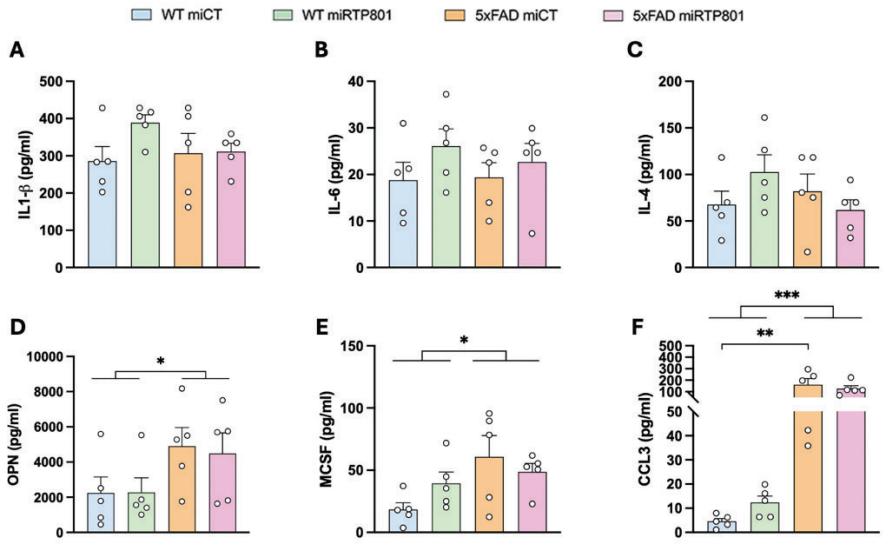

Figure 32. Astrocytic RTP801does not influence the cytokine profile. Concentration in pg/ml of cytokines measured with the Luminex (R&D Systems). (A) IL1-β, (B) IL-6 (C) IL-4 (D) OPN, (E) MCSF(F) and CCL3 (G) in hippocampal lysates of the for groups (WT miCT, WT miRTP801, 5xFAD miCT and 5xFAD miRTP801. Data are means ± SEM. Two-way ANOVA with Bonferroni's post hoc test was performed: *p < 0.05, **p< 0.01, ***p<0.001.

19. *In vitro* approaches to understand the mechanisms of RTP801 in astrocytes in the context of AD

RTP801 regulates several cellular processes, including autophagy, metabolism, oxidative stress, and cell fate. It also plays a role in the pathophysiology of inflammatory and metabolic diseases, cancer, and neurodegeneration. Higher levels of RTP801 often have negative consequences, such as muscular dystrophy, carcinogenesis, metabolic inflammation, and neurodegeneration. RTP801 has been shown to interact with 14-3-3 proteins, IκBα, thioredoxin-interacting protein, or 75 kDa glucose-regulated protein to modulate mTORC1 signaling, NF-κB activation, and cellular pro-oxidant or antioxidant activity, respectively. Its role depends on cell type, cellular context, interaction partners, and cellular localization[192]. Consequently, it is critical to comprehend the molecular processes and biological functions of RTP801 in physiological and disease conditions.

During decades the studies of the CNS have improved considerably by the establishment of *in vitro* models and recently with the establishment of brain organoids. The difficulty of dissecting molecular mechanisms in *in vivo* models is massive. Hence the combination of *in vivo* and *in vitro* approaches is crucial to understand the signaling pathways and the molecular mechanisms associated to neurodegeneration.

For these reasons, we deepened our studies regarding the physiological function of RTP801 using a novel primary culture containing neurons, astrocytes and microglia exposed to Aβ oligomers as a new *in vitro* model of AD.

19.1. Characterization of a novel *in vitro* triculture of neurons, astrocytes and microglia

Neurons, astrocytes and microglia interact closely in the brain, influencing synaptic function, neuroinflammation, and overall brain homeostasis, but in a primary culture this crosstalk is very difficult to reproduce. Hence developing a triculture prepared from the same animal is crucial for accurately studying neurodegenerative diseases, as it better mimics the complexity of the brain's microenvironment.

The supplements included to allow microglia growth were IL-34, cholesterol and TGF-β. The IL-34 is the ligand of the Colony-stimulating factor 1 (CSF1FR) and contributes to the development of microglia[280]. On the other hand, the cholesterol and the TGF-β are necessary for the activation and mobility of microglia during the brain's immune responses[281] and microglial maturation[282], respectively.

First, we characterized the mice primary triculture by immunocytochemistry, staining neurons with MAP2$^+$, astrocytes with GFAP$^+$ and microglia with Iba1$^+$. The triculture at DIV14 presented a 68% of neurons 25% of astrocytes and a 7% of microglia **(Figure 33).**

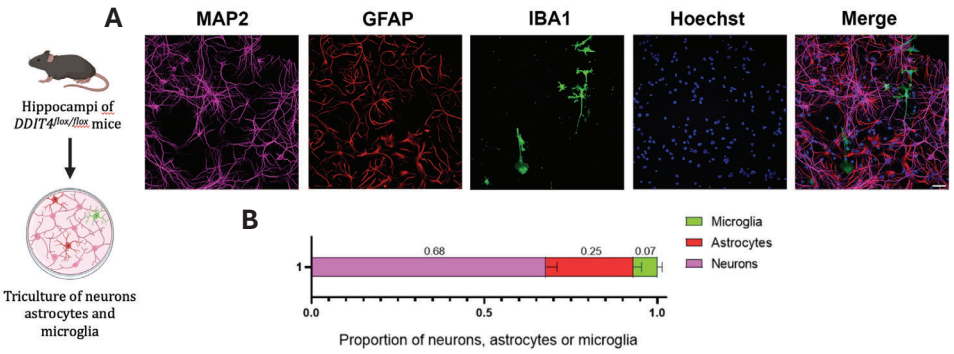

Figure 33. Proportion of neurons, astrocytes and microglia in the mice primary triculture. Cells were subjected to immunofluorescence analysis. MAP2 (magenta), GFAP (red) and Iba1 (green). A) Representative images. Scale bar of 50 μm. B)

Quantification of proportions. Values represented from three independent cultures and are represented as mean ± SEM (n=3).

We also checked whether different populations of astrocytes and neurons were present in the triculture and indeed we found PV$^+$ interneurons and S100β$^+$ astrocytes **(**¡Error! No se encuentra el origen de la referencia. **34).**

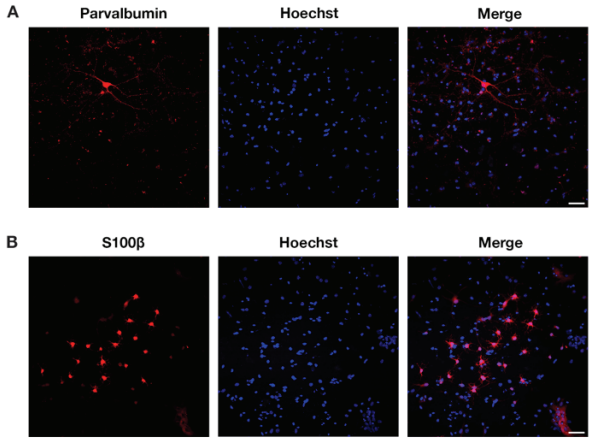

Figure 34. Parvalbumin$^+$ interneurons and S100β$^+$ astrocytes are present in the hippocampal mouse primary triculture. Immunocytochemistry for A) Parvalbumin or B) S100β (red) was performed. Representative images are shown. Scale bar of 50 μm.

We also performed an immunostaining of PSD95 and VGLUT markers of presynaptic and post-synapsis, to check the presence of synapses in the triculture model. We observed the presence of clusters PSD95/VGLUT **(**¡Error! No se encuentra el origen de la referencia. **35)**. However, further characterization of the synapses is needed to conclude that the neurons are completely mature and functional.

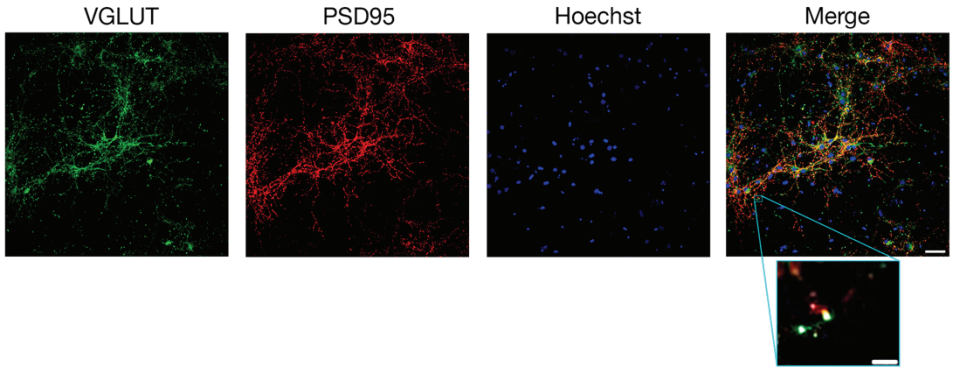

Figure 35. Presence of PSD95/VGLUT clusters in the mice primary triculture. Cells were subjected to immunofluorescence analysis. VGLUT (green) and PSD95 (red). Scale bar of 50 μm and 5 μm.

These results validated our novel hippocampal triculture model to study neuroinflammation.

19.2. Study of the toxicity of Aβ in the hippocampal triculture model

Aβ, has been extensively used to mimic certain conditions given in AD due to its toxicity. Research on Alzheimer's disease (AD) initially focused on amyloid plaques composed of Aβ. However, plaque burden didn't correlate with disease severity, as plaques were found in cognitively normal individuals. This led to a shift in focus to smaller, soluble Aβ oligomers, which were shown to cause cognitive deficits even without plaques. Studies revealed these oligomers as the toxic species, forming protofibrils that trigger inflammatory responses and neurotoxicity. Research suggests a common toxic mechanism across amyloid diseases, involving interactions with receptors and cell membranes[283]. To study whether this novel triculture is sensitive to Aβ and whether astrocytic RTP801 is directly involved in such toxicity we treated the triculture at DIV10 with 0,5 μM Aβ oligomers for 24 h. These oligomers were prepared

two days before treatment. We used the same proportion of DMSO as vehicle.

Aβ decreased the number of neurons, did not change the number of astrocytes but increased the number of microglia. Moreover, we confirmed the presence of oligomers in the triculture by immunostaining against Aβ. **(**¡Error! No se encuentra el origen de la referencia. **36).**

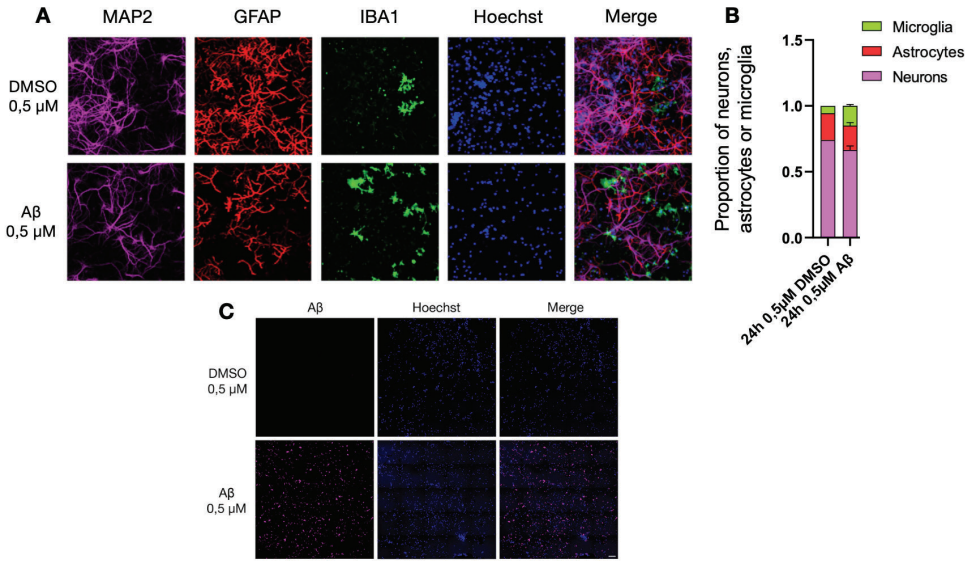

Figure 36. Characterization of the mice primary hippocampal triculture after $A\beta_{1\text{-}42}$ oligomer treatment for 24 hours. A) Representative images, cells were subjected to immunofluorescence analysis. MAP2 (magenta), GFAP (red) and Iba1 (green). Scale bar= 50 µm. B) Proportion of neurons, astrocytes or microglia. C) Immunocytochemistry of Aβ oligomers. Scale bar = 100 µm

19.3. Silencing Astrocytic RTP801 diminishes the complexity of astrocytes' morphology

To investigate whether astrocytic RTP801 contributed to Aβ toxicity, we knocked out *DDIT4* over expressing the Cre recombinase under the GFAP promoter in primary tricultures prepared from $DDIT4^{flx/flx}$ mice Specifically we used the rAAV5-GFAP-GFP-Cre or the rAVV5-GFAP-eGFP

(as a control) adeno-associated viral particles at DIV10 and at DIV14, cultures were treated with $A\beta_{1-42}$ oligomers for 24 h. Following the treatment the cells were fixed, and immunocytochemistry experiments were performed. First, we confirmed the knockout of RTP801 in astrocytes by immunostaining. Note that in controls, eGFP expression is staining the whole astrocyte but in the Cre overexpression, the staining is reduced to the nuclei, as expected **(Figure 37)**.

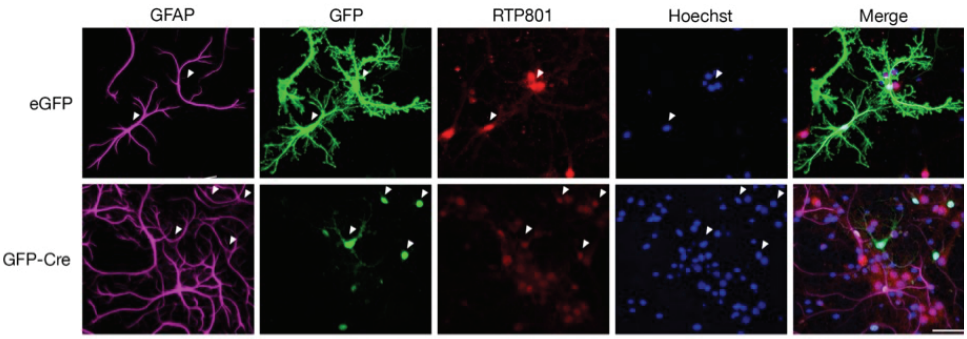

Figure 37. RTP801 expression was silenced in the hippocampal triculture model. Cells were treated at DIV10 with rAAV5-GFAP-GFP-Cre to knock out RTP801 or with rAAV5-GFAP-eGFP as a control for 5 days. Representative images, cells were subjected to immunofluorescence analysis. Astrocytes (GFAP, magenta), transduced astrocytes (GFP, green) and RTP801 (red). Scale bar = 50 μm.

Following the RTP801 silencing validation, we characterized the astrocytes phenotype after Aβ treatment. After immunocytochemistry, the relative intensity of GFAP was measured and the number of $GFAP^+$ cells was counted, but any difference was observed among conditions **(Figure 38)**

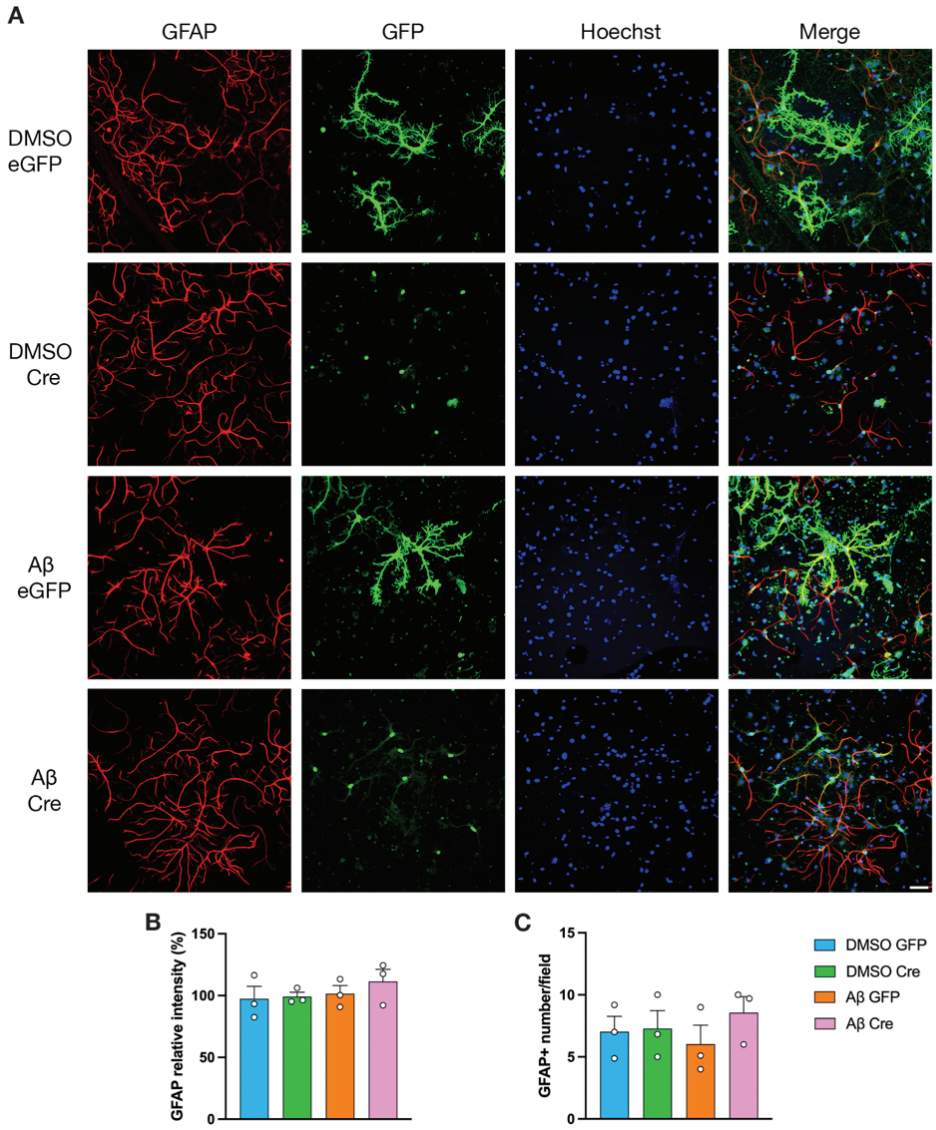

Figure 38. RTP801 does not affect GFAP intensity or in GFAP⁺ cell number in a mouse primary hippocampal triculture. A) Representative images, cells were subjected to immunofluorescence analysis. GFAP (red) and GFP (green). Scale bar= 50μM. B) Quantification GFAP relative intensity (%) C) Quantification of GFAP⁺ number of cells in each field. Values of three independent cultures are represented as mean ± SEM(n=3).

Historically, astrocytes were recognized as a distinct cell type due to their distinctive appearance. It's now known that the description of astrocytes as "star-like cells" is oversimplified and that they have very complex

morphologies. In fact, every single mature protoplasmic astrocyte found in the gray matter is composed of a soma, major branches and numerous smaller branchlets and leaflets that contact synapses. These branchlets and branchlets are commonly referred to as processes, sheets, or alternatively as perisynaptic or peripheral astrocyte processes (PAPs). The diameter of an astrocyte territory in rodent hippocampi can be of approximately 40–60 μm, while branches, branchlets, and leaflets make up 90–95% of an astrocyte's surface area. Interestingly, immunostaining for GFAP can only estimate approximately 15% of the total astrocyte. Even with the widespread use of diffraction-limited light microscopy, their PAPs have not been precisely quantifiable, leaving the organization of astrocyte morphology a mystery [284].

For this reason, here, in an attempt to have a wider perspective, we measured the amount of primary and secondary processes, being the primary processes, the major branches coming out the soma and the secondary processes the branches coming from the major branches. We observed that RTP801 silencing reduced astrocytes' complexity by reducing the number of secondary branches or processes **(**¡Error! No se encuentra el origen de la referencia. **39)**.

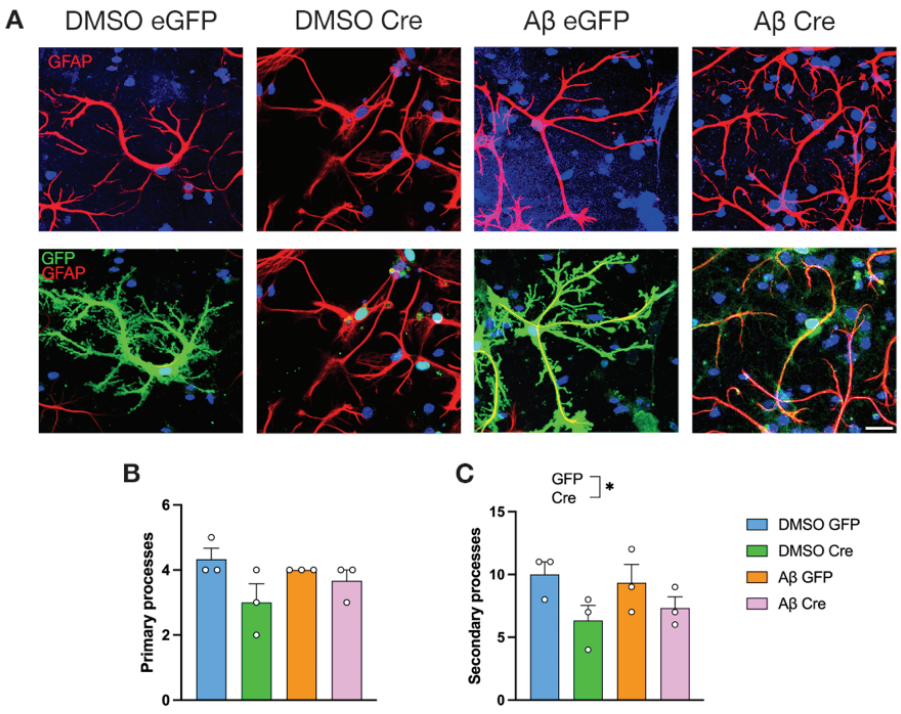

Figure 39. Astrocytic RTP801 contributes to increase astrocytic complexity. A) Representative images of cells were subjected to immunofluorescence analysis. GFAP (red) and GFP (green). Scale bar= 50μM. B) Quantification of primary processes (major branches) C) Quantification of secondary processes. > than 15 astrocytes were analyzed for each condition. Values of three independent cultures are represented as mean ± SEM(n=3). *p<0.05

19.4. Silencing astrocytic RTP801 diminishes the number of Aβ oligomers

Finally, we performed a staining of the Aβ oligomers to see if there was a difference in the number of oligomers by silencing astrocytic RTP801. We observed that after knocking out astrocytic RTP801 with the rAAV5-GFAP-GFP-Cre for 5 days and treating the cells with 0,5 μM of $A\beta_{1\text{-}42}$ for 24 h, the number of Aβ oligomers diminished comparing with the control rAAV5-GFAP-eGFP, suggesting a role of astrocytic RTP801 in the Aβ engulfment and degradation **(Figure 40).**

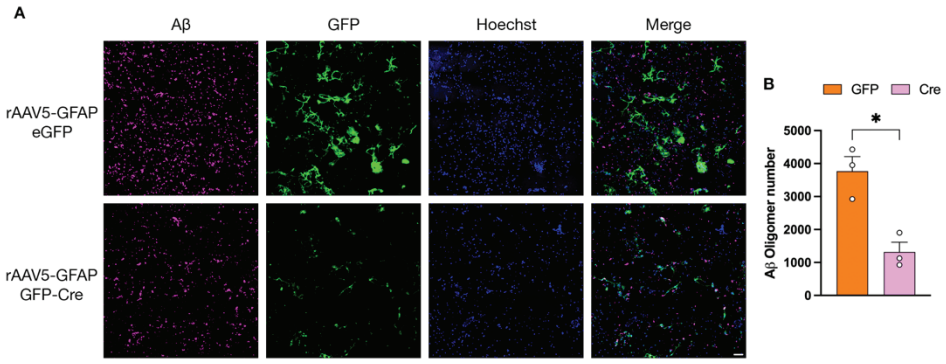

Figure 40. Silencing RTP801 decreases dramatically the Aβ oligomers in the triculture. Astrocytic RTP801 was knocked out by Cre recombinase expression under GFAP promoter at DIV10 and then the tricultures were exposed to 0,5uM Ab oligomers for 24 h and then cells were subjected to immunofluorescence analysis. A) Representative images, Aβ (magenta) and GFP (green), nuclei were visualized by Hoechst 33325 (blue). Scale bar = 50 μm. B) Quantification of $A\beta_{1\text{-}42}$ oligomer numbers. Values of three independent cultures are represented as mean ± SEM(n=3).

DISCUSION

20. Astrocytic RTP801 implications in neurodegeneration

With aging populations, both the prevalence of neurological disorders and the cost of patient care is rising. The discovery of disease-modifying medicines is hampered by the intricate biology of neurodegenerative diseases. In fact, current therapies mostly focus on symptom relief as opposed to solve or modify the underlying causes. Therefore, dissecting specific molecular mechanisms are essential to create effective pharmacological treatments to stop neurodegeneration.

The development of AD is significantly influenced by mTOR kinase signaling, an important regulator of numerous cellular and metabolic processes. Aggregation of Aβ is encouraged by autophagy inhibition caused by mTOR activation. Therefore, there is strong evidence that Aβ deposits cause mTOR to become hyperactivated, which then hyperphophorylates Tau that will evolve into NFTs [285]. In line with this notion, research on cell culture and animal models revealed that introducing Aβ oligomers into animal models causes mTOR hyperactivity, in a dose dependent manner[286]. After mTOR activity upregulation, its regulators start to increase their expression to keep pace in the modulation of the kinase. Among the many altered components of this signaling pathway, we can find RTP801.

It has become clear that RTP801 plays a significant role in the pathogenesis of neurodegenerative diseases like Parkinson's, Alzheimer's, and Huntington's. Unlike mTOR activity, which varies depending on the disease and the disease stages, and its regulation remains controversial, RTP801 levels seems to be consistently upregulated under neurodegenerative conditions.

Here in this work, we addressed for the first time the putative role of astrocytic RTP801. Our work demonstrates that the hippocampal

astrocytes of the 5xFAD mice model of AD have elevated levels of RTP801. Furthermore, by precisely silencing astrocytic RTP801, we prevented the appearance of cognitive impairment by reducing brain inflammation and hyperconnectivity. In specifics, compared to WTs, 5xFAD mice showed worse spatial memory, lower GABA levels along with fewer PV^+ interneurons, astrogliosis, microgliosis, and increased inflammasome components in the hippocampus. They also displayed functional hyperconnectivity in several resting state brain networks. Surprisingly, RTP801-specific silencing in astrocytes blocked the appearance of these features at some point.

In addition, our studies reveal the utility of a new *in vitro* triculture model containing neurons, astrocytes and microglia derived from the same animal to study neuroinflammatory events. Using the triculture, we elucidated the new role of astrocytic RTP801 in Aβ oligomer clearance. Altogether, our results proposed specifically astrocytic RTP801 as a promising therapeutic target for AD treatments.

20.1. Astrocytic RTP801 contributes to cognitive decline

The role of RTP801 in neurons has been vastly studied by our and other groups, defining its pro-apoptotic nature in high levels. However, the role of RTP801 in astrocytes was not yet elucidated. For example, by Deep Single Cell RNA sequencing it was found that there were higher levels of *DDIT4* mRNA in astrocytes compared to neurons both in humans and mice[160]. In this line, the cortical subplate and the hippocampus are the brain areas with higher amount of *DDIT4* mRNA, according to the Allen Brain Atlas[287]. Despite this evidence, the contribution of astrocytic RTP801 in AD has not been thoroughly investigated. Hence, for the first

time, we explored the specific role of astrocytic RTP801 in AD pathophysiology.

In the previous study comparing 5xFAD mice to WT mice, our group found that RTP801 levels were similarly significantly elevated in both hippocampal neurons and astrocytes. Moreover, silencing specifically neuronal levels of RTP801 with neuron-specific AAVs, also reduced the levels of RTP801 in astroglia in the 5xFAD mice[222]. This suggested that neuronal RTP801 mediates an effect from neurons to glial cells in the 5xFAD mice. With this background, we investigated the role of this protein in the hippocampal astrocytes using the 5XFAD mouse model of AD and its putative contribution to neurodegeneration as well as its influence in intercellular communication.

We discovered increased amounts of RTP801 in astrocytes of the 5xFAD mouse hippocampus both in CA1 and DG in comparison to WT. Similarly, it was discovered that the *DDIT4* gene, which codes for RTP801, is an essential regulator of Aβ toxicity, as there is a clear correlation between RTP801 levels and Aβ toxicity. Additionally, AD postmortem brains correlated with Braak and Thal phases with higher levels of RTP801 protein and higher levels of *DDIT4* mRNA in patient lymphocytes[288]. Increased levels of RTP801 can be due to Aβ mediated induction of *DDIT4* transcription[289] or by decreased proteolysis[290]. However, none of the earlier research addressed the precise mechanisms of induction specifically in astrocytes. For example, the levels of RTP801 protein in AD postmortem brains correlated with Braak and Thal phases. However, we addressed this question by assessing total protein levels by WB, and not by cell-specific immunohistochemistry.

There are many reasons to study glia cells contribution to behavior as astrocytes have been identified as important memory formation

regulators[291]. Moreover, astrocytes are crucial for synaptic plasticity phenomena including long-term potentiation[292].

Like human AD patients, the 5xFAD mouse model has substantial deficits in associative and spatial learning[293]. In terms of amyloid pathology, the disease progresses more quickly in female 5xFAD mice versus males, but there are no sex-related variations in the amount of the Aβ oligomer accumulation[294]. However, 5xFAD male mice show a more consistent cognitive impairment in the Y-maze and Morris water maze tests[295]. For these reasons, in this thesis we used only male animals. We assume that this is the major limitation of our study and females will be considered for further investigations on this topic.

Behavioral testing verified that precisely suppressing RTP801 expression in $GFAP^+$ astrocytes of the 5xFAD hippocampus led to a significant prevention of cognitive impairment. On the other hand, knocking down RTP801 partially restored the anxiety-like behavior, in agreement with bibliography supporting that 5xFAD animals are less anxious[296]

During the Plus maze, 5xFAD mice tend to spend more time and run more distance in the open arm, indicating that they are more relaxed than the WT mice, who prefer to spend more time hidden in the closed arms. In a previous study, 5xFAD mice exhibited an age-dependent reduction in anxiety. The ratio of open arm entries to total arm entries was calculated to validate this, and the results showed that the 5xFAD mice that were 6, 9, and 12 months old had significantly greater ratios than the WT animals at the same age[297]. In this line, study carried by Flanigan *et al.,* 2014, reported normal anxiety but impaired cognition and social behavior in 5xFAD transgenic mice[298]. Jawhar *et al.*, (2012), replicated these results, observing an age-dependent increase in open-arm time in these mice. However, instead of decreased anxiety, they suggest that this behavior is

due to the mice avoiding the closed arms and failing to habituate during the session. This avoidance may be linked to abnormal or excessive vibrissa sensation, potentially caused by decreased tonic inhibition or impaired sensory integration following the loss of inhibitory innervation[297]. Surprisingly, knocking down astrocytic RTP801 prevented that phenotype in the 5xFAD mice versus the WTs. It has been described that hippocampal astrocytes modulate anxiety-like behaviors in mice by controlling hippocampus DG granule cells' ATP-mediated synaptic homeostasis[299]. Hence, astrocytic RTP801 might be contributing to this phenotype by modulating the function of the hippocampal synapses, in line with the tripartite synapse theory postulated by Araque *et al.* (1999)[300]. Further studies will be needed to elucidate the exact mechanism behind astrocytic RTP801 as an anxiety-like modulator in the context of AD.

The Morris water maze test confirmed that 5XFAD mice[301,302] as AD patients[303] display severe impairments in spatial memory. However, after astrocytic RTP801 downregulation, the 5xFAD mice performance in this test was preserved, in line with previous studies where RTP801 silencing in WT mice treated with Aβ[304] or RTP801 silencing in hippocampal neurons prevented cognitive decline[222].

Despite these behavioral characteristics, RTP801 silencing did not result in changes to amyloid plaque load, suggesting that astrocytic RTP801 does not affect Aβ homeostasis in AD. This is consistent with our earlier research in which we inhibited neuronal RTP801, and no alterations in Aβ plaque load were noted[222]. When Aβ monomers misfold they clump together to create bigger soluble Aβ oligomers that are thought to be the most harmful forms of Aβ. Protofibrils are the largest of these oligomeric types. In contrast to insoluble immobilized Aβ plaques, these extremely toxic Aβ oligomers and protofibrils are free to travel across membranes or

across various cellular compartments, wreaking havoc both intracellularly and extracellularly[305]. Other research that examined postmortem AD brains and found no clear association between plaque formation and synapse/neritic loss further reinforced that idea[306,307]. Several researchers found that cognitive abnormalities in transgenic mouse models of AD developed prior to plaque formation or the discovery of insoluble amyloid aggregates in their brains, suggesting a gap between plaque disease and memory impairment[308]. So, we investigated further the causes why silencing astrocytic RTP801 was beneficial in 5xFAD mice.

In AD patients, the morphology of DGCs worsens as the disease progresses. Patients at Braak-Tau I/II stages first exhibit an unusually high number of DGCs with several major apical dendrites as their initial morphological change which increases with the disease advances[246]. This phenomenon is also seen in the 5xFAD mouse model. In this line, after astrocytic RTP801 silencing in the 5xFAD mice, the percentage of DGCs with only one apical dendrite increases. The abnormal phenotype of DGCs in AD patients may be partially driven by distinct non-cell-autonomous disturbances of DG homeostasis. In this way, pro-inflammatory stimuli change the shape of DGCs in mice[309]. It's interesting to note that during spatial exploration, the amount of primary apical dendrites of murine DGCs is negatively correlated with neuronal activity[310]. Hence, knocking down astrocytic RTP801 in hippocampus of 5xFAD mice prevents this aberrant change in DGCs morphology, possibly contributing to the cognitive symptoms' amelioration **(Figure 41)**.

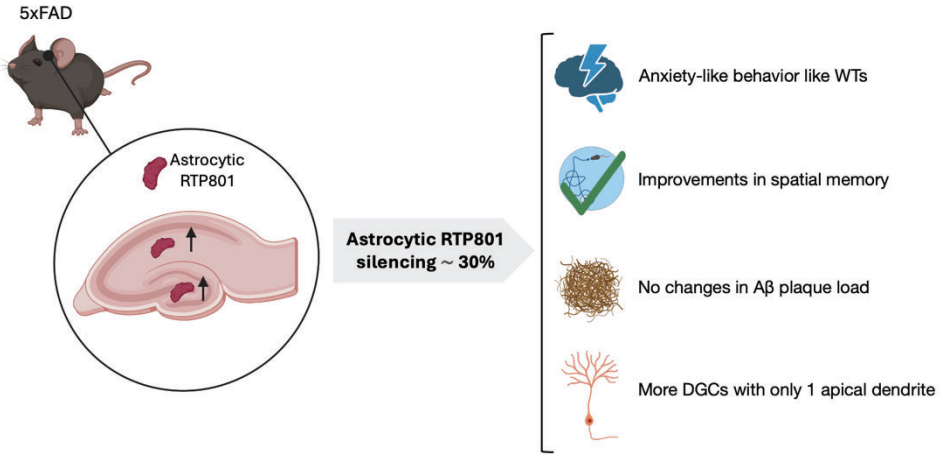

Figure 41. Phenotype characteristics of the 5xFAD mice after silencing RTP801 in hippocampal astrocytes. Figure generated with Biorender software.

20.2. Astrocytic RTP801 as a modulator of resting state functional connectivity in the context of AD

Neuroimaging techniques, mainly MRI and positron emission tomography (PET) are being increasingly used to investigate neuroimaging features in AD mouse models and provide the basis for rapid translation to the clinical setting[311]. For instance, age-dependent microstructure alterations in 5xFAD mice have been demonstrated by T1- and T2-weighted imaging and high-resolution diffusion tensor imaging[312]. Moreover, using *in vivo* resting-state fMRI and *ex vivo* Diffusion tension imaging (DTI), the organization of the functional and structural connectomes has been also studied in 5XFAD transgenic mice showing disconnection within the whole-brain network with less efficient routes taken for information exchange and hypercorrelation of structural and functional connectivity compared with WT animals[313]. Indeed, altered functional connectivity, as determined by rs-fMRI, is often regarded as a possible preclinical biomarker of AD[314]. However, to our

knowledge this is the first study in 5xFAD mice showing alterations in resting state networks (RSN) by independent component analysis (ICA).

The medial prefrontal cortex (mPFC), posterior cingulate cortex or precuneus, and bilateral inferior parietal cortices are among the core brain regions of the DMN. A set of supplementary brain regions, such as the medial temporal lobes and temporal poles, are also considered to be part of this network[315]. We have identified alterations in hippocampus, entorhinal cortex and regions of the DMN whose interconnectivity contributes to age-related alterations in memory[316]. The DMN is known to exhibit disrupted connectivity in Alzheimer's disease, contributing to important cognitive deficits both in patients[317] and in animal models[254]. Our results demonstrate that 5xFAD mice show hyperconnectivity within DMN, which can be restored by silencing RTP801.

We observed the same effect after knocking RTP801 in the salience network (SN), also affected in AD[255]. The dorsal anterior cingulate (dACC) and frontoinsular (FIC) cortices make up most of the SN, which is responsible for selecting the most pertinent internal and external stimuli from a variety of sources in order to direct behavior[318]. According to certain theories, FIC is essential for transitioning between the DMN and the central executive network (CEN)[319], which are known to interact negatively during cognitive information processing[320]. FIC functions to distinguish noteworthy stimuli from the extensive and constant flow of sensory system inputs. When the FIC detects a salient stimulus, it disengages the DMN and sends the proper temporary control signals to the CEN, which mediates attention, working memory, and other higher order cognitive functions[318].

Autonomic network, where the mammillothalamic tract is thought to be a middle channel that uses the anterior thalamus to transmit information

from the hippocampal region to the frontal cortex[321], and lateral cortex network which have also been related to spatial memory deficits showed a similar profile, pointing altogether to a therapeutical effect of astrocytic RTP801 inhibition. Our results, suggest that there might be changes in the excitatory/inhibitory input in all these networks.

20.3. GABAergic signaling and interneuron changes in the 5xFAD mice hippocampus after RTP801 silencing

Transgenic rodents and AD patients' brains have both been shown to exhibit metabolic alterations in hippocampus[322]. Our MRS study revealed that 5xFAD miCT animals have the same amount of aspartate, glutamine, glutamate, glycine and glutathione as the WT miCT animals, in contrast in different MRS studies carried in different AD mice models as the Tg2576 lower levels of glutamate were reported[323]. However, in the 5xFAD this decrease has been reported at 9-months old[324], therefore, we probably do not see this change in glutamate due to the age of our animals (7.5 months old) at the time MRS was performed. As reported in Andersen *et al.* 2021 the levels of glutamine and aspartate remained similar in 5xFAD mice after 4 months old[325]. On the other hand, in line with our results, no changes in glycine have been reported in the hippocampus, while lower levels are detected in the cortex and the thalamus of 5xFAD mice[326].

We reported a decrease in the NAA (N-acetyl aspartate) neuronal marker in the 5xFAD mice. These findings correlate with previous studies[324,327]. In fact, NAA stabilizes proteins, suppresses protein aggregation, solubilize already formed aggregates[328] and has been proposed as a potential biomarker of brain dysfunction in AD patients[322]. Furthermore, we observed a decrease in the glucose amounts in the 5xFAD hippocampus which become more evident after knocking down astrocytic RTP801. In

accordance with previous studies which described reduced glucose metabolic activity in hippocampus of the 5XFAD mice[329]. Finally, taurine showed the same effect, this metabolite is reported to have a neuroprotective effect against dementia[330].

In agreement with previous MRS studies[324,331], our results showed lower GABA levels in the 5xFAD. Stunningly, silencing astrocytic RTP801 mildly recovers the GABA levels, close to the ones seen in the WT mice. Hence, we postulate that astrocytic RTP801 is responsible for the lower levels of GABA in the 5xFAD mouse brains and their the hyperconnectivity in the RSN, since RTP801 silencing normalized both the levels of GABA and the connectivity **(Figure 42)**.

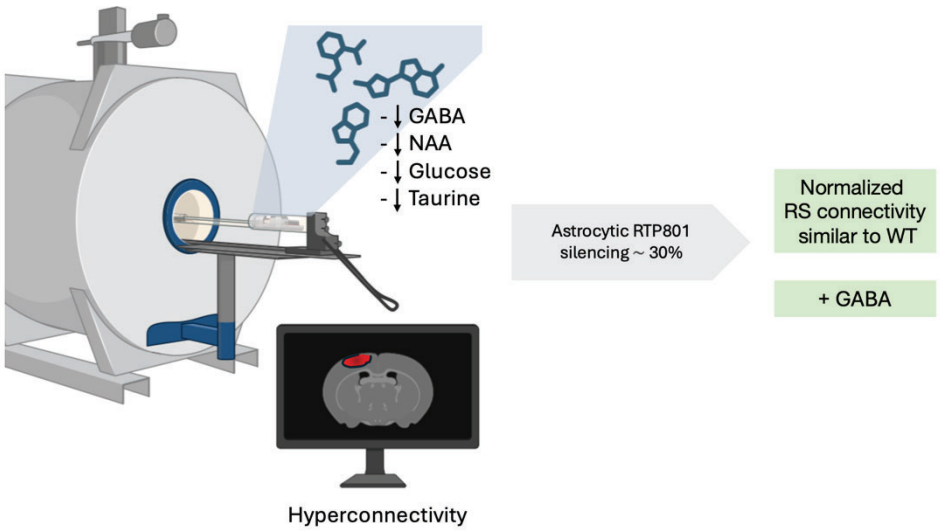

Figure 42. Changes in resting-state functional connectivity and metabolite concentrations in the 5xFAD mice model which were reverted after silencing astrocytic RTP801 in the hippocampus. Figure generated with Biorender software.

Related with the previous result, we observed lower numbers of PV^+ neurons in the 5xFAD miCT mice versus WT mice. Indeed, the 5xFAD

miRTP801 strikingly showed higher number of PV+ interneurons both in the CA1 and the DG. Moreover, PV+ cells were smaller in the DG of the 5xFAD miCT mice and seem to be bigger after silencing RTP801. Our findings are in line with other studies which use different mouse models that discovered lower density of PV-immunoreactive neurons in the entorhinal and piriform cortices[332], as well as in the hippocampal CA1 and CA2[333]. Our results also agree with studies reporting degenerating PV+ neurons in AD patients[334]. As PV+ interneurons are one of the most sensitive cells to ROS[335]. We speculate that astrocytic silencing protects interneurons from ROS.

GABAergic interneurons, particularly PV+ interneurons, make up most cells that a PNN encases[261] and it appears to shield PV+ interneurons from oxidative stress[263]. Our results showed lower amount of PNN in the CA1 which are recovered after knocking down RTP801. However, the recovery is not seeing in the DG, probably due to the lower amounts of PV+ and PNN in this area. Importantly the percentage of PV+ interneurons covered by a PNN stained by WFA does not change among conditions. Remarkably, WFA do not stain every PNN in the brain as reported in the literature[268], hence this can be a limitation of the study. In addition, although we put our focus on study the PNN as the main cellular matrix to enwrap inhibitory PV+ neurons, there are further components which need to be studied in the future**.** We hypothesized that astrocytic RTP801 change the astrocytic secretome which release different matrix component to the extracellular space.

The levels of GAD65/67 were higher in the CA1 of 5xFAD mice compared to WT. Controversially, to the study carried by Lazic *et al.* 2020, authors found lower levels of GAD65 in the cortex of 5xFAD mice[336]. Nevertheless, other studies reported that astrocytes of the 5xFAD mice hippocampus contained higher levels of GAD67 compared to WT at 6 months old[337]. We

therefore speculate that astrocytes try to compensate the loss of GABA by the interneurons' death in the hippocampus by increasing GAD65/67 expression **(Figure 43)**.

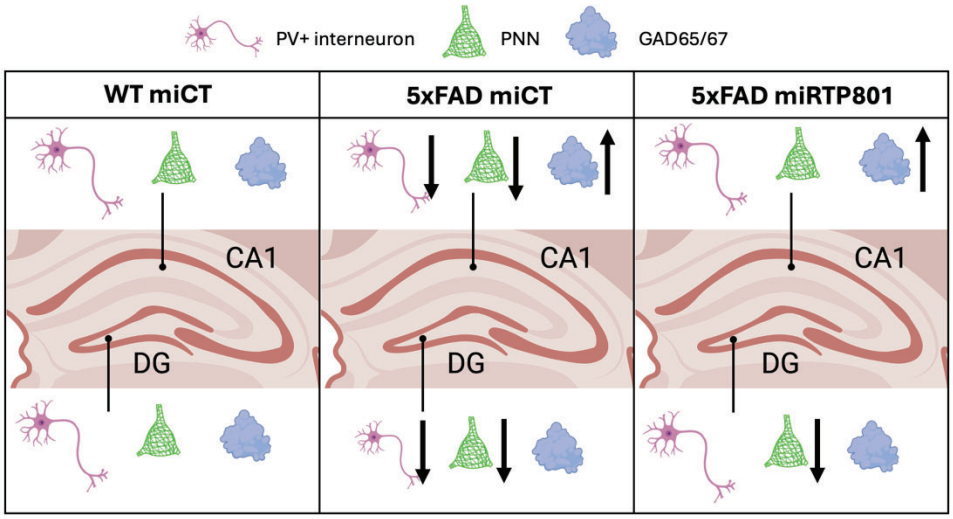

Figure 43. PV+, PNN and GAD65/67 in the hippocampus of the three different groups of animals: WT miCT, 5xFAD miCT and 5xFAD miRTP801. Figure generated with Biorender software.

21. Implications of astrocytic RTP801 in neuroinflammation

The beginning and progression of neurodegenerative disorders were postulated to be caused by a multi-component phenomenon known as "damage signals" in the 2008 publication "Theory of Neuroimmunomodulation," which raised the possibility of "multitarget" therapy for AD. This theory provides a detailed explanation of the series of molecular events that result from the overactivation of the Cdk5/p35 pathway and microglial dysfunction. The logical search for inflammatory druggable targets against AD has been made possible by all of these insights. The body of research demonstrating elevated levels of

inflammatory markers in AD patients' cerebrospinal fluid (CSF) and descriptions of CNS changes brought on by senescent immune cells in neurodegenerative diseases established a conceptual framework within which the neuroinflammation theory is being questioned from various perspectives in an effort to create novel treatments for AD[338].

One published characterization of the 5xFAD mouse model showed increases in microglial densities in the cortex of the mice starting at 8 months of age and in the hippocampus starting at 4 months of age. Immunostaining for S100β reveals markedly higher astrocyte densities in the brain and hippocampus of 5xFAD animals at 18 months of age as compared to WT mice. In the hippocampal regions, $GFAP^+$ astrocytes exhibit S100β patterns, with increased $GFAP^+$ cells visible between the ages of 8 and 18 months[339]. So, we studied astrocytic RTP801 as a possible therapeutic target to avoid neuroinflammation. We assessed the astro- and microgliosis in all the mice groups and of microglia cells in the 5xFAD. All of these neuroinflammatory events were partially or totally rescued by silencing astrocytic RTP801.

Another mechanism by which RTP801 regulates neuroinflammation is increasing the expression levels of the inflammasome proteins NLRP3, NLRP1, pro-caspase-1 and ASC. Previous studies demonstrate that dismissing its expression is beneficial in the context of AD. For instance, inhibiting NLRP3 in the TgCRND8 mice model showed fewer insoluble $A\beta_{1\text{-}42}$ in mice brains[340] and in the brains of 5xFAD mice with the ASC +/- genotype there was a notable reduction in the number of amyloid plaques[341]. To complement the *in vivo* results, we performed *in vitro* experiments using cultures of neurons with a 20% of astrocytes and demonstrated that even in physiological conditions RTP801 regulates the levels of NLRP1 inflammasome as knocking down RTP801 leaded to lower

levels of NLRP1 and overexpression of RTP801 leaded to higher levels of RTP801 **(Annex figures 47-48)**.

However, these changes in the inflammasome components levels are not correlated with the cytokines' levels detected by the Luminex array panel. Further studies with more sensitive techniques and more animals will be needed to investigate in depth the role of astrocytic RTP801 in cytokine production.

We found higher concentrations of OPN and MCSF in the 5xFAD mice hippocampus compared to WT. According to the literature, improved cognitive performance is the outcome of genetically ablation of OPN in the 5XFAD mice, which lowers proinflammatory microglia, plaque formation, and the quantity of dystrophic neurites[342]. Nonetheless, only CCL3 seems to be partially normalized by astrocytic RTP801 silencing. CCL3 seems to be detrimental for hippocampal proper functioning as reported by Marciniak *et al.* 2015, they found that CCL3 reduced LTP and impaired spatial and long-term memory[343] **(Figure 44)**.

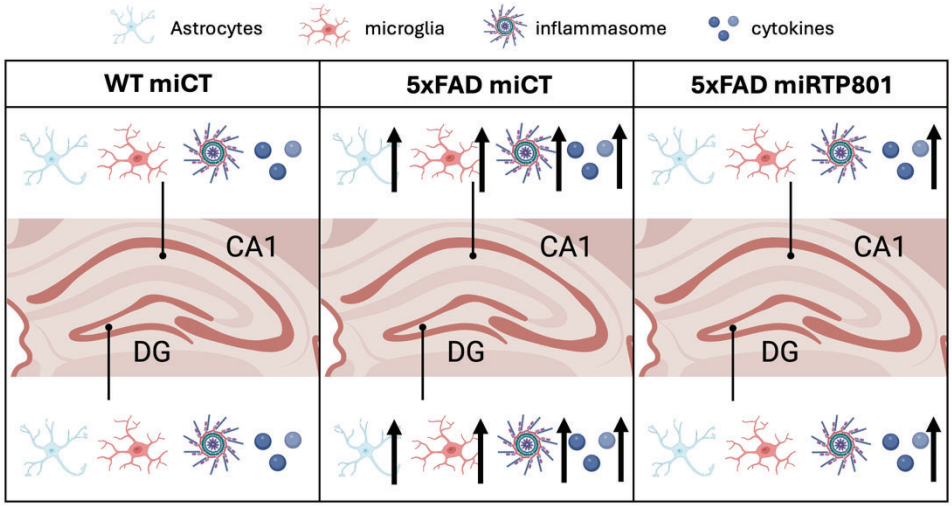

Figure 44. Astrocytes, microglia, inflammasome components and cytokines in the hippocampus (CA1 and DG) of the WT miCT, 5xFAD miCT and 5xFAD miRTP801. Figure generated with Biorender software.

Previous studies described the activation of the NF-κB pathway by RTP801 in macrophages by interacting with and sequestering IκBα[344]. In Müller glia cells it enhanced IKK-dependent degradation of IκBα[345]. Here we speculate that silencing astrocytic RTP801 could be limiting the NF-κB pathway in this way reducing the expression of inflammasome components, which are downstream of NF-κB[346].

Neuroinflammation may also be the cause of the imbalance between glutamatergic and GABAergic synapses[347]. This is because TNFα causes a rapid and long-lasting reduction in the inhibitory synaptic strength[348], which affects the homeostasis of neuronal circuits and may make excitotoxic damage from neuronal insults worse[349].

Considering all the previous results, we propose the following model; neuroinflammation leads to release of cytokines and reactive oxygen species (ROS) which can damage neurons. In fact, PV^+ interneurons are one of the most sensitive cells to these ROS[335]. Since we see

hyperconnectivity, lower levels of GABA and fewer PV+ interneurons in the hippocampus of the 5xFAD mouse model of AD, we suspect that partially suppressing the expression of astrocytic RTP801 is having a protective effect. Hence, the suppression of astrocytic RTP801 may be sufficient to correct neuroinflammatory processes, leading to the observation of considerable memory preservation in the 5xFAD model **(Figure 45)**. Nevertheless, more studies are needed to reveal the mechanism behind astrocytic RTP801 regulation of neuroinflammation and neurodegeneration.

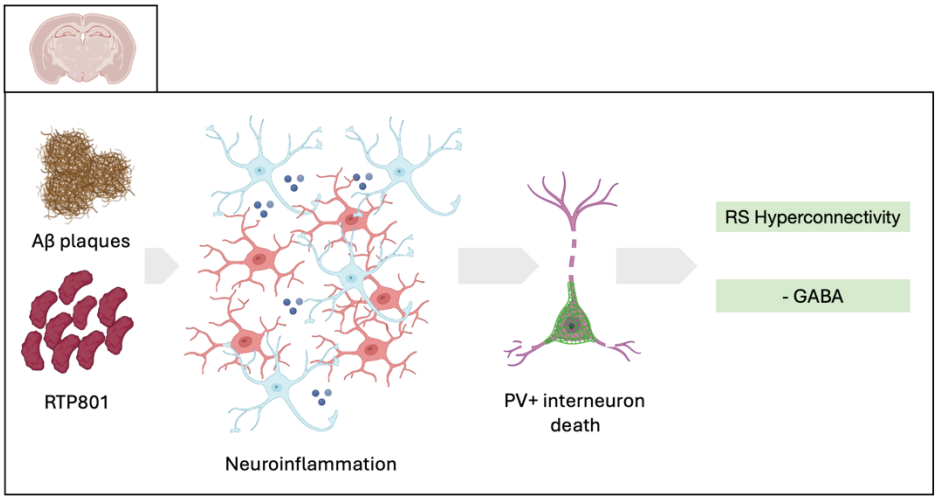

Figure 45. Proposed model of action of astrocytic RTP801: accumulation of Aβ plaques and astrocytic RTP801 in the 5xFAD mice leads to neuroinflammation and PV⁺ interneuron death leading to an hyperconnectivity and lower GABA levels. Figure generated with Biorender software.

22. Knocking out RTP801 from the equation: effects on a novel *in vitro* model of AD

The first CNS organotypic culture was created in 1962[350]. Subsequently, brain slices from the hippocampus, substantia nigra, locus coeruleus, striatum, and basal forebrain have been used to create organotypic cultures[351]. While tissue explants and organotypic slice cultures provide an accurate representation of the brain architecture, their inherent unpredictability makes experimentation with them challenging and unreproducible[352]. On the other hand, animal models of AD have been shown to replicate only Early-onset familial AD, providing incomplete depictions of human AD pathology. In fact, animal models of AD typically exhibit only a few clinical traits and lack crucial elements[353].

The reductionist methodology of *in vitro* research provides insight into a compound's mechanisms of action that may be more challenging to gain in a "whole-animal study," which is one of its main advantages. The ability to control *in vitro* studies allows for the assessment of the effect on the target process or structure without the presence of complicating variables[354]. For these reasons we stablished a new *in vitro* model containing neurons, astrocytes and microglia to further study the mechanism behind astrocytic RTP801 contribution to AD pathology.

Previous studies which pretend to study intercellular crosstalk among the three major types of cells in the brain have been performed separately and then put the cultures together in a plate after some days. For instance, a triculture stablished by to study AD, consist of culturing neurons and glia independently in separate dishes, when a monolayer of astrocytes was obtained neurons were plated above at a density of five neurons to two astrocytes. Six days later, microglia was added to the cultures in a proportion of one microglia to five neurons[355]. These cultures are more

complex to obtain as the timings are stricter for every cell cultivation which means that you must control and monitor very tightly the pregnancy of the animals. Moreover, each cell type comes from different mice, which involves differences sex segregation and in genes in each cell type.

Only a triculture of neurons, astrocytes and microglia from the same animal and in the same dish has been described by Goshi *et al* 2022, although they started from the rat cortex[356] , to study LPS-induced neuroinflammation. We adapted the protocol to achieve a hippocampal mice triculture, in this way continue using our model species *Mus musculus* and the part of the brain most affected in AD, the hippocampus.

22.1. Astrocyte characteristics after RTP801 silencing

Reactive astrocytes differ morphologically from normal astrocytes in that they show specific modifications in process extension towards the damage site, hypertrophy, elongation, and overlap of certain three-dimensional structural domains[357]. We observed no changes in the intensity of GFAP or the number of $GFAP^+$ cells, which is in line with our *in vivo* results here we only saw a mild recovery in the GFAP intensity after silencing astrocytic RTP801. However, the main objective was to assess changes in astrocytes morphology.

A single astrocyte can contact tens of neurons, hundreds of neuronal dendrites, and as many as 100,000 individual synapses because to the extensive network of astrocyte processes. Single astrocytes can also participate in bidirectional communication with nearby astrocytes[358].

In our study after Aβ treatment we did not change astrocyte morphology, meaning that 0,5 μM of Aβ oligomer is enough to affect the number of

microglia, but not the astrocyte shape. Markedly, we observed that silencing RTP801 in both conditions' (controls and after Aβ oligomer treatment) the ramification of astrocytes is reverted, showing a lower amounts of secondary processes **(Figure 46)**. We hypothesized, that as previously mentioned the role of RTP801 in the NF-κB pathway is influencing this morphology changes. Moreover, reactive morphological changes that astrocytes undergo in response to pro-inflammatory stimuli, like lipopolysaccharide (LPS), are mediated via notch signaling. In fact, the overexpression of Jag-1 by NF-κB is a prerequisite for the effects of LPS on astrocyte morphology[359].

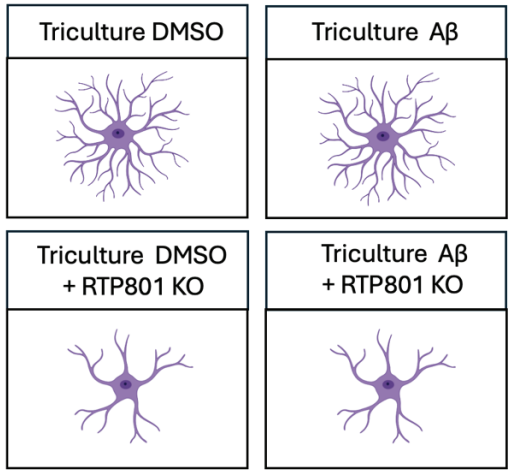

Figure 46. Morphological changes of astrocytes after knocking out astrocytic RTP801 in the triculture treated with Aβ oligomers. Figure generated with Biorender software.

In fact, astrocytes are activated in a reactive state by STAT3 in 6-month-old mice 5xFAD mice[360]. In turn, STAT3 phosphorylation is essential for *DDIT4* gene repression[361], so makes sense that upon STAT3 phosphorylation there is less RTP801 and less astrocyte reactivity.

The observed reduction in astrocytic secondary processes points to a possible disruption in cytoskeletal dynamics, which is vital for the maintenance of astrocyte architecture. Cytoskeletal components such as actin filaments, intermediate filaments (e.g., GFAP), and microtubules are known to regulate the branching and stability of astrocyte processes[362]. Astrocytic RTP801 may either directly influence cytoskeletal reorganization or modulate signaling pathways that regulate cytoskeletal dynamics.

This finding highlights the importance of this protein in maintaining astrocyte morphology and potentially protecting against Aβ-induced neurotoxicity. The structural integrity of astrocytes is crucial for their function in neuroinflammatory and neuroprotective roles, and the disruption of their processes may have far-reaching implications in the context of AD.

22.2. Astrocytic RTP801 responsible for Aβ oligomer clearance.

In the present study, we demonstrate that knocking out astrocytic RTP801 in an AD *in vitro* triculture model effectively reduces the number of Aβ oligomers, a key pathogenic factor in AD progression. Aβ oligomers are widely recognized as neurotoxic entities that contribute to synaptic dysfunction, cognitive impairment, and neuronal death, which are hallmarks of AD pathology[363]. In cultures of hippocampal neurons, Aβ oligomers induce a sharp decline in the membrane expression of memory-related receptors, which is followed by aberrant spine architecture, a drop in spine density, and a breakdown of synapses[364]. By targeting RTP801 we observed a significant decrease in Aβ oligomer levels, suggesting that this protein plays a pivotal role in the accumulation or clearance of these toxic

aggregates. Controversially, with our results in the 5xFAD where we did not observed changes in Aβ plaques load after astrocytic RTP801 silencing. However, in the *in vitro* experiment, with the Cre recombinase expression, we knocked out completely the expression of *DDIT4* in astrocytes while in the *in vivo* experiments the silencing was only about a 30%.

Our findings align with the growing body of evidence that suggests disrupting specific pathways involved in Aβ production, aggregation, or clearance can mitigate AD pathology[363]. Studies have shown that reactive astrocytes, microglia, and neurons contribute to the accumulation of Aβ, either by directly influencing Aβ production via the APP processing pathway or by modulating its clearance from the brain[365]. Given that RTP801 is involved in these processes, its knockdown may enhance Aβ degradation. Specifically, RTP801 may regulate the activity of enzymes responsible for cellular pathways critical for Aβ trafficking and clearance.

Moreover, astrocyte dysfunction has been linked to both Aβ aggregation and clearance inefficiency in AD. Reactive astrocytes, when subjected to Aβ-related stress, undergo structural and functional changes that can worsen the accumulation of toxic Aβ oligomers[366], as previously seen the astrocyte morphology changes after silencing astrocytic RTP801. The reduction in Aβ oligomers upon knocking out RTP801 might also reflect an indirect improvement in astrocyte function. Previous studies have highlighted that astrocytes possess Aβ-clearing mechanisms via endosomal-lysosomal pathways[367], and it is plausible that RTP801 interacts with these pathways to regulate Aβ turnover. By reducing the burden of Aβ oligomers, astrocytes may restore their supportive roles in synaptic maintenance and neuroprotection.

Interestingly, other studies have found that targeting Aβ oligomers specifically yields significant cognitive improvements in AD models[368]. Our findings support these observations, showing that reducing oligomeric Aβ forms through RTP801 knock out could present a promising therapeutic approach. Lower Aβ oligomer levels correlate with decreased neuroinflammation and oxidative stress, both of which are crucial mediators of neurodegeneration in AD[369]. Thus, modulating RTP801 activity not only addresses the root of Aβ aggregation but also appears to mitigate downstream consequences that exacerbate AD pathology as reported in the *in vivo* experiments of this thesis.

The observed reduction in Aβ oligomers opens avenues for further exploration into how astrocytic RTP801 may interact with Aβ clearance pathways such as those involving low-density lipoprotein receptor-related protein 1 (LRP1)[370] or receptor for advanced glycation end products (RAGE)[371]. Understanding these interactions will be critical for developing more targeted therapies aimed at halting or reversing AD progression.

Future research should focus on delineating the molecular pathways involved and assessing the long-term effects of this intervention on cognitive function and disease progression. Given the complex nature of AD, a multi-targeted approach that includes modulating astrocytic RTP801 may enhance therapeutic efficacy and lead to better outcomes for patients suffering from this devastating disorder.

CONCLUSIONS

1. The 5xFAD mouse model of Alzheimer disease presented higher levels of astrocytic RTP801 in hippocampus.

2. Normalizing the levels of astrocytic RTP801 prevents cognitive decline and restores anxiety-like behavior typical of WT mice.

3. Silencing astrocytic RTP801 mildly restores the number of DGCs with only one apical dendrite.

4. Resting-state functional connectivity is preserved by knocking down astrocytic RTP801 in 5xFAD mice.

5. Astrocytic RTP801 mediates the loss of Parvalbumin^{+} interneurons, negatively affecting the levels of GABA in the 5xFAD mice model.

6. Astrocytic RTP801 my contribute to the PNN production in hippocampus of 5xFAD mice.

7. Astrocytic RTP801 contributes to astro- and microgliosis in the 5xFAD mouse model.

8. Silencing astrocytic RTP801 changes the inflammasome protein levels but does not change the cytokine profile of the 5xFAD mice.

9. Complete silencing of astrocytic RTP801 diminishes the complexity of astrocytes morphology

10. Knocking out astrocytic RTP801 diminished the number of Aβ oligomers in a novel triculture model of AD.

REFERENCES

1. Kovacs, G. G. Cellular reactions of the central nervous system. *Handb Clin Neurol* **145**, 13–23 (2018).

2. Verkhratsky, A. & Nedergaard, M. Physiology of Astroglia. *Physiol Rev* **98**, 239 (2018).

3. Kobat, S. G. & Turgut, B. Importance of Müller Cells. *Beyoglu Eye Journal* **5**, 59 (2020).

4. Schultze, M. Observationes de retinae structura penitiori. (1859).

5. Deiters, O. Untersuchungen über Gehirn und Rückenmark des Menschen und der Säugethiere. (1865).

6. Frommann, C. Untersuchungen über die normale und pathologische Anatomie des Rückenmarks. (1864).

7. Kölliker, A. Handbuch der gewebelehre des menschen. (1867).

8. Golgi, C. Sulla fina anatomia degli organi centrali del sistema nervoso. (1885).

9. Lenhossék, M. Von. Der feinere Bau des Nervensystems im Lichte neuester Forschungen: eine allgemeine Betrachtung der Strukturprinzipien des Nervensystems; nebst einer. (1895).

10. García-Marín, V., García-López, P. & Freire, M. Cajal's contributions to glia research. *Trends Neurosci* **30**, 479–487 (2007).

11. Hertz, L. Possible role of neuroglia: a potassium-mediated neuronal--neuroglial--neuronal impulse transmission system. *Nature* **206**, 1091–1094 (1965).

12. Tasaki, I. & Chang, J. J. Electric response of glia cells in cat brain. *Science* **128**, 1209–1210 (1958).

13. Morrison, R. S. & de Vellis, J. Growth of purified astrocytes in a chemically defined medium. *Proc Natl Acad Sci U S A* **78**, 7205–7209 (1981).

14. Kriegstein, A. & Alvarez-Buylla, A. The glial nature of embryonic and adult neural stem cells. *Annu Rev Neurosci* **32**, 149–184 (2009).

15. Molofsky, A. V. & Deneen, B. Astrocyte development: A Guide for the Perplexed. *Glia* **63**, 1320–1329 (2015).

16. Breunig, J. J. *et al.* Rapid genetic targeting of pial surface neural progenitors and immature neurons by neonatal electroporation. *Neural Dev* **7**, (2012).

17. Bandeira, F., Lent, R. & Herculano-Houzel, S. Changing numbers of neuronal and non-neuronal cells underlie postnatal brain growth in the rat. *Proc Natl Acad Sci U S A* **106**, 14108–14113 (2009).

18. Ge, W. P., Miyawaki, A., Gage, F. H., Jan, Y. N. & Jan, L. Y. Local generation of glia is a major astrocyte source in postnatal cortex. *Nature* **484**, 376 (2012).

19. Schmechel, D. E. & Rakic, P. A Golgi study of radial glial cells in developing monkey telencephalon: morphogenesis and transformation into astrocytes. *Anat Embryol (Berl)* **156**, 115–152 (1979).

20. Zhu, X., Bergles, D. E. & Nishiyama, A. NG2 cells generate both oligodendrocytes and gray matter astrocytes. *Development* **135**, 145–157 (2008).

21. Huang, W. *et al.* Novel NG2-CreERT2 knock-in mice demonstrate heterogeneous differentiation potential of NG2 glia during development. *Glia* **62**, 896–913 (2014).

22. Ge, W. P. & Jia, J. M. Local production of astrocytes in the cerebral cortex. *Neuroscience* **323**, 3 (2016).

23. Jurga, A. M., Paleczna, M., Kadluczka, J. & Kuter, K. Z. Beyond the GFAP-Astrocyte Protein Markers in the Brain. *Biomolecules* **11**, (2021).

24. Bushong, E. A., Martone, M. E., Jones, Y. Z. & Ellisman, M. H. Protoplasmic astrocytes in CA1 stratum radiatum occupy separate anatomical domains. *J Neurosci* **22**, 183–192 (2002).

25. Lundgaard, I., Osório, M. J., Kress, B. T., Sanggaard, S. & Nedergaard, M. White matter astrocytes in health and disease. *Neuroscience* **276**, 161–173 (2014).

26. Feig, S. L. & Haberly, L. B. Surface-associated astrocytes, not endfeet, form the glia limitans in posterior piriform cortex and have a spatially distributed, not a domain, organization. *J Comp Neurol* **519**, 1952–1969 (2011).

27. Chan-Palay, V. & Palay, S. L. The form of velate astrocytes in the cerebellar cortex of monkey and rat: high voltage electron microscopy of rapid Golgi preparations. *Z Anat Entwicklungsgesch* **138**, 1–19 (1972).

28. Hatton, G. I. Pituicytes, glia and control of terminal secretion. *J Exp Biol* **139**, 67–79 (1988).

29. Brawer, J. R., Stein, R., Small, L., Cissé, S. & Schipper, H. M. Composition of Gomori-positive inclusions in astrocytes of the hypothalamic arcuate nucleus. *Anat Rec* **240**, 407–415 (1994).

30. Reichenbach, A. & Bringmann, A. Comparative Anatomy of Glial Cells in Mammals. *Evolutionary Neuroscience* 397–439 (2020) doi:10.1016/B978-0-12-820584-6.00016-7.

31. Liu, X. *et al.* The superficial glia limitans of mouse and monkey brain and spinal cord. *Anat Rec (Hoboken)* **296**, 995–1007 (2013).

32. Oberheim, N. A. *et al.* Uniquely hominid features of adult human astrocytes. *J Neurosci* **29**, 3276–3287 (2009).

33. Lee, H. G., Wheeler, M. A. & Quintana, F. J. Function and therapeutic value of astrocytes in neurological diseases. *Nature Reviews Drug Discovery 2022 21:5* **21**, 339–358 (2022).

34. Valles, S. L. *et al.* Functions of Astrocytes under Normal Conditions and after a Brain Disease. *Int J Mol Sci* **24**, (2023).

35. Hertz, L. & Chen, Y. Importance of astrocytes for potassium ion (K+) homeostasis in brain and glial effects of K+ and its transporters on learning. *Neurosci Biobehav Rev* **71**, 484–505 (2016).

36. Hertz, L. Possible role of neuroglia: a potassium-mediated neuronal--neuroglial--neuronal impulse transmission system. *Nature* **206**, 1091–1094 (1965).

37. Orkand, R. K., Nicholls, J. G. & Kuffler, S. W. Effect of nerve impulses on the membrane potential of glial cells in the central nervous system of amphibia. *J Neurophysiol* **29**, 788–806 (1966).

38. Kettenmann, H., Backus, K. H. & Schachner, M. gamma-Aminobutyric acid opens Cl-channels in cultured astrocytes. *Brain Res* **404**, 1–9 (1987).

39. Zanotti, S. & Charles, A. Extracellular calcium sensing by glial cells: low extracellular calcium induces intracellular calcium release and intercellular signaling. *J Neurochem* **69**, 594–602 (1997).

40. Hansen, D. B., Garrido-Comas, N., Salter, M. & Fern, R. HCO3(-)-independent pH regulation in astrocytes in situ is dominated by V-ATPase. *J Biol Chem* **290**, 8039–8047 (2015).

41. Yao, X., Hrabětová, S., Nicholson, C. & Manley, G. T. Aquaporin-4-deficient mice have increased extracellular space without tortuosity change. *J Neurosci* **28**, 5460–5464 (2008).

42. MacAulay, N. & Zeuthen, T. Water transport between CNS compartments: contributions of aquaporins and cotransporters. *Neuroscience* **168**, 941–956 (2010).

43. Bélanger, M., Allaman, I. & Magistretti, P. J. Brain energy metabolism: focus on astrocyte-neuron metabolic cooperation. *Cell Metab* **14**, 724–738 (2011).

44. Dringen, R., Gutterer, J. M. & Hirrlinger, J. Glutathione metabolism in brain metabolic interaction between astrocytes and neurons in the defense against reactive oxygen species. *Eur J Biochem* **267**, 4912–4916 (2000).

45. Bridges, R. J., Natale, N. R. & Patel, S. A. System xc^- cystine/glutamate antiporter: an update on molecular pharmacology and roles within the CNS. *Br J Pharmacol* **165**, 20–34 (2012).

46. Wilson, J. X., Peters, C. E., Sitar, S. M., Daoust, P. & Gelb, A. W. Glutamate stimulates ascorbate transport by astrocytes. *Brain Res* **858**, 61–66 (2000).

47. Makar, T. K. *et al.* Vitamin E, ascorbate, glutathione, glutathione disulfide, and enzymes of glutathione metabolism in cultures of chick astrocytes and neurons: evidence that astrocytes play an important role in antioxidative processes in the brain. *J Neurochem* **62**, 45–53 (1994).

48. Danbolt, N. C. Glutamate uptake. *Prog Neurobiol* **65**, 1–105 (2001).

49. Ortinski, P. I. *et al.* Selective induction of astrocytic gliosis generates deficits in neuronal inhibition. *Nat Neurosci* **13**, 584–591 (2010).

50. Boison, D. Adenosine as a neuromodulator in neurological diseases. *Curr Opin Pharmacol* **8**, 2–7 (2008).

51. Levitt, P., Pintar, J. E. & Breakefield, X. O. Immunocytochemical demonstration of monoamine oxidase B in brain astrocytes and serotonergic neurons. *Proc Natl Acad Sci U S A* **79**, 6385–6389 (1982).

52. Bröer, S. & Brookes, N. Transfer of glutamine between astrocytes and neurons. *J Neurochem* **77**, 705–719 (2001).

53. Norenberg, M. D. & Martinez-Hernandez, A. Fine structural localization of glutamine synthetase in astrocytes of rat brain. *Brain Res* **161**, 303–310 (1979).

54. Qu, H., Håberg, A., Haraldseth, O., Unsgård, G. & Sonnewald, U. (13)C MR spectroscopy study of lactate as substrate for rat brain. *Dev Neurosci* **22**, 429–436 (2000).

55. Suzuki, A. *et al.* Astrocyte-neuron lactate transport is required for long-term memory formation. *Cell* **144**, 810–823 (2011).

56. Patel, A. B. *et al.* Direct evidence for activity-dependent glucose phosphorylation in neurons with implications for the astrocyte-to-neuron lactate shuttle. *Proc Natl Acad Sci U S A* **111**, 5385–5390 (2014).

57. Brown, A. M. *et al.* Astrocyte glycogen metabolism is required for neural activity during aglycemia or intense stimulation in mouse white matter. *J Neurosci Res* **79**, 74–80 (2005).

58. Derouiche, A. The perisynaptic astrocyte process as a glial compartment-immunolabeling for glutamine synthetase and other glial markers. *Advances in Molecular and Cell Biology* **31**, 147–163 (2003).

59. Derouiche, A., Anlauf, E., Aumann, G., Mühlstädt, B. & Lavialle, M. Anatomical aspects of glia-synapse interaction: the perisynaptic glial sheath consists of a specialized astrocyte compartment. *J Physiol Paris* **96**, 177–182 (2002).

60. Bernardinelli, Y., Muller, D. & Nikonenko, I. Astrocyte-synapse structural plasticity. *Neural Plast* **2014**, (2014).

61. Araque, A., Parpura, V., Sanzgiri, R. P. & Haydon, P. G. Tripartite synapses: glia, the unacknowledged partner. *Trends Neurosci* **22**, 208–215 (1999).

62. Pfrieger, F. W. & Barres, B. A. Synaptic efficacy enhanced by glial cells in vitro. *Science* **277**, 1684–1687 (1997).

63. Mauch, D. H. *et al.* CNS synaptogenesis promoted by glia-derived cholesterol. *Science* **294**, 1354–1357 (2001).

64. Eroglu, Ç. *et al.* Gabapentin receptor alpha2delta-1 is a neuronal thrombospondin receptor responsible for excitatory CNS synaptogenesis. *Cell* **139**, 380–392 (2009).

65. Kucukdereli, H. *et al.* Control of excitatory CNS synaptogenesis by astrocyte-secreted proteins hevin and SPARC. *Proc Natl Acad Sci U S A* **108**, (2011).

66. Ostroff, L. E., Manzur, M. K., Cain, C. K. & Ledoux, J. E. Synapses lacking astrocyte appear in the amygdala during consolidation of Pavlovian threat conditioning. *J Comp Neurol* **522**, 2152–2163 (2014).

67. Schafer, D. P. & Stevens, B. Phagocytic glial cells: sculpting synaptic circuits in the developing nervous system. *Curr Opin Neurobiol* **23**, 1034–1040 (2013).

68. Chung, W. S. *et al.* Astrocytes mediate synapse elimination through MEGF10 and MERTK pathways. *Nature* **504**, 394–400 (2013).

69. Marcaggi, P. & Attwell, D. Role of glial amino acid transporters in synaptic transmission and brain energetics. *Glia* **47**, 217–225 (2004).

70. Rodnight, R. B. & Gottfried, C. Morphological plasticity of rodent astroglia. *J Neurochem* **124**, 263–275 (2013).

71. Zonta, M. *et al.* Neuron-to-astrocyte signaling is central to the dynamic control of brain microcirculation. *Nat Neurosci* **6**, 43–50 (2003).

72. Mulligan, S. J. & MacVicar, B. A. Calcium transients in astrocyte endfeet cause cerebrovascular constrictions. *Nature* **431**, 195–199 (2004).

73. Kur, J. & Newman, E. A. Purinergic control of vascular tone in the retina. *J Physiol* **592**, 491–504 (2014).

74. Rosenegger, D. G., Tran, C. H. T., Wamsteeker Cusulin, J. I. & Gordon, G. R. Tonic Local Brain Blood Flow Control by Astrocytes Independent of Phasic Neurovascular Coupling. *J Neurosci* **35**, 13463–13474 (2015).

75. Adamczyk, L. A. *et al.* Lymph vessels: the forgotten second circulation in health and disease. *Virchows Arch* **469**, 3–17 (2016).

76. Mathiisen, T. M., Lehre, K. P., Danbolt, N. C. & Ottersen, O. P. The perivascular astroglial sheath provides a complete covering of the brain microvessels: an electron microscopic 3D reconstruction. *Glia* **58**, 1094–1103 (2010).

77. Iliff, J. J. *et al.* A paravascular pathway facilitates CSF flow through the brain parenchyma and the clearance of interstitial solutes, including amyloid β. *Sci Transl Med* **4**, (2012).

78. Angelova, P. R. *et al.* Functional Oxygen Sensitivity of Astrocytes. *J Neurosci* **35**, 10460–10473 (2015).

79. Siepka, S. M., Yoo, S. H., Park, J., Lee, C. & Takahashi, J. S. Genetics and neurobiology of circadian clocks in mammals. *Cold Spring Harb Symp Quant Biol* **72**, 251–259 (2007).

80. Becquet, D., Girardet, C., Guillaumond, F., François-Bellan, A. M. & Bosler, O. Ultrastructural plasticity in the rat suprachiasmatic nucleus. Possible involvement in clock entrainment. *Glia* **56**, 294–305 (2008).

81. Duhart, J. M. *et al.* Suprachiasmatic astrocytes modulate the circadian clock in response to TNF-α. *J Immunol* **191**, 4656–4664 (2013).

82. Rodríguez, E. M. *et al.* Hypothalamic tanycytes: a key component of brain-endocrine interaction. *Int Rev Cytol* **247**, 89–164 (2005).

83. Balland, E. *et al.* Hypothalamic tanycytes are an ERK-gated conduit for leptin into the brain. *Cell Metab* **19**, 293–301 (2014).

84. Han, R. T., Kim, R. D., Molofsky, A. V. & Liddelow, S. A. Astrocyte-immune cell interactions in physiology and pathology. *Immunity* **54**, 211–224 (2021).

85. Kucukdereli, H. *et al.* Control of excitatory CNS synaptogenesis by astrocyte-secreted proteins hevin and SPARC. *Proc Natl Acad Sci U S A* **108**, (2011).

86. Christopherson, K. S. *et al.* Thrombospondins are astrocyte-secreted proteins that promote CNS synaptogenesis. *Cell* **120**, 421–433 (2005).

87. Allen, N. J. *et al.* Astrocyte glypicans 4 and 6 promote formation of excitatory synapses via GluA1 AMPA receptors. *Nature* **486**, 410–414 (2012).

88. Liddelow, S. A. *et al.* Neurotoxic reactive astrocytes are induced by activated microglia. *Nature* **541**, 481–487 (2017).

89. Guttenplan, K. A. *et al.* Knockout of reactive astrocyte activating factors slows disease progression in an ALS mouse model. *Nat Commun* **11**, (2020).

90. Hong, S. *et al.* Complement and microglia mediate early synapse loss in Alzheimer mouse models. *Science* **352**, 712–716 (2016).

91. Maragakis, N. J. & Rothstein, J. D. Glutamate transporters: Animal models to neurologic disease. *Neurobiol Dis* **15**, 461–473 (2004).

92. Panattoni, G. *et al.* Diverse inflammatory threats modulate astrocytes Ca2+ signaling via connexin43 hemichannels in organotypic spinal slices. *Mol Brain* **14**, (2021).

93. Dong, Q. *et al.* Mechanism and consequence of abnormal calcium homeostasis in Rett syndrome astrocytes. *Elife* **7**, (2018).

94. Dong, Q. P., He, J. Q. & Chai, Z. Astrocytic Ca(2+) waves mediate activation of extrasynaptic NMDA receptors in hippocampal neurons to aggravate brain damage during ischemia. *Neurobiol Dis* **58**, 68–75 (2013).

95. Reichenbach, N. *et al.* P2Y1 receptor blockade normalizes network dysfunction and cognition in an Alzheimer's disease model. *J Exp Med* **215**, 1649–1663 (2018).

96. Cvetkovic, C. *et al.* Assessing Gq-GPCR-induced human astrocyte reactivity using bioengineered neural organoids. *J Cell Biol* **221**, (2022).

97. Patani, R., Hardingham, G. E. & Liddelow, S. A. Functional roles of reactive astrocytes in neuroinflammation and neurodegeneration. *Nature Reviews Neurology 2023 19:7* **19**, 395–409 (2023).

98. Haim, L. Ben *et al.* The JAK/STAT3 Pathway Is a Common Inducer of Astrocyte Reactivity in Alzheimer's and Huntington's Diseases. *The Journal of Neuroscience* **35**, 2817 (2015).

99. Ceyzériat, K., Abjean, L., Carrillo-de Sauvage, M. A., Ben Haim, L. & Escartin, C. The complex STATes of astrocyte reactivity: How are they controlled by the JAK-STAT3 pathway? *Neuroscience* **330**, 205–218 (2016).

100. Lane, C. A., Hardy, J. & Schott, J. M. Alzheimer's disease. *Eur J Neurol* **25**, 59–70 (2018).

101. Bondi, M. W., Edmonds, E. C. & Salmon, D. P. Alzheimer's Disease: Past, Present, and Future. *J Int Neuropsychol Soc* **23**, 818–831 (2017).

102. Briggs, R., Kennelly, S. P. & O'Neill, D. Drug treatments in Alzheimer's disease. *Clin Med (Lond)* **16**, 247–253 (2016).

103. Petersen, R. C. Mild Cognitive Impairment. *Continuum (Minneap Minn)* **22**, 404–418 (2016).

104. What Are the Signs of Alzheimer's Disease? | National Institute on Aging. https://www.nia.nih.gov/health/alzheimers-symptoms-and-diagnosis/what-are-signs-alzheimers-disease.

105. Serrano-Pozo, A. *et al.* Thal Amyloid Stages Do Not Significantly Impact the Correlation Between Neuropathological Change and Cognition in the Alzheimer Disease Continuum. *J Neuropathol Exp Neurol* **75**, 516–526 (2016).

106. Cummings, J. L., Tong, G. & Ballard, C. Treatment Combinations for Alzheimer's Disease: Current and Future Pharmacotherapy Options. *J Alzheimers Dis* **67**, 779–794 (2019).

107. Bagaria, J., Bagyinszky, E. & An, S. S. A. Genetics, Functions, and Clinical Impact of Presenilin-1 (PSEN1) Gene. *Int J Mol Sci* **23**, 10970 (2022).

108. Rabinovici, G. D. Late-onset Alzheimer Disease. *Continuum : Lifelong Learning in Neurology* **25**, 14 (2019).

109. Corder, E. H. *et al.* Gene dose of apolipoprotein E type 4 allele and the risk of Alzheimer's disease in late onset families. *Science* **261**, 921–923 (1993).

110. Rajan, K. B. *et al.* Population estimate of people with clinical Alzheimer's disease and mild cognitive impairment in the United States (2020-2060). *Alzheimers Dement* **17**, 1966–1975 (2021).

111. Chêne, G. *et al.* Gender and incidence of dementia in the Framingham Heart Study from mid-adult life. *Alzheimers Dement* **11**, 310–320 (2015).

112. Ahmadi-Abhari, S. *et al.* Temporal trend in dementia incidence since 2002 and projections for prevalence in England and Wales to 2040: modelling study. *BMJ* **358**, (2017).

113. Wolters, F. J. *et al.* Twenty-seven-year time trends in dementia incidence in Europe and the United States: The Alzheimer Cohorts Consortium. *Neurology* **95**, E519–E531 (2020).

114. Freedman, V. A., Kasper, J. D., Spillman, B. C. & Plassman, B. L. Short-Term Changes in the Prevalence of Probable Dementia: An Analysis of the 2011-2015 National Health and Aging Trends Study. *J Gerontol B Psychol Sci Soc Sci* **73**, S48–S56 (2018).

115. Tom, S. E. *et al.* Association of Demographic and Early-Life Socioeconomic Factors by Birth Cohort With Dementia Incidence

Among US Adults Born Between 1893 and 1949. *JAMA Netw Open* **3**, (2020).

116. American Psychiatric Association. Diagnostic and Statistical Manual of Mental Disorders. *Diagnostic and Statistical Manual of Mental Disorders* (2013) doi:10.1176/APPI.BOOKS.9780890425596.

117. Graham, N. L. & Hodges, J. R. Distinctive cognitive profiles in Alzheimer's disease and subcortical vascular dementia. *J Neurol Neurosurg Psychiatry* **75**, 61–71 (2004).

118. Price, J. L., Davis, P. B., Morris, J. C. & White, D. L. The distribution of tangles, plaques and related immunohistochemical markers in healthy aging and Alzheimer's disease. *Neurobiol Aging* **12**, 295–312 (1991).

119. D'Onofrio, G. *et al.* Neuropsychiatric symptoms and functional status in Alzheimer's disease and vascular dementia patients. *Curr Alzheimer Res* **9**, 759–771 (2012).

120. Clarfield, A. M. The decreasing prevalence of reversible dementias: an updated meta-analysis. *Arch Intern Med* **163**, 2219–2229 (2003).

121. van der Flier, W. M., de Vugt, M. E., Smets, E. M. A., Blom, M. & Teunissen, C. E. Towards a future where Alzheimer's disease pathology is stopped before the onset of dementia. *Nature Aging 2023 3:5* **3**, 494–505 (2023).

122. Festari, C. *et al.* European consensus for the diagnosis of MCI and mild dementia: Preparatory phase. *Alzheimers Dement* **19**, 1729–1741 (2023).

123. Nakamura, A. *et al.* High performance plasma amyloid-β biomarkers for Alzheimer's disease. *Nature* **554**, 249–254 (2018).

124. Wood, M. J. A., O'Loughlin, A. J. & Lakhal, S. Exosomes and the blood-brain barrier: implications for neurological diseases. *Ther Deliv* **2**, 1095–1099 (2011).

125. Jia, L. *et al.* Concordance between the assessment of Aβ42, T-tau, and P-T181-tau in peripheral blood neuronal-derived exosomes and cerebrospinal fluid. *Alzheimer's & Dementia* **15**, 1071–1080 (2019).

126. Kiani, L. Finger-prick blood test for Alzheimer disease. *Nature Reviews Neurology 2023 19:9* **19**, 507–507 (2023).

127. Wattmo, C. & Wallin, Å. K. Early- versus late-onset Alzheimer's disease in clinical practice: cognitive and global outcomes over 3 years. *Alzheimers Res Ther* **9**, (2017).

128. Wilson, R. S. *et al.* Cognitive decline in incident Alzheimer disease in a community population. *Neurology* **74**, 951 (2010).

129. Knopman, D. S. *et al.* Alzheimer disease. *Nat Rev Dis Primers* **7**, (2021).

130. Perl, D. P. Neuropathology of Alzheimer's disease. *Mt Sinai J Med* **77**, 32–42 (2010).

131. Apostolova, L. G. *et al.* Hippocampal atrophy and ventricular enlargement in normal aging, mild cognitive impairment (MCI), and Alzheimer Disease. *Alzheimer Dis Assoc Disord* **26**, 17–27 (2012).

132. Kao, Y. H., Chou, M. C., Chen, C. H. & Yang, Y. H. White Matter Changes in Patients with Alzheimer's Disease and Associated Factors. *J Clin Med* **8**, (2019).

133. Coulson, E. J., Paliga, K., Beyreuther, K. & Masters, C. L. What the evolution of the amyloid protein precursor supergene family tells us about its function. *Neurochem Int* **36**, 175–184 (2000).

134. Belyaev, N. D. *et al.* The transcriptionally active amyloid precursor protein (APP) intracellular domain is preferentially produced from the 695 isoform of APP in a {beta}-secretase-dependent pathway. *J Biol Chem* **285**, 41443–41454 (2010).

135. Müller, U. C., Deller, T. & Korte, M. Not just amyloid: physiological functions of the amyloid precursor protein family. *Nat Rev Neurosci* **18**, 281–298 (2017).

136. Kuhn, A. J., Abrams, B. S., Knowlton, S. & Raskatov, J. A. The Alzheimer's Disease "non-amyloidogenic" p3 peptide revisited: a case for Amyloid-α. *ACS Chem Neurosci* **11**, 1539 (2020).

137. Richter, M. C. *et al.* Distinct in vivo roles of secreted APP ectodomain variants APPsα and APPsβ in regulation of spine density, synaptic plasticity, and cognition. *EMBO J* **37**, (2018).

138. Grimm, M. O. W. *et al.* APP intracellular domain derived from amyloidogenic β-and ?-secretase cleavage regulates neprilysin expression. *Front Aging Neurosci* **7**, 135278 (2015).

139. Bukhari, H. *et al.* Small things matter: Implications of APP intracellular domain AICD nuclear signaling in the progression and pathogenesis of Alzheimer's disease. *Prog Neurobiol* **156**, 189–213 (2017).

140. Flagmeier, P. *et al.* Direct measurement of lipid membrane disruption connects kinetics and toxicity of Aβ42 aggregation. *Nat Struct Mol Biol* **27**, 886–891 (2020).

141. Esparza, T. J. *et al.* Amyloid-β oligomerization in Alzheimer dementia versus high-pathology controls. *Ann Neurol* **73**, 104–119 (2013).

142. Koffie, R. M. *et al.* Oligomeric amyloid beta associates with postsynaptic densities and correlates with excitatory synapse loss near senile plaques. *Proc Natl Acad Sci U S A* **106**, 4012–4017 (2009).

143. Walker, L. C. & Jucker, M. Neurodegenerative diseases: expanding the prion concept. *Annu Rev Neurosci* **38**, 87–103 (2015).

144. Thal, D. R., Rüb, U., Orantes, M. & Braak, H. Phases of A beta-deposition in the human brain and its relevance for the development of AD. *Neurology* **58**, 1791–1800 (2002).

145. Bancher, C. *et al.* Accumulation of abnormally phosphorylated τ precedes the formation of neurofibrillary tangles in Alzheimer's disease. *Brain Res* **477**, 90–99 (1989).

146. Moloney, C. M., Lowe, V. J. & Murray, M. E. Visualization of neurofibrillary tangle maturity in Alzheimer's disease: A clinicopathologic perspective for biomarker research. *Alzheimer's & Dementia* **17**, 1554–1574 (2021).

147. Iwata, M., Watanabe, S., Yamane, A., Miyasaka, T. & Misonou, H. Regulatory mechanisms for the axonal localization of tau protein in neurons. *Mol Biol Cell* **30**, 2441 (2019).

148. Waheed, Z. *et al.* The Role of Tau Proteoforms in Health and Disease. *Mol Neurobiol* **60**, 5155–5166 (2023).

149. Despres, C. *et al.* Identification of the Tau phosphorylation pattern that drives its aggregation. *Proc Natl Acad Sci U S A* **114**, 9080–9085 (2017).

150. Fan, X. *et al.* Tau Acts in Concert With Kinase/Phosphatase Underlying Synaptic Dysfunction. *Front Aging Neurosci* **14**, 908881 (2022).

151. Martin, L. *et al.* Tau protein kinases: involvement in Alzheimer's disease. *Ageing Res Rev* **12**, 289–309 (2013).

152. Martin, L. *et al.* Tau protein phosphatases in Alzheimer's disease: the leading role of PP2A. *Ageing Res Rev* **12**, 39–49 (2013).

153. Braak, H. & Braak, E. Neuropathological stageing of Alzheimer-related changes. *Acta Neuropathol* **82**, 239–259 (1991).

154. Perry, V. H. & Teeling, J. Microglia and macrophages of the central nervous system: the contribution of microglia priming and systemic inflammation to chronic neurodegeneration. *Semin Immunopathol* **35**, 601 (2013).

155. Rickenbach, C. & Gericke, C. Specificity of Adaptive Immune Responses in Central Nervous System Health, Aging and Diseases. *Front Neurosci* **15**, 806260 (2022).

156. Chen, X. & Holtzman, D. M. Emerging roles of innate and adaptive immunity in Alzheimer's Disease. *Immunity* **55**, 2236 (2022).

157. Miao, J. *et al.* Microglia in Alzheimer's disease: pathogenesis, mechanisms, and therapeutic potentials. *Front Aging Neurosci* **15**, 1201982 (2023).

158. Keren-Shaul, H. *et al.* A Unique Microglia Type Associated with Restricting Development of Alzheimer's Disease. *Cell* **169**, 1276-1290.e17 (2017).

159. Clayton, K. *et al.* Plaque associated microglia hyper-secrete extracellular vesicles and accelerate tau propagation in a humanized APP mouse model. *Mol Neurodegener* **16**, (2021).

160. Li, Q. *et al.* Developmental Heterogeneity of Microglia and Brain Myeloid Cells Revealed by Deep Single-Cell RNA Sequencing. *Neuron* **101**, 207-223.e10 (2019).

161. Yeh, F. L., Wang, Y., Tom, I., Gonzalez, L. C. & Sheng, M. TREM2 Binds to Apolipoproteins, Including APOE and CLU/APOJ, and Thereby Facilitates Uptake of Amyloid-Beta by Microglia. *Neuron* **91**, 328–340 (2016).

162. Fonseca, M. I. *et al.* Cell-specific deletion of C1qa identifies microglia as the dominant source of C1q in mouse brain. *J Neuroinflammation* **14**, (2017).

163. Britschgi, M. *et al.* Deficiency of terminal complement pathway inhibitor promotes neuronal tau pathology and degeneration in mice. *J Neuroinflammation* **9**, (2012).

164. Heneka, M. T. *et al.* NLRP3 is activated in Alzheimer's disease and contributes to pathology in APP/PS1 mice. *Nature* **493**, 674–678 (2013).

165. Heneka, M. T. *et al.* NLRP3 is activated in Alzheimer's disease and contributes to pathology in APP/PS1 mice. *Nature* **493**, 674–678 (2013).

166. Flores, J., Fillion, M. L. & LeBlanc, A. C. Caspase-1 inhibition improves cognition without significantly altering amyloid and inflammation in aged Alzheimer disease mice. *Cell Death Dis* **13**, (2022).

167. McDonald, C. L. *et al.* Inhibiting TLR2 activation attenuates amyloid accumulation and glial activation in a mouse model of Alzheimer's disease. *Brain Behav Immun* **58**, 191–200 (2016).

168. Liddelow, S. A. *et al.* Neurotoxic reactive astrocytes are induced by activated microglia. *Nature* **541**, 481–487 (2017).

169. Li, C. *et al.* Astrocytes: implications for neuroinflammatory pathogenesis of Alzheimer's disease. *Curr Alzheimer Res* **8**, 67–80 (2011).

170. Patel, N. S. *et al.* Inflammatory cytokine levels correlate with amyloid load in transgenic mouse models of Alzheimer's disease. *J Neuroinflammation* **2**, (2005).

171. Brown, M. R., Radford, S. E. & Hewitt, E. W. Modulation of β-Amyloid Fibril Formation in Alzheimer's Disease by Microglia and Infection. *Front Mol Neurosci* **13**, 609073 (2020).

172. Kanekiyo, T. *et al.* Neuronal Clearance of Amyloid-β by Endocytic Receptor LRP1. *Journal of Neuroscience* **33**, 19276–19283 (2013).

173. Fleeman, R. M. & Proctor, E. A. Astrocytic Propagation of Tau in the Context of Alzheimer's Disease. *Front Cell Neurosci* **15**, 645233 (2021).

174. Saroja, S. R., Gorbachev, K., Tcw, J., Goate, A. M. & Pereira, A. C. Astrocyte-secreted glypican-4 drives APOE4-dependent tau hyperphosphorylation. *Proc Natl Acad Sci U S A* **119**, e2108870119 (2022).

175. Xu, X. *et al.* Yes-associated protein regulates glutamate homeostasis through promoting the expression of excitatory amino acid transporter-2 in astrocytes via β-catenin signaling. *Glia* **71**, 1197–1216 (2023).

176. Ahadiat, S.-A. & Hosseinian, Z. Astrocytes' innate role in neurodegenerative disorders. *Bulletin of the National Research Centre 2023 47:1* **47**, 1–11 (2023).

177. Li, W.-P. *et al.* Archival Report Astrocytes Mediate Cholinergic Regulation of Adult Hippocampal Neurogenesis and Memory Through M 1 Muscarinic Receptor. doi:10.1016/j.biopsych.2022.04.019.

178. Singh, S., Agrawal, N. & Goyal, A. Role of Alpha-7-Nicotinic Acetylcholine Receptor in Alzheimer's Disease. *CNS Neurol Disord Drug Targets* **23**, 384–394 (2023).

179. Nagele, R. G., D'Andrea, M. R., Lee, H., Venkataraman, V. & Wang, H. Y. Astrocytes accumulate Aβ42 and give rise to astrocytic amyloid plaques in Alzheimer disease brains. *Brain Res* **971**, 197–209 (2003).

180. Se Thoe, E., Fauzi, A., Tang, Y. Q., Chamyuang, S. & Chia, A. Y. Y. A review on advances of treatment modalities for Alzheimer's disease. *Life Sci* **276**, (2021).

181. Dooley, M. & Lamb, H. M. Donepezil: a review of its use in Alzheimer's disease. *Drugs Aging* **16**, 199–226 (2000).

182. Birks, J. S. & Grimley Evans, J. Rivastigmine for Alzheimer's disease. *Cochrane Database Syst Rev* **2015**, (2015).

183. Scott, L. J. & Goa, K. L. Galantamine: a review of its use in Alzheimer's disease. *Drugs* **60**, 1095–1122 (2000).

184. Winblad, B., Jones, R. W., Wirth, Y., Stöffler, A. & Möbius, H. J. Memantine in moderate to severe Alzheimer's disease: a meta-analysis of randomised clinical trials. *Dement Geriatr Cogn Disord* **24**, 20–27 (2007).

185. Calhoun, A., King, C., Khoury, R. & Grossberg, G. T. An evaluation of memantine ER + donepezil for the treatment of Alzheimer's disease. *Expert Opin Pharmacother* **19**, 1711–1717 (2018).

186. Budd Haeberlein, S. *et al.* Two Randomized Phase 3 Studies of Aducanumab in Early Alzheimer's Disease. *Journal of Prevention of Alzheimer's Disease* **9**, 197–210 (2022).

187. CH, van D. *et al.* Lecanemab in Early Alzheimer's Disease. *N Engl J Med* **388**, 142–143 (2023).

188. Sims, J. R. *et al.* Donanemab in Early Symptomatic Alzheimer Disease: The TRAILBLAZER-ALZ 2 Randomized Clinical Trial. *JAMA* **330**, 512–527 (2023).

189. Sperling, R. A. *et al.* Trial of Solanezumab in Preclinical Alzheimer's Disease. *N Engl J Med* **389**, 1096–1107 (2023).

190. Novak, G. *et al.* Changes in Brain Volume with Bapineuzumab in Mild to Moderate Alzheimer's Disease. *J Alzheimers Dis* **49**, 1123–1134 (2016).

191. Arora, S., Santiago, J. A., Bernstein, M. & Potashkin, J. A. Diet and lifestyle impact the development and progression of Alzheimer's dementia. *Front Nutr* **10**, (2023).

192. Kim, J. Y., Kwon, Y. G. & Kim, Y. M. The stress-responsive protein REDD1 and its pathophysiological functions. *Experimental and Molecular Medicine* vol. 55 1933–1944 Preprint at https://doi.org/10.1038/s12276-023-01056-3 (2023).

193. Shoshani, T. *et al.* Identification of a Novel Hypoxia-Inducible Factor 1-Responsive Gene, RTP801 , Involved in Apoptosis . *Mol Cell Biol* **22**, 2283–2293 (2002).

194. Ellisen, L. W. *et al. REDD1, a Developmentally Regulated Transcriptional Target of P63 and P53, Links P63 to Regulation of Reactive Oxygen Species Ily to Transcriptional Activation of the Cyclin-Dependent Kinase Inhibitor P21 Cip1 (Deng et al While a Number of Candidate Target Genes Have Been Implicated in P53-Dependent Apoptosis, Including Bax, TRAIL-DR5, PERP, Noxa, and APAF-1 (Miyashita and Reed, 1995; Attardi*. *Molecular Cell* vol. 10 (2002).

195. Vega-Rubin-de-Celis, S. *et al.* Structural analysis and functional implications of the negative mTORC1 regulator REDD1. *Biochemistry* **49**, 2491–2501 (2010).

196. Michel, G. *et al.* Plasma membrane translocation of REDD1 governed by GPCRs contributes to mTORC1 activation. *J Cell Sci* **127**, 773–787 (2014).

197. Cho, S. S. *et al.* Induction of REDD1 via AP-1 prevents oxidative stress-mediated injury in hepatocytes. *Free Radic Biol Med* **124**, 221–231 (2018).

198. Deyoung, M. P., Horak, P., Sofer, A., Sgroi, D. & Ellisen, L. W. Hypoxia regulates TSC1/2-mTOR signaling and tumor suppression through REDD1-mediated 14-3-3 shuttling. *Genes Dev* **22**, 239–251 (2008).

199. Kim, M. Y. *et al.* Gadd45 is a novel mediator of cardiomyocyte apoptosis induced by ischaemia/hypoxia. *Cardiovasc Res* **87**, 119–126 (2010).

200. Dennis, M. D., Kimball, S. R., Fort, P. E. & Jefferson, L. S. Regulated in development and DNA damage 1 is necessary for hyperglycemia-

induced vascular endothelial growth factor expression in the retina of diabetic rodents. *Journal of Biological Chemistry* **290**, 3865–3874 (2015).

201. Jin, H. O., Hong, S. E., Kim, J. Y., Jang, S. K. & Park, I. C. Amino acid deprivation induces AKT activation by inducing GCN2/ATF4/REDD1 axis. *Cell Death Dis* **12**, (2021).

202. Qi, Y. *et al.* Sphingosine kinase 1 protects hepatocytes from lipotoxicity via down-regulation of IRE1α protein expression. *Journal of Biological Chemistry* **290**, 23282–23290 (2015).

203. Schupp, M. *et al. Metabolite and Transcriptome Analysis during Fasting Suggest a Role for the P53-Ddit4 Axis in Major Metabolic Tissues*. http://www.biomedcentral.com/1471-2164/14/758 (2013).

204. Lin, L., Stringfield, T. M., Shi, X. & Chen, Y. Arsenite induces a cell stress-response gene, RTP801, through reactive oxygen species and transcription factors Elk-1 and CCAAT/enhancer-binding protein. *Biochemical Journal* **392**, 93–102 (2005).

205. Jin, H. O. *et al.* TXNIP potentiates Redd1-induced mTOR suppression through stabilization of Redd1. *Oncogene* **30**, 3792–3801 (2011).

206. Quigley, M. *et al.* Vitamin D Modulation of Mitochondrial Oxidative Metabolism and mTOR Enforces Stress Adaptations and Anticancer Responses. *JBMR Plus* **6**, (2022).

207. Lee, D. K. *et al.* Lipopolysaccharide induction of REDD1 is mediated by two distinct CREB-dependent mechanisms in macrophages. *FEBS Lett* **589**, 2859–2865 (2015).

208. Kimball, S. R., Do, A. N. D., Kutzler, L., Cavener, D. R. & Jefferson, L. S. Rapid turnover of the mTOR complex 1 (mTORC1) repressor REDD1 and activation of mTORC1 signaling following inhibition of protein synthesis. *Journal of Biological Chemistry* **283**, 3465–3475 (2008).

209. Tan, C. Y. & Hagen, T. mTORC1 Dependent Regulation of REDD1 Protein Stability. *PLoS One* **8**, (2013).

210. Katiyar, S. *et al.* REDD1, an inhibitor of mTOR signalling, is regulated by the CUL4A-DDB1 ubiquitin ligase. *EMBO Rep* **10**, 866–872 (2009).

211. Romaní-Aumedes, J. *et al.* Parkin loss of function contributes to RTP801 elevation and neurodegeneration in Parkinson's disease. *Cell Death & Disease 2014 5:8* **5**, e1364–e1364 (2014).

212. Canal, M. *et al.* Loss of NEDD4 contributes to RTP801 elevation and neuron toxicity: implications for Parkinson's disease. *Oncotarget* **7**, 58813 (2016).

213. Kim, J. & Guan, K. L. mTOR as a central hub of nutrient signalling and cell growth. *Nature Cell Biology* vol. 21 63–71 Preprint at https://doi.org/10.1038/s41556-018-0205-1 (2019).

214. Benvenuto, G. *et al. The Tuberous Sclerosis-1 (TSC1) Gene Product Hamartin Suppresses Cell Growth and Augments the Expression of the TSC2 Product Tuberin by Inhibiting Its Ubiquitination*. www.nature.com/onc.

215. Zhang, Y. *et al. Rheb Is a Direct Target of the Tuberous Sclerosis Tumour Suppressor Proteins*. *NATURE CELL BIOLOGY* vol. 5 (2003).

216. Dennis, M. D., Coleman, C. S., Berg, A., Jefferson, L. S. & Kimball, S. R. REDD1 enhances protein phosphatase 2A-mediated dephosphorylation of Akt to repress mTORC1 signaling. *Sci Signal* **7**, (2014).

217. Malagelada, C. *et al.* RTP801/REDD1 regulates the timing of cortical neurogenesis and neuron migration. *Journal of Neuroscience* **31**, 3186–3196 (2011).

218. Lee, D. K. *et al.* REDD1 promotes obesity-induced metabolic dysfunction via atypical NF-κB activation. *Nat Commun* **13**, (2022).

219. Wu, Y. *et al.* REDD1 is a major target of testosterone action in preventing dexamethasone-induced muscle loss. *Endocrinology* **151**, 1050–1059 (2010).

220. Solana-Balaguer, J. *et al.* RTP801 mediates transneuronal toxicity in culture via extracellular vesicles. *J Extracell Vesicles* **12**, (2023).

221. Choi, H. S., Ahn, J. H., Park, J. H., Won, M. H. & Lee, C. H. Age-dependent changes in the protein expression levels of Redd1 and mTOR in the

gerbil hippocampus during normal aging. *Mol Med Rep* **13**, 2409–2414 (2016).

222. Pérez-Sisqués, L. *et al.* RTP801/REDD1 contributes to neuroinflammation severity and memory impairments in Alzheimer's disease. *Cell Death Dis* **12**, (2021).

223. Canal, M., Romaní-Aumedes, J., Martín-Flores, N., Pérez-Fernández, V. & Malagelada, C. RTP801/REDD1: A stress coping regulator that turns into a troublemaker in neurodegenerative disorders. *Front Cell Neurosci* **8**, (2014).

224. Ota, K. T. *et al.* REDD1 is essential for stress-induced synaptic loss and depressive behavior. *Nat Med* **20**, 531–535 (2014).

225. Malagelada, C., Zong, H. J. & Greene, L. A. RTP801 is induced in Parkinson's disease and mediates neuron death by inhibiting Akt phosphorylation/activation. *Journal of Neuroscience* **28**, 14363–14371 (2008).

226. Martín-Flores, N. *et al.* Synaptic RTP801 contributes to motor-learning dysfunction in Huntington's disease. *Cell Death Dis* **11**, (2020).

227. Pérez-Sisqués, L. *et al.* Rtp801/redd1 is involved in neuroinflammation and modulates cognitive dysfunction in huntington's disease. *Biomolecules* **12**, (2022).

228. Oakley, H. *et al.* Intraneuronal β-Amyloid Aggregates, Neurodegeneration, and Neuron Loss in Transgenic Mice with Five Familial Alzheimer's Disease Mutations: Potential Factors in Amyloid Plaque Formation. *Journal of Neuroscience* **26**, 10129–10140 (2006).

229. Kanno, T., Tsuchiya, A. & Nishizaki, T. Hyperphosphorylation of Tau at Ser396 occurs in the much earlier stage than appearance of learning and memory disorders in 5XFAD mice. *Behavioural Brain Research* **274**, 302–306 (2014).

230. Boza-Serrano, A., Yang, Y., Paulus, A. & Deierborg, T. Innate immune alterations are elicited in microglial cells before plaque deposition in the Alzheimer's disease mouse model 5xFAD. *Sci Rep* **8**, (2018).

231. Moon, M., Cha, M. Y. & Mook-Jung, I. Impaired hippocampal neurogenesis and its enhancement with ghrelin in 5XFAD mice. *J Alzheimers Dis* **41**, 233–241 (2014).

232. Eimer, W. A. & Vassar, R. Neuron loss in the 5XFAD mouse model of Alzheimer's disease correlates with intraneuronal Aβ42 accumulation and Caspase-3 activation. *Mol Neurodegener* **8**, (2013).

233. Crouzin, N. *et al.* Area-Specific Alterations of Synaptic Plasticity in the 5XFAD Mouse Model of Alzheimer's Disease: Dissociation between Somatosensory Cortex and Hippocampus. *PLoS One* **8**, (2013).

234. Girard, S. D. *et al.* Evidence for early cognitive impairment related to frontal cortex in the 5XFAD mouse model of Alzheimer's disease. *J Alzheimers Dis* **33**, 781–796 (2013).

235. Girard, S. D. *et al.* Onset of hippocampus-dependent memory impairments in 5XFAD transgenic mouse model of Alzheimer's disease. *Hippocampus* **24**, 762–772 (2014).

236. Sahu, M. P., Nikkilä, O., Lagas, S., Kolehmainen, S. & Castrén, E. Culturing primary neurons from rat hippocampus and cortex. *Neuronal Signal* **3**, 20180207 (2019).

237. Haddad-Tóvolli, R. *et al.* Food craving-like episodes during pregnancy are mediated by accumbal dopaminergic circuits. *Nature Metabolism 2022 4:4* **4**, 424–434 (2022).

238. Grandjean, J. *et al.* Common functional networks in the mouse brain revealed by multi-centre resting-state fMRI analysis. *Neuroimage* **205**, (2020).

239. Winkler, A. M., Ridgway, G. R., Webster, M. A., Smith, S. M. & Nichols, T. E. Permutation inference for the general linear model. *Neuroimage* **92**, 381–397 (2014).

240. Ly, P. T. T., Cai, F. & Song, W. Detection of neuritic plaques in Alzheimer's disease mouse model. *J Vis Exp* (2011) doi:10.3791/2831.

241. Canal, M., Romaní-Aumedes, J., Martín-Flores, N., Pérez-Fernández, V. & Malagelada, C. RTP801/REDD1: A stress coping regulator that turns

into a troublemaker in neurodegenerative disorders. *Front Cell Neurosci* **8**, (2014).

242. Malagelada, C., Zong, H. J. & Greene, L. A. RTP801 is induced in Parkinson's disease and mediates neuron death by inhibiting Akt phosphorylation/activation. *Journal of Neuroscience* **28**, 14363–14371 (2008).

243. Martín-Flores, N. *et al.* Synaptic RTP801 contributes to motor-learning dysfunction in Huntington's disease. *Cell Death Dis* **11**, (2020).

244. Pérez-Sisqués, L. *et al.* Rtp801/redd1 is involved in neuroinflammation and modulates cognitive dysfunction in huntington's disease. *Biomolecules* **12**, (2022).

245. Kameno, K. *et al.* Loss of body weight in old 5xFAD mice and the alteration of gut microbiota composition. *Exp Gerontol* **166**, (2022).

246. Márquez-Valadez, B., Rábano, A. & Llorens-Martín, M. Progression of Alzheimer's disease parallels unusual structural plasticity of human dentate granule cells. *Acta Neuropathol Commun* **10**, 125 (2022).

247. Llorens-Martín, M., Jurado-Arjona, J., Avila, J. & Hernández, F. Novel connection between newborn granule neurons and the hippocampal CA2 field. *Exp Neurol* **263**, 285–292 (2015).

248. Hainmueller, T. & Bartos, M. Dentate gyrus circuits for encoding, retrieval and discrimination of episodic memories. *Nature Reviews Neuroscience 2020 21:3* **21**, 153–168 (2020).

249. Damoiseaux, J. S. *et al.* Consistent resting-state networks across healthy subjects. *Proc Natl Acad Sci U S A* **103**, 13848–13853 (2006).

250. Agosta, F. *et al.* Language networks in semantic dementia. *Brain* **133**, 286–299 (2010).

251. Binnewijzend, M. A. A. *et al.* Resting-state fMRI changes in Alzheimer's disease and mild cognitive impairment. *Neurobiol Aging* **33**, 2018–2028 (2012).

252. Ma, Y. *et al.* In vivo 3D digital atlas database of the adult C57BL/6J mouse brain by magnetic resonance microscopy. *Front Neuroanat* **2**, 175 (2008).

253. Kucikova, L. *et al.* Resting-state brain connectivity in healthy young and middle-aged adults at risk of progressive Alzheimer's disease. *Neurosci Biobehav Rev* **129**, 142–153 (2021).

254. Tudela, R., Muñoz-Moreno, E., Sala-Llonch, R., López-Gil, X. & Soria, G. Resting state networks in the TGF344-AD rat model of Alzheimer's disease are altered from early stages. *Front Aging Neurosci* **10**, 475162 (2019).

255. He, X. *et al.* Abnormal salience network in normal aging and in amnestic mild cognitive impairment and Alzheimer's disease. *Hum Brain Mapp* **35**, 3446–3464 (2014).

256. Li, B. S. Y., Wang, H. & Gonen, O. Metabolite ratios to assumed stable creatine level may confound the quantification of proton brain MR spectroscopy. *Magn Reson Imaging* **21**, 923–928 (2003).

257. Walls, A. B. *et al.* Knockout of GAD65 has major impact on synaptic GABA synthesized from astrocyte-derived glutamine. *Journal of Cerebral Blood Flow & Metabolism* **31**, 494 (2011).

258. Liu, J., Feng, X., Wang, Y., Xia, X. & Zheng, J. C. Astrocytes: GABAceptive and GABAergic Cells in the Brain. *Front Cell Neurosci* **16**, 892497 (2022).

259. Carulli, D. *et al.* Animals lacking link protein have attenuated perineuronal nets and persistent plasticity. *Brain* **133**, 2331–2347 (2010).

260. Brückner, G. *et al.* Extracellular matrix organization in various regions of rat brain grey matter. *J Neurocytol* **25**, 333–346 (1996).

261. Enwright, J. F. *et al.* Reduced Labeling of Parvalbumin Neurons and Perineuronal Nets in the Dorsolateral Prefrontal Cortex of Subjects with Schizophrenia. *Neuropsychopharmacology 2016 41:9* **41**, 2206–2214 (2016).

262. Cabungcal, J. H., Steullet, P., Kraftsik, R., Cuenod, M. & Do, K. Q. Early-life insults impair parvalbumin interneurons via oxidative stress: reversal by N-acetylcysteine. *Biol Psychiatry* **73**, 574–582 (2013).

263. Cabungcal, J. H. *et al.* Perineuronal nets protect fast-spiking interneurons against oxidative stress. *Proc Natl Acad Sci U S A* **110**, 9130–9135 (2013).

264. Morawski, M., Brückner, M. K., Riederer, P., Brückner, G. & Arendt, T. Perineuronal nets potentially protect against oxidative stress. *Exp Neurol* **188**, 309–315 (2004).

265. Wiese, S., Karus, M. & Faissner, A. Astrocytes as a source for extracellular matrix molecules and cytokines. *Front Pharmacol* **3**, (2012).

266. Chaunsali, L., Tewari, B. P. & Sontheimer, H. Perineuronal Net Dynamics in the Pathophysiology of Epilepsy. *Epilepsy Curr* **21**, 273–281 (2021).

267. Fitch, M. T. & Silver, J. CNS injury, glial scars, and inflammation: Inhibitory extracellular matrices and regeneration failure. *Exp Neurol* **209**, 294–301 (2008).

268. Matthews, R. T. *et al.* Aggrecan glycoforms contribute to the molecular heterogeneity of perineuronal nets. *J Neurosci* **22**, 7536–7547 (2002).

269. Norden, D. M., Trojanowski, P. J., Villanueva, E., Navarro, E. & Godbout, J. P. Sequential activation of microglia and astrocyte cytokine expression precedes increased iba-1 or GFAP immunoreactivity following systemic immune challenge. *Glia* **64**, 300–316 (2016).

270. Viviani, B. *et al.* Interleukin-1β Enhances NMDA Receptor-Mediated Intracellular Calcium Increase through Activation of the Src Family of Kinases. *Journal of Neuroscience* **23**, 8692–8700 (2003).

271. Hickman, S. E., Allison, E. K. & El Khoury, J. Microglial dysfunction and defective beta-amyloid clearance pathways in aging Alzheimer's disease mice. *J Neurosci* **28**, 8354–8360 (2008).

272. Zaben, M. *et al.* Role of proinflammatory cytokines in the inhibition of hippocampal neurogenesis in mesial temporal lobe epilepsy. *The Lancet* **389**, S105 (2017).

273. Escartin, C. *et al.* Reactive astrocyte nomenclature, definitions, and future directions. *Nature Neuroscience 2021 24:3* **24**, 312–325 (2021).

274. Gao, C., Jiang, J., Tan, Y. & Chen, S. Microglia in neurodegenerative diseases: mechanism and potential therapeutic targets. *Signal Transduction and Targeted Therapy 2023 8:1* **8**, 1–37 (2023).

275. Martinon, F., Burns, K. & Tschopp, J. The inflammasome: a molecular platform triggering activation of inflammatory caspases and processing of proIL-beta. *Mol Cell* **10**, 417–426 (2002).

276. Eng, L. F., Vanderhaeghen, J. J., Bignami, A. & Gerstl, B. An acidic protein isolated from fibrous astrocytes. *Brain Res* **28**, 351–354 (1971).

277. Michetti, F. *et al.* The S100B story: from biomarker to active factor in neural injury. *J Neurochem* **148**, 168–187 (2019).

278. Silva, I., Silva, J., Ferreira, R. & Trigo, D. Glymphatic system, AQP4, and their implications in Alzheimer's disease. *Neurol Res Pract* **3**, (2021).

279. Zeppenfeld, D. M. *et al.* Association of Perivascular Localization of Aquaporin-4 With Cognition and Alzheimer Disease in Aging Brains. *JAMA Neurol* **74**, 91–99 (2017).

280. Wang, Y. *et al.* IL-34 is a tissue-restricted ligand of CSF1R required for the development of Langerhans cells and microglia. *Nature Immunology 2012 13:8* **13**, 753–760 (2012).

281. Miller, Y. I., Navia-Pelaez, J. M., Corr, M. & Yaksh, T. L. Thematic Review Series: Biology of Lipid Rafts: Lipid rafts in glial cells: role in neuroinflammation and pain processing. *J Lipid Res* **61**, 655 (2020).

282. Spittau, B., Dokalis, N. & Prinz, M. The Role of TGFβ Signaling in Microglia Maturation and Activation. *Trends Immunol* **41**, 836–848 (2020).

283. Sengupta, U., Nilson, A. N. & Kayed, R. The Role of Amyloid-β Oligomers in Toxicity, Propagation, and Immunotherapy. *EBioMedicine* **6**, 42 (2016).

284. Baldwin, K. T., Murai, K. K. & Khakh, B. S. Astrocyte morphology. *Trends Cell Biol* **34**, 547–565 (2024).

285. Uddin, M. S. *et al.* Autophagy and Alzheimer's disease: From molecular mechanisms to therapeutic implications. *Front Aging Neurosci* **10**, (2018).

286. Oddo, S., Caccamo, A., Kitazawa, M., Tseng, B. P. & LaFerla, F. M. Amyloid deposition precedes tangle formation in a triple transgenic model of Alzheimer's disease. *Neurobiol Aging* **24**, 1063–1070 (2003).

287. Gene Detail :: Allen Brain Atlas: Mouse Brain. https://mouse.brain-map.org/gene/show/50588.

288. Damjanac, M. *et al.* PKR, a cognitive decline biomarker, can regulate translation via two consecutive molecular targets p53 and Redd1 in lymphocytes of AD patients. *J Cell Mol Med* **13**, 1823–1832 (2009).

289. Kim, J. R. *et al.* Identification of amyloid beta-peptide responsive genes by cDNA microarray technology: involvement of RTP801 in amyloid beta-peptide toxicity. *Exp Mol Med* **35**, 403–411 (2003).

290. Oh, S. *et al.* Amyloid peptide attenuates the proteasome activity in neuronal cells. *Mech Ageing Dev* **126**, 1292–1299 (2005).

291. Gibbs, M. E., Hutchinson, D. & Hertz, L. Astrocytic involvement in learning and memory consolidation. *Neurosci Biobehav Rev* **32**, 927–944 (2008).

292. Henneberger, C., Papouin, T., Oliet, S. H. R. & Rusakov, D. A. Long-term potentiation depends on release of D-serine from astrocytes. *Nature* **463**, 232–236 (2010).

293. De Pins, B. *et al.* Conditional BDNF delivery from astrocytes rescues memory deficits, spine density, and synaptic properties in the 5xFAD mouse model of alzheimer disease. *Journal of Neuroscience* **39**, 2441–2458 (2019).

294. Mukhin, V. N., Pavlov, K. I. & Klimenko, V. M. Mechanisms of Neuron Loss in Alzheimer's Disease. *Neuroscience and Behavioral Physiology 2017 47:5* **47**, 508–516 (2017).

295. Poon, C. H. *et al.* Sex Differences between Neuronal Loss and the Early Onset of Amyloid Deposits and Behavioral Consequences in 5xFAD Transgenic Mouse as a Model for Alzheimer's Disease. *Cells* **12**, (2023).

296. Schneider, F., Baldauf, K., Wetzel, W. & Reymann, K. G. Effects of methylphenidate on the behavior of male 5xFAD mice. *Pharmacol Biochem Behav* **128**, 68–77 (2015).

297. Jawhar, S., Trawicka, A., Jenneckens, C., Bayer, T. A. & Wirths, O. Motor deficits, neuron loss, and reduced anxiety coinciding with axonal degeneration and intraneuronal Aβ aggregation in the 5XFAD mouse model of Alzheimer's disease. *Neurobiol Aging* **33**, 196.e29-196.e40 (2012).

298. Flanigan, T. J., Xue, Y., Rao, S. K., Dhanushkodi, A. & McDonald, M. P. Abnormal vibrissa-related behavior and loss of barrel field inhibitory neurons in 5xFAD transgenics. *Genes Brain Behav* **13**, 488–500 (2014).

299. Cho, W. H. *et al.* Hippocampal astrocytes modulate anxiety-like behavior. *Nature Communications 2022 13:1* **13**, 1–14 (2022).

300. Araque, A., Parpura, V., Sanzgiri, R. P. & Haydon, P. G. Tripartite synapses: glia, the unacknowledged partner. *Trends Neurosci* **22**, 208–215 (1999).

301. Xiao, N. A. *et al.* Reduction of Glucose Metabolism in Olfactory Bulb is an Earlier Alzheimer's Disease-related Biomarker in 5XFAD Mice. *Chin Med J (Engl)* **128**, 2220–2227 (2015).

302. Griñán-Ferré, C. *et al.* Pharmacological inhibition of G9a/GLP restores cognition and reduces oxidative stress, neuroinflammation and β-Amyloid plaques in an early-onset Alzheimer's disease mouse model. *Aging* **11**, 11591–11608 (2019).

303. Quenon, L., De Xivry, J. J. O., Hanseeuw, B. & Ivanoiu, A. Investigating Associative Learning Effects in Patients with Prodromal Alzheimer's Disease Using the Temporal Context Model. *J Int Neuropsychol Soc* **21**, 699–708 (2015).

304. Yi, J. H. *et al.* REDD1 Is Involved in Amyloid β-Induced Synaptic Dysfunction and Memory Impairment. *Int J Mol Sci* **21**, 1–13 (2020).

305. Paranjape, G. S., Gouwens, L. K., Osborn, D. C. & Nichols, M. R. Isolated amyloid-β(1-42) protofibrils, but not isolated fibrils, are robust stimulators of microglia. *ACS Chem Neurosci* **3**, 238–247 (2012).

306. Dickson, D. W. *et al.* Correlations of synaptic and pathological markers with cognition of the elderly. *Neurobiol Aging* **16**, 285–298 (1995).

307. Masliah, E., Terry, R. D., Mallory, M., Alford, M. & Hansen, L. A. Diffuse plaques do not accentuate synapse loss in Alzheimer's disease. *ncbi.nlm.nih.govE Masliah, RD Terry, M Mallory, M Alford, LA HansenThe American journal of pathology, 1990•ncbi.nlm.nih.gov* **13**, (1990).

308. Mucke, L. *et al.* High-level neuronal expression of Aβ1–42 in wild-type human amyloid protein precursor transgenic mice: synaptotoxicity without plaque formation. *Soc NeuroscienceL Mucke, E Masliah, GQ Yu, M Mallory, EM Rockenstein, G Tatsuno, K Hu, D KholodenkoJournal of Neuroscience, 2000•Soc Neuroscience* (2000).

309. Llorens-Martín, M. *et al.* Peripherally triggered and GSK-3β-driven brain inflammation differentially skew adult hippocampal neurogenesis, behavioral pattern separation and microglial activation in response to ibuprofen. *Transl Psychiatry* **4**, e463 (2014).

310. Diamantaki, M., Frey, M., Berens, P., Preston-Ferrer, P. & Burgalossi, A. Sparse activity of identified dentate granule cells during spatial exploration. *Elife* **5**, (2016).

311. Correia, C. *et al.* Neuroimaging of Mouse Models of Alzheimer's Disease. *Biomedicines 2022, Vol. 10, Page 305* **10**, 305 (2022).

312. Maharjan, S. *et al.* Age-dependent microstructure alterations in 5xFAD mice by high-resolution diffusion tensor imaging. *Front Neurosci* **16**, (2022).

313. Kesler, S. R., Acton, P., Rao, V. & Ray, W. J. Functional and structural connectome properties in the 5XFAD transgenic mouse model of Alzheimer's disease. *Network Neuroscience* **02**, 241–258 (2018).

314. Sheline, Y. I. & Raichle, M. E. Resting state functional connectivity in preclinical Alzheimer's disease. *Biol Psychiatry* **74**, 340–347 (2013).

315. Mars, R. B. *et al.* On the relationship between the 'default mode network' and the 'social brain'. *Front Hum Neurosci* **6**, 1–9 (2012).

316. Ward, A. M. *et al.* Relationships between default-mode network connectivity, medial temporal lobe structure, and age-related memory deficits. *Neurobiol Aging* **36**, 265–272 (2015).

317. Ereira, S., Waters, S., Razi, A. & Marshall, C. R. Early detection of dementia with default-mode network effective connectivity. *Nature Mental Health 2024 2:7* **2**, 787–800 (2024).

318. Menon, V. & Uddin, L. Q. Saliency, switching, attention and control: a network model of insula function. *Brain Struct Funct* **214**, 655–667 (2010).

319. Sridharan, D., Levitin, D. J. & Menon, V. A critical role for the right fronto-insular cortex in switching between central-executive and default-mode networks. *Proc Natl Acad Sci U S A* **105**, 12569–12574 (2008).

320. Fox, M. D. *et al.* The human brain is intrinsically organized into dynamic, anticorrelated functional networks. *Proc Natl Acad Sci U S A* **102**, 9673–9678 (2005).

321. Kim, E. *et al.* Mammillothalamic functional connectivity and memory function in Wernicke's encephalopathy. *Brain* **132**, 369–376 (2009).

322. Wang, H. *et al.* Magnetic Resonance Spectroscopy in Alzheimer's Disease: Systematic Review and Meta-Analysis. *J Alzheimers Dis* **46**, 1049–1070 (2015).

323. Dedeoglu, A., Choi, J. K., Cormier, K., Kowall, N. W. & Jenkins, B. G. Magnetic resonance spectroscopic analysis of Alzheimer's disease mouse brain that express mutant human APP shows altered neurochemical profile. *Brain Res* **1012**, 60–65 (2004).

324. Mlynárik, V. *et al.* Proton and Phosphorus Magnetic Resonance Spectroscopy of a Mouse Model of Alzheimer's Disease. *Journal of Alzheimer's Disease* **31**, S87–S99 (2012).

325. Andersen, J. V. *et al.* Hippocampal disruptions of synaptic and astrocyte metabolism are primary events of early amyloid pathology in the 5xFAD mouse model of Alzheimer's disease. *Cell Death Dis* **12**, (2021).

326. Ohno, K. *et al.* GlyCEST: Magnetic Resonance Imaging of Glycine—Distribution in the Normal Murine Brain and Alterations in 5xFAD Mice. *Contrast Media Mol Imaging* **2021**, (2021).

327. Klunk, W. E., Panchalingam, ; K, Moossy, ; J, Mcclure, ; R J & Pettegrew, J. W. *N-Acetyl-L-Aspartate and Other Amino Acid Metabolites in Alzheimer's Disease Brain: A Preliminary Proton Nuclear Magnetic Resonance Study*. https://www.neurology.org (1991).

328. Warepam, M. *et al.* Brain Metabolite, N-Acetylaspartate Is a Potent Protein Aggregation Inhibitor. *Front Cell Neurosci* **15**, 617308 (2021).

329. Macdonald, I. R. *et al.* Early Detection of Cerebral Glucose Uptake Changes in the 5XFAD Mouse. *Curr Alzheimer Res* **11**, 450 (2014).

330. Oh, S. J. *et al.* Evaluation of the neuroprotective effect of taurine in Alzheimer's disease using functional molecular imaging. *Sci Rep* **10**, (2020).

331. Yoo, C. H., Kim, J., Baek, H. M., Chang, K. A. & Choe, B. Y. Neurodegenerative Changes in the Brains of the 5xFAD Alzheimer's Disease Model Mice Investigated by High-Field and High-Resolution Magnetic Resonance Imaging and Multi-Nuclei Magnetic Resonance Spectroscopy. *Int J Mol Sci* **24**, (2023).

332. Saiz-Sanchez, D., Ubeda-Baon, I., De La Rosa-Prieto, C. & Martinez-Marcos, A. Differential expression of interneuron populations and correlation with amyloid-β deposition in the olfactory cortex of an AβPP/PS1 transgenic mouse model of Alzheimer's disease. *J Alzheimers Dis* **31**, 113–129 (2012).

333. Takahashi, H. *et al.* Hippocampal interneuron loss in an APP/PS1 double mutant mouse and in Alzheimer's disease. *Brain Struct Funct* **214**, 145–160 (2010).

334. Satoh, J., Tabira, T., Sano, M., Nakayama, H. & Tateishi, J. Parvalbumin-immunoreactive neurons in the human central nervous system are decreased in Alzheimer's disease. *Acta Neuropathol* **81**, 388–395 (1991).

335. Steullet, P. *et al.* Oxidative stress-driven parvalbumin interneuron impairment as a common mechanism in models of schizophrenia. *Mol Psychiatry* **22**, 936–943 (2017).

336. Lazic, D. *et al.* Every-other-day feeding exacerbates inflammation and neuronal deficits in 5XFAD mouse model of Alzheimer's disease. *Neurobiol Dis* **136**, 104745 (2020).

337. Wu, Z., Guo, Z., Gearing, M. & Chen, G. Tonic inhibition in dentate gyrus impairs long-term potentiation and memory in an Alzhiemer's disease model. *Nat Commun* **5**, 4159 (2014).

338. Wong-Guerra, M., Calfio, C., Maccioni, R. B. & Rojo, L. E. Revisiting the neuroinflammation hypothesis in Alzheimer's disease: a focus on the druggability of current targets. *Front Pharmacol* **14**, (2023).

339. Forner, S. *et al.* Systematic phenotyping and characterization of the 5xFAD mouse model of Alzheimer's disease. *Sci Data* **8**, (2021).

340. Yin, J. *et al.* NLRP3 inflammasome inhibitor ameliorates amyloid pathology in a mouse model of Alzheimer's disease. *Mol Neurobiol* **55**, 1977 (2018).

341. Couturier, J. *et al.* Activation of phagocytic activity in astrocytes by reduced expression of the inflammasome component ASC and its implication in a mouse model of Alzheimer disease. *J Neuroinflammation* **13**, (2016).

342. Qiu, Y. *et al.* Definition of the contribution of an Osteopontin-producing CD11c+ microglial subset to Alzheimer's disease. *Proc Natl Acad Sci U S A* **120**, 2218915120 (2023).

343. Marciniak, E. *et al.* The Chemokine MIP-1α/CCL3 impairs mouse hippocampal synaptic transmission, plasticity and memory. *Scientific Reports 2015 5:1* **5**, 1–11 (2015).

344. Lee, D. K. *et al.* REDD-1 aggravates endotoxin-induced inflammation VIA atypical NF-κB activation. *The FASEB Journal* **32**, 4585–4599 (2018).

345. Sunilkumar, S. *et al.* Stress response protein REDD1 promotes diabetes-induced retinal inflammation by sustaining canonical NF-κB signaling. *J Biol Chem* **298**, 102638 (2022).

346. Yu, H., Lin, L., Zhang, Z., Zhang, H. & Hu, H. Targeting NF-κB pathway for the therapy of diseases: mechanism and clinical study. *Signal Transduction and Targeted Therapy 2020 5:1* **5**, 1–23 (2020).

347. El-Ansary, A. & Al-Ayadhi, L. GABAergic/glutamatergic imbalance relative to excessive neuroinflammation in autism spectrum disorders. *J Neuroinflammation* **11**, (2014).

348. Pribiag, H. & Stellwagen, D. TNF-α downregulates inhibitory neurotransmission through protein phosphatase 1-dependent trafficking of GABA(A) receptors. *J Neurosci* **33**, 15879–15893 (2013).

349. Stellwagen, D., Beattie, E. C., Seo, J. Y. & Malenka, R. C. Differential regulation of AMPA receptor and GABA receptor trafficking by tumor necrosis factor-alpha. *J Neurosci* **25**, 3219–3228 (2005).

350. biologie, J. B.-C. rendus des seances de la S. de & 1962, undefined. Organotypic culture, on natural and artificial media, of fragments of the adult rat hypophysis. *europepmc.org*.

351. LaVail, J. H. & Wolf, M. K. Postnatal development of the mouse dentate gyrus in organotypic cultures of the hippocampal formation. *American Journal of Anatomy* **137**, 47–65 (1973).

352. Walsh, K., Megyesi, J. & Hammond, R. Human central nervous system tissue culture: a historical review and examination of recent advances. *Neurobiol Dis* **18**, 2–18 (2005).

353. De Strooper, B. Lessons from a failed γ-secretase Alzheimer trial. *Cell* **159**, 721–726 (2014).

354. Huber, M., Rembiałkowska, E., Średnicka, D., Bügel, S. & Van De Vijver, L. P. L. Organic food and impact on human health: Assessing the status quo and prospects of research. *NJAS - Wageningen Journal of Life Sciences* **58**, 103–109 (2011).

355. Luchena, C. *et al.* A neuron, microglia, and astrocyte triple coculture model to study Alzheimer disease. *bioRxiv* 2021.12.13.472367 (2021) doi:10.1101/2021.12.13.472367.

356. Goshi, N., Kim, H. & Seker, E. Primary Cortical Cell Tri-Culture-Based Screening of Neuroinflammatory Response in Toll-like Receptor Activation. *Biomedicines* **10**, (2022).

357. Schiweck, J., Eickholt, B. J. & Murk, K. Important Shapeshifter: Mechanisms Allowing Astrocytes to Respond to the Changing Nervous System During Development, Injury and Disease. *Front Cell Neurosci* **12**, (2018).

358. Bushong, E. A., Martone, M. E., Jones, Y. Z. & Ellisman, M. H. Protoplasmic astrocytes in CA1 stratum radiatum occupy separate anatomical domains. *J Neurosci* **22**, 183–192 (2002).

359. Acaz-Fonseca, E., Ortiz-Rodriguez, A., Azcoitia, I., Garcia-Segura, L. M. & Arevalo, M. A. Notch signaling in astrocytes mediates their morphological response to an inflammatory challenge. *Cell Death Discovery 2019 5:1* **5**, 1–14 (2019).

360. Choi, M., Kim, H., Yang, E. J. & Kim, H. S. Inhibition of STAT3 phosphorylation attenuates impairments in learning and memory in 5XFAD mice, an animal model of Alzheimer's disease. *J Pharmacol Sci* **143**, 290–299 (2020).

361. Garcia-Segura, P., Malagelada, C., Garcia-Segura, C. P. & Malagelada, C. STAT3 and REDD1: an unconventional story of gene repression. *FEBS J* **290**, 1735–1739 (2023).

362. Oberheim, N. A., Wang, X., Goldman, S. & Nedergaard, M. Astrocytic complexity distinguishes the human brain. *Trends Neurosci* **29**, 547–553 (2006).

363. Walsh, D. M. & Selkoe, D. J. A beta oligomers - a decade of discovery. *J Neurochem* **101**, 1172–1184 (2007).

364. Hampel, H. *et al.* The Amyloid-β Pathway in Alzheimer's Disease. *Molecular Psychiatry 2021 26:10* **26**, 5481–5503 (2021).

365. Heneka, M. T. *et al.* Neuroinflammation in Alzheimer's disease. *The Lancet Neurology* vol. 14 388–405 Preprint at https://doi.org/10.1016/S1474-4422(15)70016-5 (2015).

366. Frost, G. R. & Li, Y. M. The role of astrocytes in amyloid production and Alzheimer's disease. *Open Biol* **7**, (2017).

367. Wong, C. O. Endosomal-Lysosomal Processing of Neurodegeneration-Associated Proteins in Astrocytes. *Int J Mol Sci* **21**, 1–17 (2020).

368. Selkoe, D. J. Soluble oligomers of the amyloid beta-protein impair synaptic plasticity and behavior. *Behavioural brain research* **192**, 106–113 (2008).

369. Butterfield, D. A. & Halliwell, B. Oxidative stress, dysfunctional glucose metabolism and Alzheimer disease. *Nat Rev Neurosci* **20**, 148–160 (2019).

370. Kanekiyo, T., Liu, C. C., Shinohara, M., Li, J. & Bu, G. LRP1 in brain vascular smooth muscle cells mediates local clearance of Alzheimer's amyloid-β. *J Neurosci* **32**, 16458–16465 (2012).

371. Chaney, M. O. *et al.* RAGE and amyloid beta interactions: Atomic force microscopy and molecular modeling. *Biochimica et Biophysica Acta (BBA) - Molecular Basis of Disease* **1741**, 199–205 (2005).

ANNEX

23. RTP801 regulates astrocytic NLRP1 levels *in vitro*

We wondered whether astrocytic RTP801 could regulate inflammation related proteins in physiological conditions. We studied the capability of RTP801 to regulate NLRP1 levels in astrocytes and in basal conditions.

First, we characterized our primary rat culture of neurons and observed that there were a 90% of neurons (MAP2$^+$ cells) and 10% of astrocytes (GFAP$^+$ cells). **(Figure 47).**

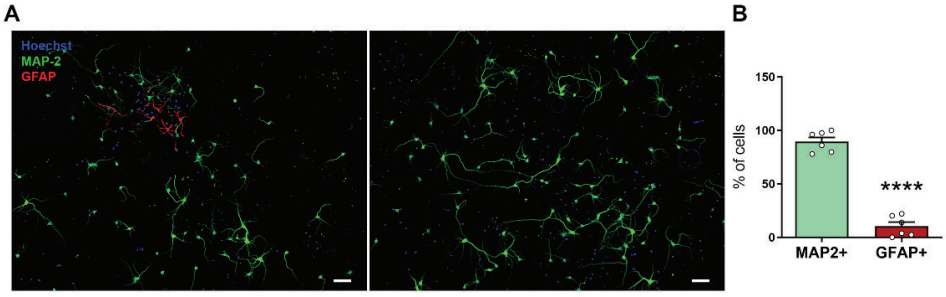

Figure 47. Characterization of neuronal cultures. (A) Immunocytochemistry for MAP-2 (green) was performed to visualize neurons and for GFAP (red), to visualize astrocytes. Hoechst 33342 (blue) was used to visualize nuclei. Representative culture fields are shown (B) Quantification of MAP-2 positive cells vs. GFAP positive cells. Values represent culture replicates of two independent neuronal cultures (mean ±SEM). Data was analyzed by Student's T-test (****P<0.0001 vs. MAP-2+). Obtained from Solana-Balaguer J. dissertation.

At DIV14 we knock down RTP0801 in the whole culture transducing the culture with lentiviral particles containing the vectors pLL3.7-shCT (control) or pLL3.7-shRTP801. We checked the levels of the inflammasome protein NLRP1 specifically on transduced astrocytes, by immunocytochemistry, under these two conditions. Surprisingly, we observed lower relative intensity (%) of NLRP1 in astrocytes after RTP801 silencing **(Figure 48).**

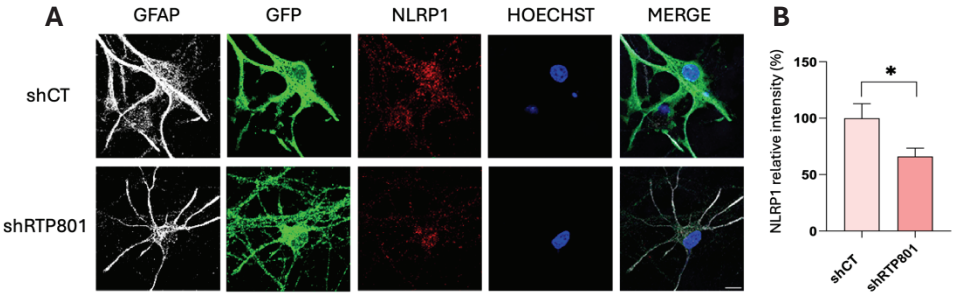

Figure 48. RTP801 regulates levels of NLRP1 in astrocytes. RTP801 was knocked down in hippocampal astrocytes with lentiviral particles. Cells were subjected to immunofluorescence analysis. GFP as an indicator of infected cells (green), GFAP (grey) and NALP1 (red). Scale bar of 10 μm. Intensity was measured with ImageJ software and data was analyzed by two-way ANOVA (*P<0.05). Values represented different astrocytes (>5 per experiment) from three independent cultures and are represented as mean ± SEM(n=3).

Afterwards, we performed the same experiment however overexpressing RTP801. This time, the culture was transduced with lentiviral particles containing the FUGWm-eGFP (control) or the FUGWm eGFP-RTP801 to overexpress RTP801 in the whole primary culture. We observed the opposite effect seen after silencing. Under these conditions the levels of the inflammasome protein NLRP1 were increased after overexpressing RTP801 in transduced astrocytes **(Figure 49).**

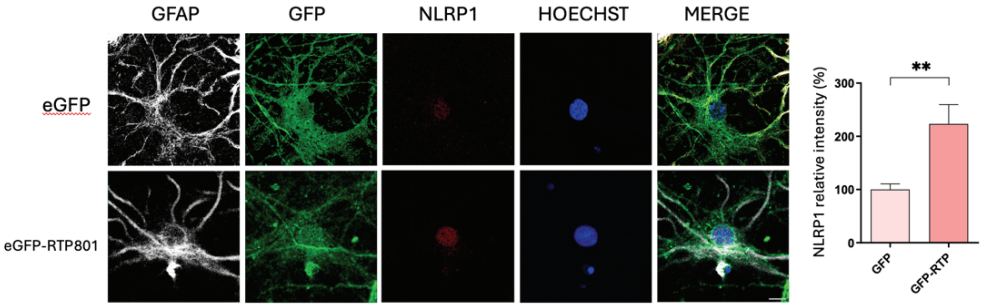

Figure 49. RTP801 regulates levels of NLRP1 in astrocytes. RTP801 overexpressed in hippocampal astrocytes with lentiviral particles. A) Cells were subjected to immunofluorescence analysis. GFP as an indicator of infected cells (green), GFAP (grey) and NALP1 (red). Scale bar of 10 μm. Intensity was measured with ImageJ software and data was analyzed by two-way ANOVA (**P<0.01). B) NLRP1 relative intensity (%) quantification. Values represented different astrocytes (>5 per experiment) from three independent cultures and are represented as mean ± SEM(n=3).

These results suggest that RTP801 in astrocytes is somehow regulating the levels of the inflammasome protein NLRP1 in physiological conditions. However, as this primary culture contains around a 90% of neurons and RTP801 was silenced in the whole culture we do not discard that this effect is also regulated by neuron intercommunication with astrocytes.

In neurodegenerative diseases, like Alzheimer's disease the levels of RTP801 are higher, as well as the levels of NLRP1 in astrocytes. As depicted in our results it seems that RTP801 is regulating inflammasome levels even in the absence of inflammation.